Functionalisation of gold nanoparticles with short synthetic peptides and their potential therapeutic use against the influenza virus infections

Thesis submitted in accordance with the requirements of the University of Liverpool for the degree of Doctor of Philosophy

Zaid Khalaf Abdullah Alghrair

Institute of Integrative Biology

University of Liverpool

Supervisors:

Prof. David Fernig

Dr. Bahram Ebrahimi

April 2018

`

Declaration

I hereby declare that the work contained within this thesis is my own and has not been submitted for any other degree at any University. The work of others is acknowledged as appropriate.

`

Acknowledgements

I would like to extend my thanks and gratitude to those who have helped me both in terms of guidance and advice, but also support and friendship.

Firstly, I would like to express my sincere thanks to both Prof. Dave Fernig and Dr. Bahram Ebrahimi as the work here would not have been possible without their knowledge and experience. They have provided great support in my pursuit of this PhD, and have also been kind enough to offer advice on matters that extend further than the confines of academia. I would like to thank the dozens of people who I have met and worked with during my time at Liverpool, especially those in Lab D. Without their friendship this experience would not have been as enjoyable. They too have offered a variety of useful advice during the much more informal 'lab meetings' held on Monday morning.

I would like to thank those who have supported me much longer than the duration of the PhD, my wife and two lovely daughters. They have given me all the support that I have required throughout my life and I hope that this goes someway to paying back their faith.

Finally, I would appreciate Iraqi ministry of higher education and scientific research who support my PhD work.

Table of contents

Abstract

Influenza (‘flu) virus is a major health concern for humans and animals. The mode of transmission is predominantly by the respiratory route. 'Flu infection occurs seasonally and can cause global pandemics, with the most recent ‘flu pandemic, the 2009 H1N1 Swine ‘flu, resulted in more than 18,000 deaths worldwide. ‘Flu poses major challenges, because the virus has an RNA genome, which has a high potential to recombine and produce new strains through a mechanism termed re-assortment. The constant appearance of new strains requires new vaccines; the time between virus identification and the deployment of the vaccine is an important challenge in ‘flu control. Therefore, anti-influenza drugs, which can control the virus infection irrespective the virus strain are important. Such antivirals are usually cheaper compared to vaccination and can be self-administered. However, drug treatment is usually less effective over time due to the rapid evolution of the virus genome and the acquisition by the virus of drug resistance.

The approval of the first peptide anti-viral, Enfuvirtidie, by the Food and Drug Administration (USA) illustrates the potential of peptides to combat infectious diseases. “Flupep”, a peptide originally identified as a mimic of the suppressor of cytokine signalling (SOCS) protein, was subsequently found to inhibit the infectivity of influenza A virus, including the H1N1 subtype. To understand how Flupep exerts its effects, it has been incorporated into the ligand shell of gold nanoparticles. The gold nanoparticles provide a very sensitive probe that can be detected optically, and are a model for a potential future nanoparticle formulations. The results demonstrate that the nanoparticle-Flupep conjugates have enhanced

anti-‘flu virus activity compared to free peptide in a cell-based plaque assay. Nanoparticle-Flupep conjugates do not bind to influenza virus *in vitro*. However, the nanoparticle-Flupep conjugates bind to cells and, following binding, remain cell-associated and able to inhibit ‘flu virus infectivity. The cell bound nanoparticle-Flupep conjugates may be removed by washing the cells with 1 M NaCl, indicating that ionic interactions are likely to underpin their binding to cells. Treatment of cells with heparinases I and II neuraminidases, but not chondroitinase ABC reduces binding of Flupep-nanoparticle conjugates, indicating that heparan sulfate and sialic acid are major cellular binding sites of the peptide. Since the Flupep sequence has a basic C-terminus likely to be involved in binding these polysaccharides, heparan sulfate binding sequences from growth factors were added to the FluPep sequence. These additions enhanced its anti-viral activity, showing that engineering extracellular matrix binding of peptides inhibiting ‘flu virus is a route to increasing their effective potency.

Overall the thesis demonstrates that Flupep, contrary to published work, exerts its anti-viral effects by binding to cells, and FluPep binding sites include heparan sulfate and sialic acid. Other binding sites are likely involved, since the IC_{50} of Flupep and its derivatives is orders of magnitude lower than the likely affinity of the peptides for polysaccharide binding sites. Thus, the hypothesis is put forward that Flupep interacts with one of more dual receptor systems consisting of polysaccharide and protein(s) and that this underlies the efficacy and mode of action of the peptide

List of abbreviations

AgNP	Silver nanoparticles
AuNP	Gold nanoparticle
BSA	Bovine serum albumin
CV-N	Cyanovirin-N
DEAE	Diethylaminoethanol
DIBO	Dibenzocylooctyne
DMEM	Dulbecco's modified eagle medium
DMSO	Dimethyl sulfoxide
DTT	Dithiothreitol
EB	Entry blocker
FBS	Fetal bovine serum
FGF	Fibroblast growth factor
HA	Hemagglutinin
HCV	Hepatitis C virus
HIV	Human immunodeficiency virus
LSPR	Local surface plasmon resonance
MDCK	Madine-Darby canine kidney cells
MOI	Multiplicity of infection
NA	Neuraminidase
Ni–NTA	Nickel–nitrilotriacetic
NP	Nanoparticle
PBS	Phosphate buffered saline
PEG	Polyethylene glycol

PFU	Plaque forming unit
QD	Quantum dot
SEF	Surface-enhanced fluorescence
SERS	Surface-enhanced Raman scattering
TEM	Transmission electron microscopy
Tkip	Tyrosine kinase inhibitor peptide
UV-Vis	Ultraviolet-visible

`

Chapter 1

1 General introduction

1.1 Pandemic Influenza virus

1.1.1 Overview

Influenza (‘flu) virus is is an infectious disease for humans, farm and wild animals (Chavas et al., 2010). The ‘flu virus is a member of the to the Orthomyxoviridae family, a negative-stranded RNA viruses with a segmented genome, which is nearly spherical, but somewhat pleomorphic with a particle size of around ~100 nm in diameter (Bouvier and Palese, 2008). The influenza A virion is embedded with spikes of haemagglutinin (HA) and neuraminidase (NA) glycoproteins that projecting from a host cell–derived lipid membrane (Fig. 1). Virus nomenclature is according to H number (for the type of haemagglutinin) and an N number (for the type of neuraminidase). There are 18 known H antigens (H1 to H18) and 11 different N antigens (N1 to N11) (Gamblin and Skehel, 2010). Heamagglutinin HA is a trimeric glycoprotein, which is considered responsible for receptor binding and membrane fusion (Hamilton et al., 2012), while neuraminidase NA is a tetramer glycoprotein that cleaves sialic acids from cell surface N-glycans to aid the release of newly synthesised viruses (Fig. 1). The M2 protein is a tetrameric integral membrane protein that forms an ion channel that is responsible for the acidification of the interior of the viral particle during viral infection (Skalickova et al., 2015a). M1 is a matrix protein located under the viral lipid envelope associated with the viral ribonucleoprotein (vRNP) complex, from which it dissociates upon

acidification of the interior environment of the viral particle due to the action of the ion channel formed by M2 (Fig. 1)

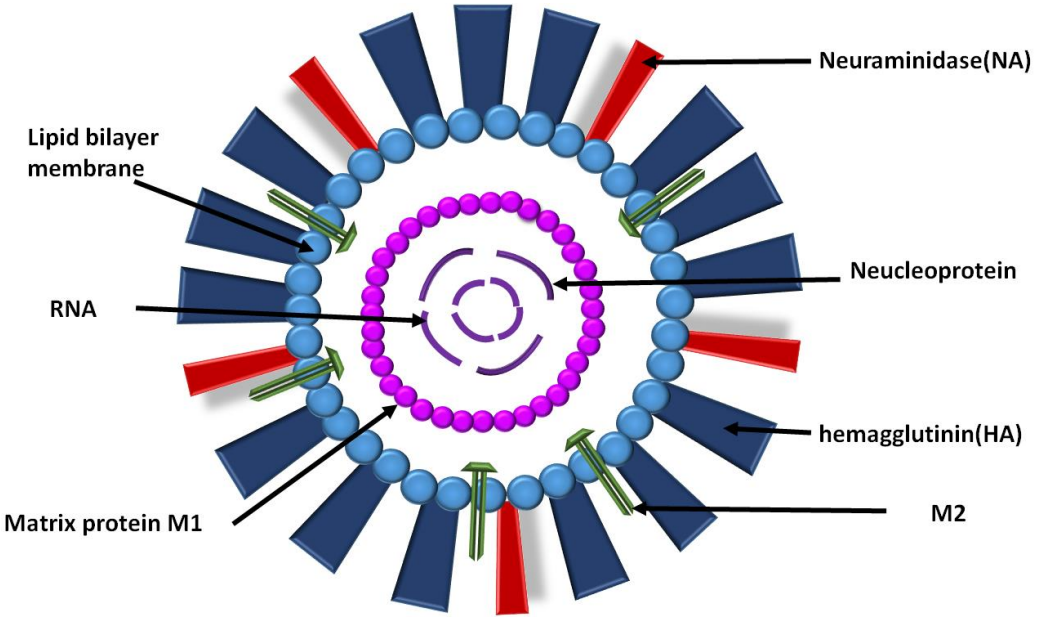

Fig. 1. Schematic of influenza virus structure. Derived from (Skalickova et al; 2015)

All eight vRNA segments inside the virion are bound to the nucleoprotein NP and to the influenza virus RNA polymerases to form ribonucleoprotein (RNP) complexes (Fig. 1) (Lamb and Choppin, 1983).

There are three influenza viral types; A, B and C (Blumel et al., 2009). Influenza A viruses circulate in a wide range of avian and mammalian hosts, whereas influenza B and C are human viruses. Influenza A and B viruses are the predominant causative agent of the vast majority of human infections. Past epidemics and pandemics are mainly associated with type A, while type B is less frequently associated with epidemics. Type C causes a very mild respiratory influenza illness.

`

1.1.2 Seasonal ‘flu, epidemics and pandemics

Influenza is a highly infectious viral disease which can occur as sporadic cases, an epidemic or a pandemic (Morens et al., 2009). In temperate and cold climates, most common are seasonal outbreaks whereas in tropical climates outbreaks may occur throughout the year (Lowen and Palese, 2009). These forms of ‘flu have varying ranges of infection from severe illness to death, and those with chronic medical conditions, elderly people and pregnant women are usually the most vulnerable to infection (Barker, 1986, Barker and Mullooly, 1980). An epidemic is a seasonal outbreak, which infects many people and spreads to neighbouring countries, generally due to the re-emergence of the previous year’s virus strain. Slight changes in the virus’ surface binding proteins may result in it not being recognised by the host's immune system, enabling infection and spread. In contrast, pandemic ‘flu is a worldwide outbreak or a severe epidemic resulting from a introduced new influenza A virus strain (Saunders-Hastings and Krewski, 2016). This can spread quickly from person to person due to the lack of pre-existing immunity, so the pool of hosts is very large (Morens et al., 2009). Pandemic ‘flu occurs sporadically, and over the last 300 years there have been about three influenza pandemics in each century (Hill et al., 2017). The most recent ‘flu pandemic was the 2009 H1N1 Swine ‘flu, which resulted in more than 18,000 deaths worldwide (Pasricha et al., 2013). The worst pandemic on record was the so-called 1918 Spanish ‘flu, which caused an estimated ~50 million deaths worldwide (Taubenberger and Morens, 2006).

`

1.1.3 Virus transmission

The three main routes of viral transmission among humans are (i) inhalation of virus-laden aerosols, (ii) contact with infected individuals, and (iii) contact with contaminated fomites. Which of these is the most common mode of transmission still unknown (Mubareka et al., 2009). Speaking, singing and even normal breathing can produce sufficient aerosols for respiratory transmission. Coughing and sneezing produce heavier aerosols, which eventually fall to the ground within a few meters and infect only those in close proximity (Cowling et al., 2013). Transmission by direct contact occurs by physical contact with, for example, hands containing nasal secretions. Research has shown that up to 60% of objects in homes with infected individuals harbor influenza viral RNA, which can mediate virus transmission (Barker et al., 2001). Thus, hands often become contaminated with respiratory viruses. Thereafter the touching of the nasal mucosa or the conjunctivae enables the virus to infect the individual (Ansari et al., 1991)

1.1.4 Virus replicative cycle

The conventional view of the virus replication cycle is that it starts with attachment to the host epithelial cells of the respiratory tract via the surface glycoprotein haemagglutinin (HA) (Mair et al., 2014). This interaction with cell-surface molecules is followed by endocytosis and fusion of the viral and endosomal membranes, which then allows delivery of the viral genetic material to the nucleocytoplasmic space (Skehel and Wiley, 2000). Haemagglutinin is a trimer that binds to sialic acids carried on the glycan portion of cell surface proteins (Das et al., 2010). This interaction triggers endocytosis of the virus. Endosomes are

acidified by the action of the vacuolar H^+ATPase, which triggers a conformational change in HA (Guinea and Carrasco, 1995). This exposes the N-terminus of haemagglutinin 2 (HA2), allowing its insertion into the endosomal membrane, which causes fusion of the viral and endosomal membranes. The ion channel formed by the M2 protein acidifies the interior environment of the viral particle (Skalickova et al., 2015a). The lower pH in the virus leads to the dissociation of viral matrix protein (M1) from viral ribonucleoprotein (vRNP) complex, which is then released into the host cytoplasm to be transported to the nucleus (Skalickova et al., 2015a). Here the viral RNA is replicated and transcribed, which is catalysed by RNA polymerase complex (Brunotte et al., 2014, Stubbs and te Velthuis, 2014). The host cell ribosomes translate the viral mRNA to produce new viral proteins. HA, neuraminidase (NA) and M2 proteins are transported to the plasma membrane where new viral particles will assemble and be released (Leser and Lamb, 2005). Neuraminidase, the second main surface glycoprotein is considered to facilitate the release of the new assembled virion particles from the cell surface, so allowing these to infect other cells (Takimoto et al., 2002, Rossman et al., 2010).

1.2 Prevention and treatment

1.2.1 The challenge

The treatment of ‘flu infections is difficult, because the virus has RNA genome, which has a high potential to recombine and create new strains through re-assortment (Treanor, 2004). From the host perspective, this results antigenic drift and shift, which result in antigenic mutants of the virus that alter the virus immunological and pharmacological identity periodically. Antigenic drift is when

small changes in the viral genome happen frequently over time, resulting in a series of minor changes in the surface antigens, which can occur in all three influenza types. In contrast, antigenic shift is the result of a large change in one or both surface antigens (HA or NA) and is a result of a genetic recombination between influenza A viruses, and is most common in those that affect humans and birds (Shao et al., 2017).

1.2.2 Prevention

The most effective means to combat 'flu infection is by vaccination. Vaccines need to be administered annually before the season of influenza. No attempts at herd immunity levels of vaccination have been attempted. Instead, all those over 6 months who are at risk of developing severe or complicated influenza, are targeted for vaccination. The prioritised groups are (Baek et al., 2014):

- Elderly people aged 65 years or older
- People with chronic diseases, such as diabetes, cardiovascular disorders (except controlled hypertension).
- Those on immunosuppressive drugs
- Women (within 2 weeks after delivery)
- Healthcare workers (Baek et al., 2014).

According to the Centers for Disease Control and Prevention (CDC), getting the seasonal flu vaccinate would reduce the risk of getting the ‘flu by at least between 40% and 60% among the overall population when most circulating flu viruses are well-matched to the flu vaccine.

However, the efficacy of the vaccine is not guaranteed. Vaccine efficacy depends on the degree of antigenic resemblance between the virus circulating wild strain and the immunizing strains (Santak et al., 2013), the antibody response to vaccine, which is lowest in aged and in immunosuppressed patients and greatest in younger, healthy adults. Other important factors are the number of doses administered (in terms of generating partial or local herd immunity within a community) and the viral strains vaccinated in past years, which will influence the immunogenicity and effectiveness of current-season vaccination (DiazGranados et al., 2016, Ruggiero and Utili, 1992). The appearance of new strains requires new vaccines. Thus, one disadvantage of using vaccination is the gap between virus identification and the time to deployment of the vaccine. Influenza vaccines must be updated annually due to changes in the virus (Section 1.2.1), which involves a prediction of the likely virus (es) circulating in the following year. After virus identification follow vaccine manufacture (usually in eggs), testing and distribution of the influenza vaccine. The entire process takes 6-9 months.

There are several contributing factors that limit the efficacy of the virus. The long lead time of the production process means that the circulating strain(s) can change, and so partially (or wholly) escape the immune system's priming by vaccination. An issue that has recently come to light is that production of vaccine in chicken resulted in partial masking by a glycan of a key antigenic determinant in the vaccine from 2016–2017(Zost et al., 2017).

`

1.2.3 Treatment

1.2.3.1 Drug treatment overview

Due to the partial coverage of the seasonal ‘flu vaccine and the possibility that one day the vaccine will not have much efficacy against a major outbreak, drugs that prevent or mitigate ‘flu infection are an important target. Generally, there are two types of anti-influenza drugs, based on their mechanism of action. The first class are neuraminidase inhibitors such as Oseltamivir (Tamiflu) and Zanamivir. The second class are virus ion-channel blockers such as Amantadine and Rimantadine (Symetrel).

The effectiveness of Tamiflu has been questioned by Cohen (Cohen, 2014). Moreover, due to the virus strains changing from one season to next or even in the same season, drug resistance occurs. For example influenza viruses resistant to neuraminidase inhibitors arise through mutations in NA which can change the catalytic site of NA and thus reducing inhibitor, but not substrate binding (Colman et al., 1993). ‘Flu virus resistance to adamantines such as amantadine and rimantadine has increased substantially over the last few years (Bright et al., 2005). The frequency and distribution of M2 gene mutations in adamantane-resistant influenza variants circulated in the world between 1902 and 2013 and different HA -subtypes A viruses (H1– H17) was investigated. The results demonstrated that a high-level resistance to adamantanes was exhibited by H1, H3, H5, H7, H9, and H17 subtype influenza A viruses, associated with specific resistance-associated mutations in their M2 genes. However, a rarer resistance to adamantanes was found

in H2, H4, H6, H10, and H11 subtypes, whereas HA subtypes H8, H12–H16 didn't show any resistance to this class of drugs (Dong et al., 2015).

The resistance of virus to drugs and the questioned efficacy of Tamiflu (Sections 1.2.3.2 and 1.2.3.3) mean that there is a need for the development of new drugs (Rodewald et al., 2006). One type of new drug, peptides, one of which is the focus of this thesis are described in (Section 1.5.2.3)

1.2.3.2 Ion channel blocker and evidence for the lack of effectiveness

Until 2003, adamantines were highly active against all community isolates of influenza A virus (Deyde et al., 2007). This might be result of the increased use of amantadine that accompanied the spread of influenza A subtype H5N1 (influenza A/H5N1) virus. Now the majority of the influenza A virus subtypes, especially the most common H1N1 and H3N2 that circulate globally are resistant to adamantanes and so these are largely ineffective anti-influenza A virus drugs. The adamantanes mechanism of action is to inhibit the release of vRNP and so influenza A virus replication by binding to the M2 channel pore. This blocks proton conductance and so the pH decrease in the virus necessary for the dissociation of M1 protein from vRNP and the release of the latter into host cell cytoplasm does not occure (Ma et al., 2009). Influenza A virus resistant to adamantanes occurs either by amino acid mutations (L26F, V27A, A30T/V, S31N, G34E, and L38F) in M2 transmembrane domain that line the channel pore; mutation of V27, A30, and G34 lead to narrowing of the pore whereas the other three mutations (L26, S31, and L38), destabilize helix–helix assembly required for pore formation (Cady et al., 2010, AshaRani et al., 2009, Pielak et al., 2009).

`

1.2.3.3 Tamiflu and evidence of the lack of effectiveness

In 1999, the US Food and Drug Administration approved Oseltamivir (Tamiflu), a neuraminidase inhibitor for seasonal flu. The efficacy of the drug was established by meta-analysis, systematic reviews of a number of randomized controlled trials, which were funded and marketed by Roche (Gupta et al., 2015). Tamiflu was recommended by many organisations, such as the World Health Organization (WHO), the Centers for Disease Control and Prevention and the European Medicines Agency, for its prophylaxis of influenza. Consequently, it was stockpiled as a means to tide over 'flu crises, especially after swine influenza pandemic of 2009 (Gupta et al., 2015). Thus, since the first cases of H1N1 'flu, the drug was widely prescribed, and U.S. government spent more than $1.5 billion stockpiling Tamiflu since 2005, as part of their protective plan against 'flu pandemic (Lenzer, 2009).

Roche claimed that their drug reduced hospital admissions by 61% complications such as bronchitis, pneumonia, and sinusitis by 67%, and lower respiratory tract infections requiring antibiotics by 55% (Lenzer, 2009). Then some discrepancies were found, published in a study led by Chris Del Mar from the Cochrane team at Bond University in Australia. They re-examined the previous studies and re-analysed the data. They concluded that there was at best weak evidence that Tamiflu reduces complications, hospitalizations, or deaths, and any benefit offered by the drug was slight (Jefferson et al., 2014). There were asymptomatic reported cases of 'flu in a school in the UK at 2009, which led to 7 days prophylaxis of oseltamivir to all the children due to an order from the Health Protection Agency (HPA) (Gupta et al., 2015). The purpose was to reduce the risk of contact between the

asymptomatic patients and the rest of the children causing an outbreak. However, follow-up indicated that the drug didn't reduce the risk of transmission and infection (Toovey et al., 2008, Gupta et al., 2015). A cohort study in children in Japan demonstrated that oseltamivir intake was associated with events of abnormal behaviour and disturbance of consciousness and instance of deaths (Jefferson et al., 2012). Abnormal behaviour on the 1st day after drug intake were recognised in the studies by Roche. However, other data indicated that this was more serious, with over 50% increased risk of abnormal behaviour associated with oseltamivir and occurrence of unconsciousness in a number of patients on the 1st day after drug intake (Gupta et al., 2015). Therefore, Japan developed a package with a warning showing the dangerous effect of the drug to children and restricted the use of oseltamivir for adults (Muthuri et al., 2014). However, there was no evidence of increased risk of neuropsychiatric events in the Roche review of 2007 (Cohen, 2014). Nevertheless, label warning against rare adverse events, e.g., hallucination, self-injury, abnormal behaviour were updated due to the global accumulation of adverse events overseas oseltamivir (Gupta et al., 2015).

Thus, Tamiflu may not be effective and has serious side effects in children, one group who are particularly at risk from 'flu (Rudavsky, 2018). In addition, resistance to NA and M2 channel inhibitors has arisen rapidly. Therefore, new anti-influenza drugs remain a major priority.

`

1.3 Viral assays

1.3.1 Plaque assay

One of the most common viral assays, used to determine the virus titre or concentration of virus in a sample, is the plaque assay. Derived from work on bacteriophage, it was first adapted by Renato Dulbecco to make it suitable for animal virology in the late 1950s (Kevles, 1993).

The principle of the assay is that a monolayer of cells is infected with virus. Following a set time to allow viruses to bind to the cells, the excess is removed and an overlay of a semi-solid medium such as agarose is applied, which prevent viruses from diffusing across the cell monolayer and resulting secondary plaques. Virus bound to the susceptible cell delivers its genetic material and viral replication takes place within the cell nucleus. The virus infected cell will lyse and spread the infection to adjacent cells, where the infection-to-lysis cycle is repeated. Over a period of a days (depending on virus and cell type used) the area of lysed cells enlarges and upon staining of the cells with toluidine blue it becomes visible to the naked eye (Fig.2). Plaques are counted manually, and the results are used to determine the plaque forming units per sample unit volume (pfu/mL), which is the combination of the dilution factor used to prepare the plate and the plaque number. Based on the assumption that each plaque is due to one original infective virus particle, the pfu/mL is considered to represent the number of infective virus particles within the sample (Baek et al., 2014).

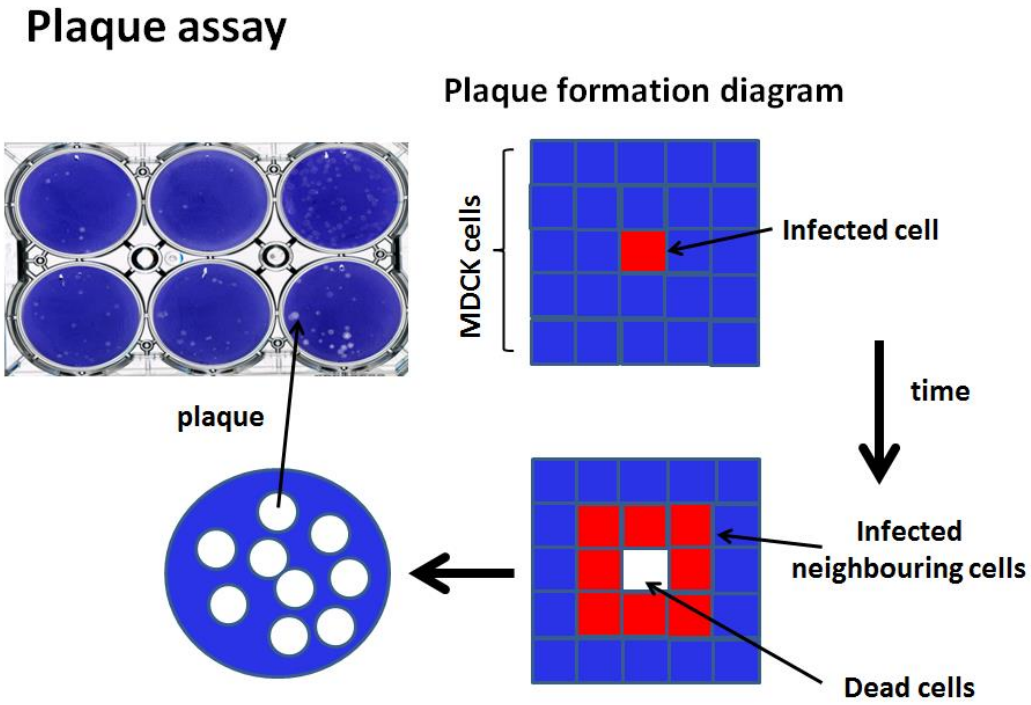

Fig. 2. Plaque forming mechanism in plaque assay

The plaque-forming unit (PFU) refers to a virus or group of viruses which cause a plaque and is one measure of virus quantity. The multiplicity of infection or MOI is the ratio of the infectious agents to infection targets (e.g., cells) is another measure. For example, the MOI of a group of cells inoculated with virus particles is the ratio of the number of virus particles to the number of target cells present.

The cell line used in this thesis, which is susceptible to influenza virus is MDCK (Madin-Darby canine kidney), which was derived in 1958 by Madin and Darby from a kidney of a normal cocker spaniel (Lugovtsev et al., 2013). The first evidence of the susceptibility of these cells to virus infection was published by Green (Green, 1962). Thereafter, the immunologic and cytogenetic properties of MDCK cells, as well as their susceptibility to several viruses were characterised by Gaush and co-workers (Gaush et al., 1966). Thus, the MDCK cell line is a widely

used in influenza virus research (Audsley and Tannock, 2004) and cell lines derived from upper respiratory tract are used less frequently. The reasons for this are not clear, but may relate to theneed to transform human primary cells to immortalise them, which is usually accomplished with retroviral genes. This may alter the antiviral response of the cells. In addition, changing established practice requires considerable benchmarking. Moreover, there other data demonstrating the utility of this cell line in influenza virus research. For example, MDCK cells have been used to select influenza vaccine strain candidates as a platform for vaccine development, since the original antigenic properties of a strain are maintained during the propagation process in MDCK cells (Katz et al., 1990, Saito et al., 2004).

1.4 nanoparticles

Nanoparticles are particles between 1 and 1000 nanometres in diameter, but as probes in biology diameters of 100 nm or less are usually considered, as this is in the size range of biological macromolecules (Kreuter, 2007). There are many nanomaterials, but for as labels in biology, the electronic and optical properties of noble metal and of semiconductor quantum dot nanoparticles make these the most appealing, because the optical techniques for their detection are standard in biological laboratories.

1.4.1 Quantum dots (QDS)

Quantum dots are usually between 2 - 10 nm in diameter and are fluorescent. Their emission can be easily tuned to cover from the blue to the red with increasing nanoparticle size. This is because quantum dots, semiconductor nanoparticles such as (CdSe), show a strong restriction of excited electrons and holes, which leads to

significantly different optical and electronic properties compared to bulk CdSe (Qu and Peng, 2002). Quantum dots have other unique optical and electronic properties, giving them many advantages over conventional fluorophores, such as organic dyes, fluorescent proteins and lanthanide chelates (Wang et al., 2006). These properties include the width of the excitation spectrum, the width of the emission spectrum, photostability, and the decay lifetime. Normal dyes suffer from narrow excitation spectrum; therefore, they require excitation by light at a certain wavelength, which is variable among different dyes. Quantum dots have a wide absorption spectrum so they can be excited by a wide range of wavelengths, a characteristic which may be used to excite many different coloured QDs at the same time using a single wavelength (Han et al., 2001)

Because of the small size of QDs, their electrons are restricted in a small space when the radius of the semiconductor nanocrystal is smaller than the exciton Bohr radius (this is the average distance between the electron in the conduction band and the hole it leaves behind in the valence band) (Shaalan et al., 2016). There is quantization of the energy levels according to Pauli's exclusion principle, which is the principle that two identical fermions, e.g., electrons, cannot occupy the same quantum state in a body such as an atom (Reimann and Manninen, 2002, Bawendi et al., 1990). Overall, as the size of the crystal reduces, the difference in energy between the highest valence band and the lowest conduction band increases. Additional energy is then required to promote the electron to the conduction band, and so, additional energy is released when the crystal returns to its ground state, resulting in a colour shift from red to blue in the emitted light. As a result of this phenomenon, quantum dots can send out any colour of light from the same material

by changing the quantum dot. Thus, due to the high level of control possible over the size of the nanocrystals produced, quantum dots can be tuned during manufacturing to emit any colour of light (Yoffe, 2001).

1.4.2 Gold nanoparticles AuNPs

Gold is likely one of the first metals to have been discovered, since it exists as a metal rather than an oxide(Materials, 2012). Historically, Chinese, Arabian, and Indian cultures managed to produce colloidal gold and utilized it for medicinal purposes (Chinese "golden solution" and Indian "liquid gold") (Dykman and Khlebtsov, 2011). Francisco Antonii, a philosopher and doctor of medicine, published what is considered to be the first book on colloidal gold in 1618 (Dykman and Khlebtsov, 2011). The use of gold nanoparticles in biology started in 1971 when Faulk and Taylor described a method of antibody conjugation with colloidal gold for direct electron microscopy visualization of the surface antigens of salmonellae (Faulk and Taylor, 1971). This pioneering work led to the adoption of immunogold electron microscopy as a means to identify at molecular scale resolution the location of specific macromolecules in cells. Since, they have a large surface to volume ratio, AuNPs possess strong size-dependent properties. The electronic and optical properties of these metal nanoparticles give rise to local surface plasmon resonance (LSPR)((Crespilho et al., 2009), (Endo et al., 2007), surface-enhanced Raman scattering (SERS) (Zou et al., 2015), and surface-enhanced fluorescence (SEF) (Rosi et al., 2006).

`

1.4.3 Optical properties of gold nanoparticles: scattering and absorption nanolabels

Noble metal nanoparticles have historically been of great interest throughout the ages due to their optical properties (Heiligtag and Niederberger, 2013). These properties have made them useful for optical and plasmonic detection techniques, due to their strong interaction with light. Gold nanoparticles have been the subject of much research, and there is very good control of their size and shape during their manufacture (Robertson et al., 2016). The importance of such synthetic capabilities are that the diameter and shape of the nanoparticles affects greatly the optical properties they exhibit. For example, spherical gold nanoparticles of diameter ~ 10 nm possess a clear single plasmon band at 520 nm (He et al., 2005).

The surface plasmon resonance absorption peak moves towards the infra-red (IR) portion of the spectrum and most visible wavelengths are reflected, giving the nanoparticles clear or translucent color, as the particle size is increased toward the limit of bulk gold (Juve et al., 2013). In contrast, the optical properties of nanorods depend on both their size and aspect ratio (Smitha et al., 2013). This is because they possess two plasmon absorption bands; a longitudinal localized surface plasmon resonance (longitudinal LSPR) band located in a longer wavelength region, which can be tuned by varying the aspect ratio of the nanorods from the visible to the near-IR region and a transverse localized surface plasmon resonance (transverse LSPR) band located in the visible region around 520 nm (Jayabal et al., 2015).

When any object is exposed to light this may be absorbed or scattered. With gold nanoparticles these processes are due to the interaction of their free electrons with photons. When gold nanoparticles are exposed to light, the electrical field of the

light causes the collective oscillation of the conduction electrons at the surface of the particle with respect to the core of the nanoparticle (Venkatesh and Prasad, 1983). The oscillation of these electrons relative to atomic lattice is due to the displacement of the electron cloud relative to the nuclei and a restoring force from Coulomb attraction between electrons and nuclei. The consequence is the collective oscillation of the electrons. There are four factors that determine the oscillation frequency: the electron mass, the density of electrons and the shape and size of the charge distribution i.e., the size and shape of the nanoparticle. This explains, for example, why gold nanorods have two plasmon resonances, one corresponding to oscillations along the long axis and the second to the oscillations along the short axis (Zhu et al., 2005, Jain et al., 2006, Sokolov et al., 2003).

Early techniques for the optical detection of single particles relied on the scattering of light with labels such as plastic beads (μm in diameter) and then large (> 40 nm) gold nanoparticles (Kusumi et al., 1993). The use of scattering labels in single molecule analysis resulted in new insights into the organisation and dynamics of molecular systems, particularly those at the cell surface, where labelling was easier. An example of early work is the tracking latex bead labelled alpha-amino-3-hydroxy-5-methyl-4-isoxazole propionic acid (AMPA) receptors - glutamate receptors in the central nervous system) on neurites of cultured neuronal cells (Borgdorff and Choquet, 2002). In the case of scattering nanoparticles, the interaction of the particles with light waves, known as Rayleigh scattering, occurs when the electromagnetic waves in light are scattered by particles with diameters much smaller than the wavelength of the light (Turzhitsky et al., 2014). With noble metals such as gold, the free electrons are called plasmons and so their oscillation

local surface plasmon resonance, The surface plasmon absorption, scattering and total extinction efficiencies are described by Mie theory (Haiss et al., 2007). For spherical nanoparticles, scattering scales to the sixth power of the radius (r^6) while absorption scales to the volume (r^3) (Madjet et al., 1995). When the diameter of gold nanoparticles is ≥40, the scattering starts to dominate. The absorption of light in the blue-green portion of the spectrum (~520 nm for ~10 nm diameter gold nanoparticles) and reflection of red light (~700 nm) produces a rich red colour for nanoparticles of diameter ~ 10 nm (Fig. 4). There are factors other than nanoparticle size that affect the wavelength of which plasmon resonance occurs (Nehl and Hafner, 2008). One is the local environment, which includes the solvent and molecules adsorbed to the nanoparticle surface.

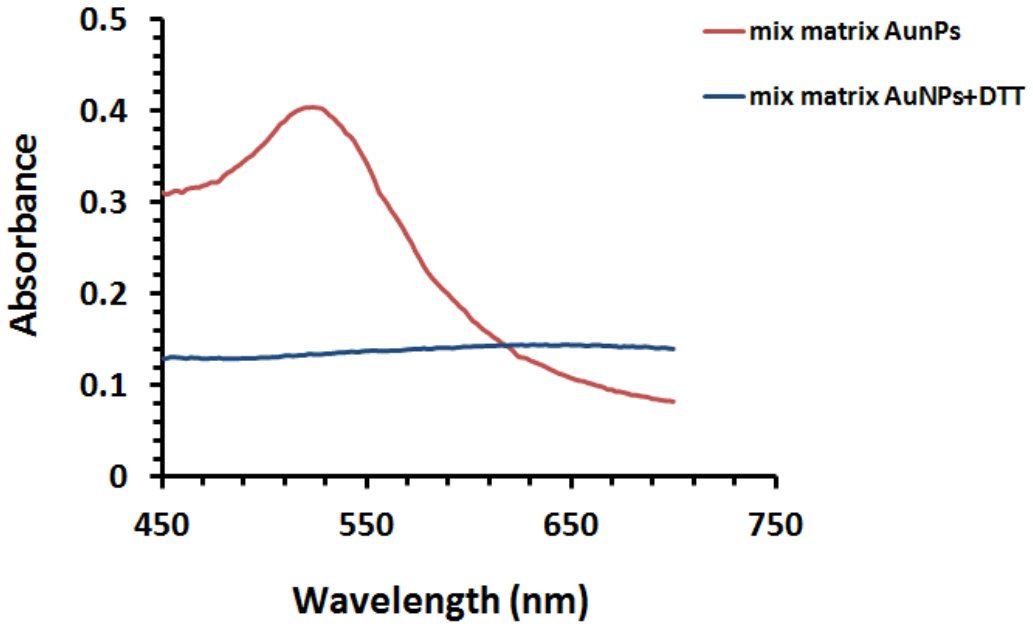

Fig. 4. AuNPs maximum absorption peak before and after aggregation. Mix matrix AuNPs are gold nanoparticles of diameter 8.8 nm with a mix matrix ligand shell (Section 2.3.1). Mix matrix AuNPs + DTT are the same gold nanoparticles aggregated after prolonged treatment with DTT in the presence of electrolytes (Sections 2.6.1 and 2.9.1).

The wavelength of surface plasmon resonance related absorption shifts to longer, redder wavelengths as particle size increases. At the limit, when the nanoparticles aggregate, the spectrum become featureless (Fig. 4).

Silver, a noble metal like gold has entirely analogous optical properties. However, silver nanoparticles have a stronger absorbance and scattering than gold nanoparticles, and they are also strong enhancers of Raman scattering. There is a long-standing use of silver and more recently silver nanoparticles in health fields, due to their antimicrobial properties. These they are drawing increasing attention for potential prevention of bacterial/fungal and viral infection, in part due to growing antibiotic resistance (Franci et al., 2015).

1.4.4 Synthesis of gold nanoparticles:

Gold nanoparticles are usually synthesised by the reduction of the metal salt for example by citrate (equations 1 and 2). Other common reductants include $NaBH_4$, aldehydes, which include biological compounds such as glucose. It is known that $HAuCl_4$ can be hydrolyzed to various gold complexes (Zhao et al., 2012) in a manner that is dependent on the pH of the reaction solution, as shown in equation (1). After the addition of the reducing agent, both hydroxyl groups and chloride ions will be released upon reduction of the gold precursors, as shown in equation (2). Growth of nanoparticles is by nucleation of Au^0 and accretion of further atoms on the nucleus. Binding of ligands such as citrate, the starting concentration of Au^+ and reductant will determine the size of the nanoparticle product.

$$HAuCl_4 + n\ H_2O \rightleftharpoons AuCl_{4-n}OH^- + (n+1)\ H^+ + n\ Cl^- \quad \ldots\ldots(1)$$

$$AuCl_{(4-n)}OH_n \longrightarrow Au_{(particle)} + (4-n)\ Cl^- + n\ OH^- \quad \ldots\ldots(2)$$

For nanoparticles of diameter ≥ 20 nm small nanoparticles are synthesised and used as seeds in a subsequent reaction.

1.4.5 Silver nanoparticles

Silver is a noble metal and nanoparticles of silver (AgNPs) have similar properties to gold nanoparticles. Thus, their conduction electrons react to photons in much the same way. However, they are stronger scatterers and absorbers of light than gold nanoparticles (Haiss et al., 2007), (Paramelle et al., 2014). Silver nanoparticles of diameter ~10 nm with a mix matrix ligand shell (Section 2.3.1) have a plasmon peak at ~ 410 nm, which is narrower than that of gold (Fig. 5 for silver, Fig. 4 for gold). The position of this peak is dependent on the nanoparticle size and shifts towards the red as the silver nanoparticles get larger; when they aggregate the nanoparticle become electronically coupled and the spectrum becomes featureless (Fig. 5). The plasmon absorption of silver nanoparticles is more sensitive to the immediate environment that corresponding gold ones. For example, without a ligand shell, the silver nanoparticles in Fig. 5 have a plasmon peak at ~395 nm, indicating that the self-assembled monolayer of the ligand shell shifts the plasmon band by ~ 15 nm. The corresponding shift for gold nanoparticles is less than 2 nm (Levy et al., 2004).

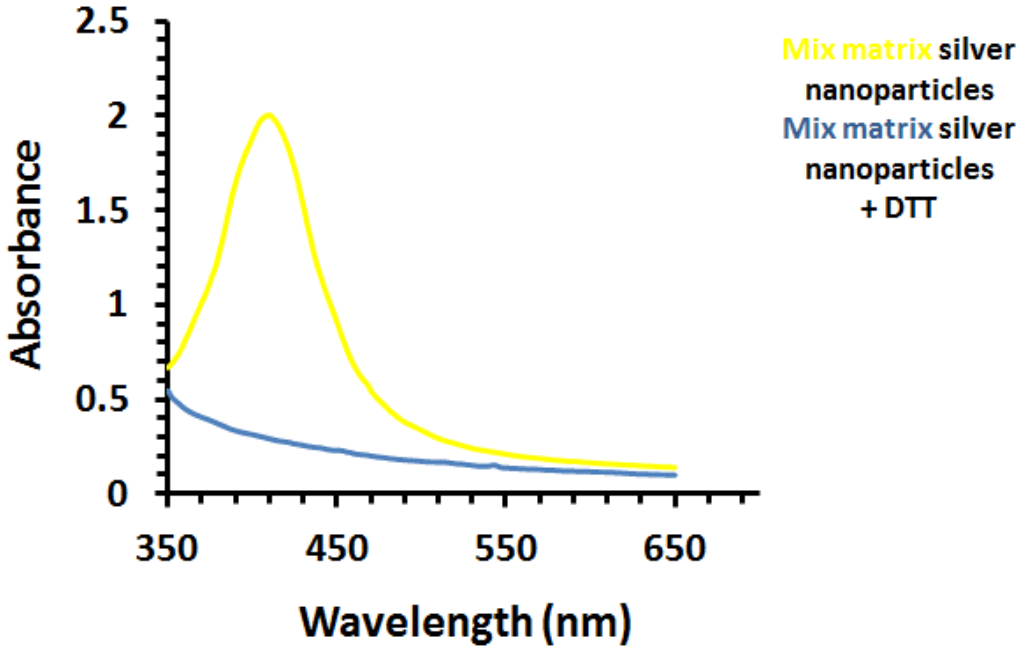

Fig. 5. AgNPs maximum absorption peak before and after aggregation. Mix matrix AgNPs are silver nanoparticles of diameter 8.8 nm with a mix matrix ligand shell (Section 2.3.1). Mix matrix AgNPs + DTT are the same silver nanoparticles aggregated after prolonged treatment with DTT (Sections 2.6.1 and 2.9.1).

In contrast to gold, silver ions inhibit a range of microorganisms, including pathogenic ones. Indeed, silver nitrate has long been used clinically to prevent the infection of wounds, though more recently this has been questioned (Storm-Versloot et al., 2010), and, as the authors of this Cochrane review point out, clinical data in the area is of poor quality. In any event, the historical association of silver ions and anti-microbial activity, which is experimentally demonstrable, has led to an interest in developing silver nanoparticles as slow release agents for silver ions at sites of infection (Wang et al., 2016). The increasing resistance of pathogenic microorganisms to drugs has fuelled this interest.

Silver ions have a strong bacteriostatic action; that is they halt bacterial growth (Slawson et al., 1992, Spadaro et al., 1974), and though there are documented cases of resistant bacterial strains, these remain rare (Pooley, 1982, Klaus et al., 1999). The slow release of silver ions by nanoparticles in the context of inhibition of bacterial growth was demonstrated with E. coli grown in Luria–Bertani (LB) medium on solid agar plates. Addition of different concentrations of silver nanoparticles and lysis of the bacteria was evidenced by scanning and transmission electron microscopy (SEM and TEM), which showed that the E. coli cells were damaged. This was due to the formation of "pits" in the cell wall of the bacteria, resulting in an increasing permeability of the cell wall and cell death. The silver nanoparticles were found to accumulate in the bacterial membrane. Such experiments have led to the idea that silver nanoparticles may be suitable for the formulation of new types of bactericidal nanomaterials (Sondi and Salopek-Sondi, 2004).

Silver nanoparticles, presumably through the release of silver ions have also been shown to exert showed potent anti-fungal activity against clinical isolates and ATCC strains of *Trichophyton mentagrophytes* and *Candida species* at concentrations of 1–7 μg/mL *in vitro*, which was comparable to that of amphotericin B, but superior to that of fluconazole (amphotericin B IC80, 1-5 μg/ml; fluconazole IC80, 10- 30 μg/ml) (Kim et al., 2008). While high, such concentrations are attainable topically.

Silver nanoparticle have also been shown to possess inhibitory activity towards a range of unrelated human viruses in a variety of model systems. AgNPs effectively inhibited Herpesviridae and Paramyxoviridae viruses in Vero cells (Gaikwad et al.,

2013). The antiviral activity of silver nanoparticles against hepatitis B virus was measured by incubating 5-50 µM ~10 nm AgNPs with hepatoblastoma cells, which secrete HBV-like particles containing hepatitis B virus DNA into the medium (Ladner et al., 1997). After 48 h incubation, total DNA was extracted and HBV DNA was quantified by real-time PCR, and the AgNPs were shown to the level of inhibit hepatitis B virus DNA in the medium by 38% at 5 µM and 80% at 50 µM (Lu et al., 2008). Similarly, in a model of HIV-1 infectivity using Hut/CCR5 cells AgNPs were shown, after 3 days infection, to reduce in a dose-dependent manner the in inhibiting HIV-1 replication with 50 µM AgNPs causing a 98% inhibition. (Sun et al., 2005).

Silver nanoparticles have also been shown to inhibit the infectivity of H1N1 influenza A virus (Li et al., 2016). To determine the inhibitory activity of silver nanoparticles on H1N1 influenza A virus, the embryo inoculation assay and MDCK cells were used as the infection model. Electron microscopy analysis and flow cytometry assays demonstrated that silver nanoparticles reduced H1N1 influenza A virus activity. (Xiang et al., 2011),

1.4.6 Ligand shells

Noble metal nanoparticles, as synthesised, are generally not useful in biology. These bare metal nanoparticles are not colloidally stable and will aggregate in physiological concentrations of electrolytes (Moore et al., 2015). Moreover, the surface of AuNPs and AgNPs bind groups found in biological molecules: thiols, amines and carbonyls (Sainsbury et al., 2007). Thus, though gold is considered to be relatively non-reactive, it will bind non-specifically to with proteins, polysaccharides and DNA/RNA and silver nanoparticles likewise. Consequently,

the surface of the noble metal nanoparticles needs to be protected. What follows is focussed on gold nanoparticles, since the most work has been done on these, though the same principles apply to silver nanoparticles.

Stabilization of metal nanoparticles has different meanings, dependent on the context. Stability from a physical perspective means that the nanoparticle maintains its integrity as a nanoparticle colloidal solution and the material does not change chemically. From a biological point of view there are additional features, which are that the nanoparticles remain soluble and dispersed in physiological environments, having low to not detectable non-specific binding to biological macromolecules. This may be achieved by means of a passivating shell, which is the coating of the metal surface. There are different strategies for the passivation nanoparticles, which include (Kim et al., 2015, Li et al., 2013, Gajan et al., 2009, Nune et al., 2009):

- Silica
- Layer-by-layer (LBL)
- Polymers
- Self-assembled monolayer (SAM)

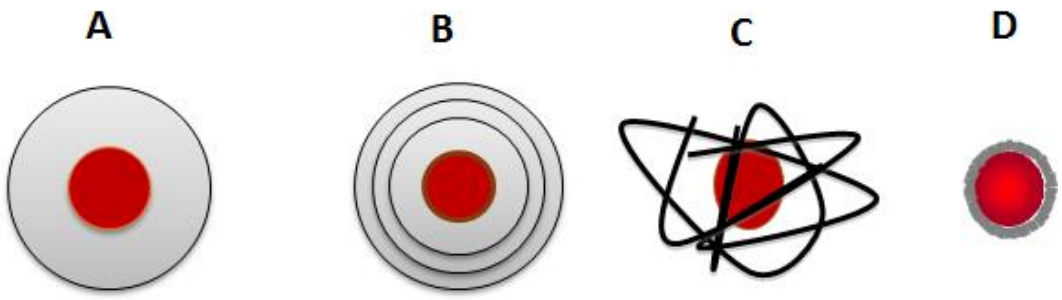

Fig 6. Diagram to show the results of the four different passivation strategies. Nanoparticle and passivation layer roughly to scale for a ~10 nm diameter nanoparticle. A. silica shell, B. LBL shell .C. polymer. D. SAM.

`

1.4.6.1 Silica passivation of nanoparticles

One approach to passivation is the deposition of a homogeneous shell of an inorganic material, such as silica. This achieves colloidal stabilization and generates what is called core–shell geometry (Liz-Marzan et al., 1996). Silica shells not only provides greatly enhanced colloidal stability in water, but also can be used to determine the distance between core particles within assemblies by controlling the shell thickness (Ung et al., 1998). Three steps have used in to make silica encapsulated nanoparticles: (1) By using silane coupling agents such as silicon alkoxides with an amino or thiol group as surface primer, modification of the metal nanoparticle surface to make it vitreophilic; (2) slow silica deposition in water from a sodium silicate solution, and (3) extensive growth of the silica shells through sol–gel reaction using silicon alkoxide in ethanol/ammonia mixtures (Ung et al., 1998).

One obvious drawback of the silica shell for biology is that it makes the nanoparticle a lot larger (Fig. 6A). This goes against the idea of using a small nanoparticle in the first place and may cause problems due to the large hydrodynamic radius of the silica covered nanoparticle preventing this accessing all parts of the biological system. In addition, the silica shell does not impart stability that is suitable for the direct use in cell biology, because biological molecules bind silica and some means of functionalization is required, a layer of polymer is often attached to the silica shell. This will make the nanoparticle even larger. So silica core-shell nanoparticles have important drawbacks in terms of their use in biology.

`

1.4.6.2 The layer by layer (LBL) passivation of nanoparticles

The LBL approach generates another kind of ligand shell to protect metal nanoparticles. This involves coating of nanoparticles with successive layers of polyelectrolytes of opposing charges, which assemble into a layered structure. The ability to control the deposition and achieve a uniform layer of polyelectrolytes with nanometre thick precision is one a feature of electrostatically driven LBL assembly. The LBL approach provides a general route to tailor the general characteristic of nanoparticles, because polyelectrolytes readily adsorb onto different surfaces and can be modified or reacted to incorporate different functional groups. Furthermore, the outer polyelectrolyte provides colloidal stability to the nanoparticles by giving well defined surface charge to the nanoparticles. However, this surface charge will attract biological molecules of the opposite charge, so leading to a specific binding. In addition, there will be several layers, so the nanoparticle hydrodynamic radius will be increased (Fig. 6B). Finally, the polyelectrolytes do not form a complete physical barrier, so biological molecules may penetrate to a greater or lesser extent into the layers.

1.4.6.3 Polymer passivation of nanoparticles

Polymers are another commonly used ligand shell. Generally polymers with one or more functional groups (particularly thiols) that bind to gold are used. These can displace existing ligands, which includes thiol ligands if the polymer is at high enough concentration and/or possesses multiple thiols (Lu et al., 2002). Polymers can also be used to attach biological molecules using other functional groups present, such as amines or carboxylic acids. Polymers that have been used include

mercapto polyethylene glycol and mercapto dextans (Costanzo and Beyer, 2007), Polymer ligand shells have some disadvantages. As with the silica and LBL approaches, they increase the hydrodynamic radius of the nanoparticle considerably (Fig. 6C). In addition, like the LBL system, the polymer shell is not a physical barrier that is biological molecules can penetrate it and either take up residence (changing the biological functionality of the nanoparticle) or access the underlying gold surface and exchange for the polymer. This could ultimately destroy the polymer ligand shell.

1.4.6.4 Self-assembled monolayer (SAM) passivation of nanoparticles

Self-assemble monolayers (SAMs) are another strategy used to protect AuNPs. SAMs ensure the passivation keeps the hydrodynamic radius of the nanoparticle to a minimum, since the ligands that make up the monolayer are short (Fig. 6D), There are many examples of self-assembling ligand shells, including PEGylated alkanethiols and peptides. All of them follow the same design principal, they start with a thiol group for bonding to the metal, a hydrophobic core, allowing packing of the monolayer, and a hydrophilic terminus exposed to solvent to enable solubility in physiological environments. They give excellent solubility to the metal nanoparticle. For example, PEGylated alkanethiols and peptides, such as CALNN, have been found to protect gold and silver nanoparticles from aggregation by electrolyte induced aggregation and also to protect silver from oxidation in water containing electrolytes (Levy et al., 2004a, Doty et al., 2005). Moreover, SAMs formed from peptides only impose a small increase in nanoparticles hydrodynamic radius (Octeau et al., 2009)

Functionalisation of SAM protected nanoparticles can be achieved through a group that is exposed to solvent or, in some systems, by the incorporation of a ligand with a functional group exposed to solvent. In addition, it is possible to control the valency of functionalisation. Thus, the CALNN pentapeptide ligand system was shown to allow a simple means for producing nanoparticles carrying a single biomolecular recognition function (Levy, 2006). In these experiments a ligand shell of the peptide CALNN was assembled on 6 nm diameter AuNPs. Functionalisation of the nanoparticles was achieved by incorporating into the initial ligand solution a a functional ligand (CALNNGHHHHHHGK$_{biotin}$G) as a mole % of the CALNN ligand. The functional ligand had the same initial five amino acids, to ensure it packed into the SAM similarly to the matrix CALNN peptides and towards its C-terminus a hexahistidine sequence. The latter would allow separation of functionalised from non-functionalised nanoparticles by immobilised metal ion affinity chromatography, using a standard nitrilotriacetic acid-Ni^{2+} column. The C-terminal biotin provided a further means of detection and separation. Following purification of the nanoparticles from excess ligand by size-exclusion chromatography (Levy et al., 2004b) the binding and elution of functionalised nanoparticles form the nickel affinity column was demonstrated. Moreover, it was shown that the fraction of bound, so functionalised nanoparticles, depended on the mole % of the peptide CALNNGHHHHHHGK$_{biotin}$G in the initial ligand mixture. Thus incorporation of the functional ligand was random, dependent only on its relative concentration. This allowed the analysis of populations of functionalised nanoparticles and the partial separation of ones bearing 1, 2 or more functional ligands. The relative proportions of nanoparticles in these different fractions

corresponded reasonably to that expected from random incorporation of ligands into the self-assembled monolayer. Thus, the assumption that the probability P_f of reaction of a functional peptide with a gold NP is simply equal to the molar ratio of functional versus matrix peptide present in solution and does not change during the capping process holds. A consequence is that for small values of P_f, the proportion of labelled NPs tends to zero, but essentially all labelled NPs have exactly one label and in practical terms when 10 % of the nanoparticles are functionalised, so bind to the affinity column, ~95% of these will carry just one functional ligand, and the remaining 5% two or more (Levy at al 2005, Figure 2A).

There are, however, drawbacks to both peptide and PEGylated alkane thiol ligands. The peptide SAMs carry a high negative charge, due to the C-terminal carboxylic acid group that is exposed to solvent. This results in binding positively charged molecules (Duchesne et al., 2008a), which are abundant in biological systems, e.g., any protein with a basic isoelectric point or which possesses an uneven charge distribution on its surface. In addition, the peptide ligands are not stable when challenged by small thiol-containing molecules. That is, they undergo ligand exchange, where the thiol in solution replaces the peptides on the surface of the nanoparticle and this includes cysteine, which is present at ~ mM concentrations in cell culture medium (Chen et al., 2012, Duchesne et al., 2008a). Both the non specific interactions of the nanoparticles and ligand exchange must be prevented, because these can lead to a change and/or loss of the functionality of the nanoparticle. Whereas SAMSs formed from PEGylated alkane thiol ligands do not suffer from these disadvantages, they are more limited in their capacity for functionalisation. With peptide ligands, extension of the amino acid sequence at the

C-terminus and/or incorporation of particular functional groups such as biotin is part of the options available during commercial peptide synthesis. In contrast PEGylated alkane thiol ligands are available with a limited number of functional groups, generally requiring synthetic chemistry to attach a biological function. Moreover, it was found that addition of a very small mole % of peptide ligands did not give rise to the stoichiolmetric incorporation of these into a PEGylated alkane thiol ligand shell (Duchesne et al., 2008a). This may be due to the preference of the alkane for packing against alkanes, to the exclusion of the peptide ligand.

1.4.6.5 The 'mix matrix' SAM ligand shell

To overcome these drawbacks, a ligand shell of thiolated pentapeptidols and alkane thiol ethylene glycol, was designed and called a 'mix matrix', as it is composed of two different ligands, typically 70% (mole/mole) of the peptidol H-CVVVT-ol and 30 % (mole/mole) of the ethylene glycol–terminated alkane thiol HS-C_{11}-EG_4 (Duchesne et al., 2008) Fig. 7A.

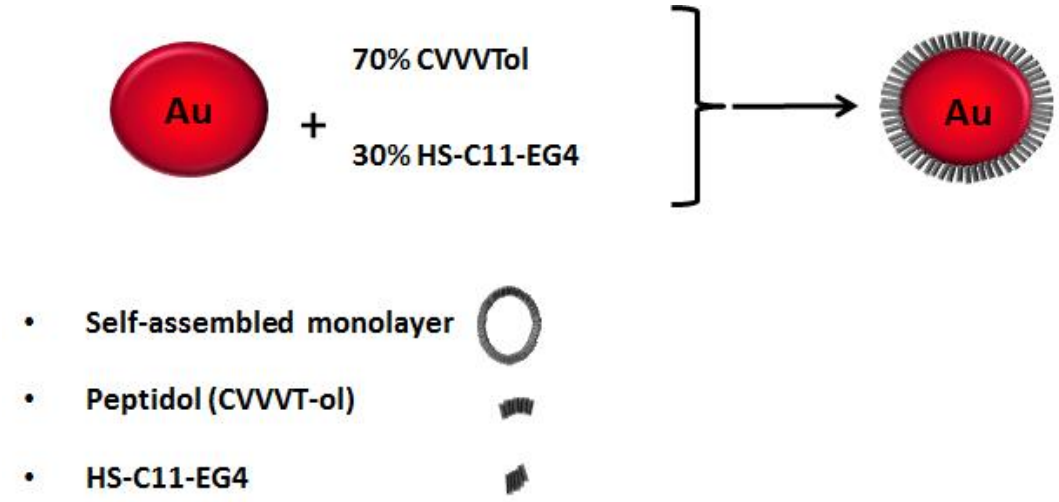

Fig. 7. Diagram of gold nanoparticle passivation with the mix matrix ligands. The pentapeptidol (darker ligand) and alkane thiol ethylene glycol (lighter ligand) are shown. The organisation, if any, of the two ligands on the surface is unknown.

The thiol groups (HS on the cysteine of the peptidol and –SH on the alkane thiol ethylene glycol) have a high affinity for gold and silver, and the N-terminal amino group of the cysteine provides for a further interaction. The central section of both ligands is hydrophobic and will, in aqueous solutions, pack together, which drives self-assembly. The C-terminal hydroxyl of the peptidol is hydrophilic and aids solubility, but is insufficient to prevent aggregation; the four terminal ethylene glycol units are highly mobile and they provide both hydrophilicity and steric repulsion, which prevents aggregation (Duchesne et al., 2008a)(Duchesne et al 2008). Mix-matrix capping ligands have been shown to provide both gold and silver nanoparticles with excellent solubility, stability to electrolyte- induced aggregation, resistance to nonspecific binding to biological molecules, ligand exchange with

small thiols such as dithiothreitol (Duchesne et al., 2008a, Chen et al., 2012, Duchesne et al., 2012), and to degradation by cyanide (Free et al., 2012).

By having both the peptidol and alkane thiol ethyleneglycol ligands in the SAM, it is then possible to include one or both types of ligand carrying a functional group and these are now incorporated stoichiometrically into the ligand shell, that is according to their mole % in the initial ligand mixture (Section 1.4.6.4) (Fig 7 B).

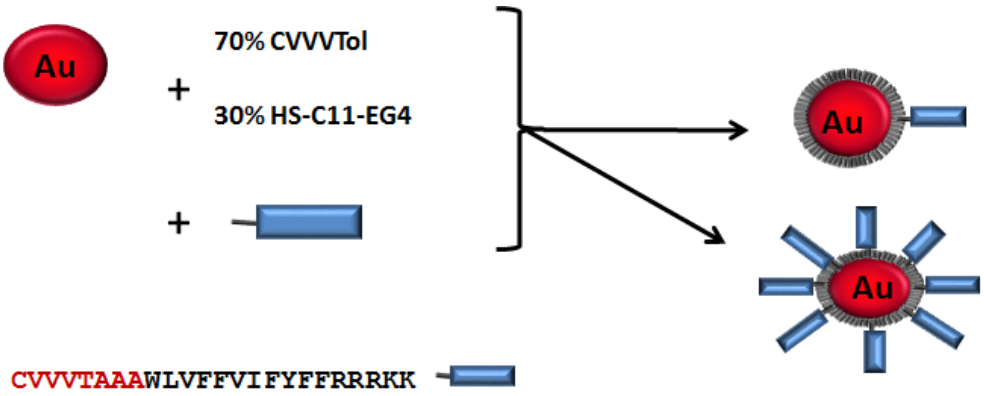

Fig. 7. Gold nanoparticles passivation and functionalisation. B Principle of functionalisation of gold nanoparticles using different mole% of the functional ligand (shown here is FluPep ligand, Section 2.3) to produce nanoparticles with different grafting densities of the functional ligand.

Thus the mix matrix SAM ligand shell is easily functionalised by the incorporation of a ligand with an extension. Mix matrix ligand shells have been functionalised using ligands possessing affinity tags (Duchesne et al., 2008a), such as tris nitriloacetic acid to enable stoichiometric conjugation to proteins with a hexahistidine tag (Duchesne et al., 2012). This approach has been used to increase the efficacy of loading nanoparticles into a protein cage containing hexahistidine tags (Paramelle et al., 2016). In addition, using the same principle, selective

chemical conjugation of proteins and oligosaccharides has been achieved by first functionalising the nanoparticles with an azide. This was then converted to a thiol to react with maleimide-functionalised oligosaccharides or to a maleimide to react with a single accessible cysteine side chain on the surface of a protein (Nieves et al., 2015).

Thus, the SAM formed by the mix matrix allows good stabilisation of noble metal nanoparticles, only causes a small increase in the nanoparticle hydrodynamic volume. Importantly, for the purposes of this thesis, the mix matrix ligand shell can easily be functionalised with peptide ligands with some control over the stoichiometry of functionalisation. For these reasons, this will be the system that will be explored first to determine whether it may be functionalised with peptides that inhibit 'flu virus infectivity.

1.5 Antiviral peptides

1.5.1 Examples of antiviral proteins and peptides

Peptide-based drugs are becoming established as viable therapeutics after the successful use of Enfuvirtidie against HIV. This is the first peptide-based antiviral drug approved by the Food and Drug Administration (USA) (Cooper and Lange, 2004). Peptide-based drugs potentially offer many advantages, as they are biologics, so can carry in their structure a lot of information relating to selectivity and specificity of their targets, so they might have fewer off target effects than small molecules. Production can be scaled and is cheaper than protein biologics. Moreover, aspects of their pharmacodynamics, to their lifetime in the body can be tuned. Thus, peptides will be rapidly cleared from the circulation and degraded *in*

vivo to amino acids (a non-toxic end product), whereas the incorporation of D-amino acids and/or alternative linkages to peptide bonds, e.g., isopeptide bond, will prolong their lifetime *in vivo* (Skalickova et al., 2015b).

The antiviral peptides target different aspects of the virus replicative cycle: (i) entry blocker peptides, which inhibit viral attachment and virus-cell membrane fusion; (ii) viral envelope targeting peptides, which disrupt the viral envelope; (iii) viral polymerase peptides, which inhibit replication of influenza virus by interacting with viral polymerase (Skalickova et al., 2015b).

Several viral diseases have been treated successfully with antiviral peptides including HIV. The infection with human immunodeficiency virus (HIV) results in CD4+ T cell depletion and the subsequent loss of immune function, which eventually leads to death from AIDS. It has been demonstrated that some peptides inhibit the fusion of the HIV virus. Thus, the membrane-associated and secreted C46 peptides efficiently block infection of cells by interfering with the function of HIV-1 gp41. Peptides derived from the heptad repeat 2 (HR2) region of the HIV fusogenic protein gp41 are also potent inhibitors of viral infection, and one of them, called enfuvirtide, is now used for the treatment of therapy-experienced AIDS patients. An understanding of the mechanism of these peptides, which interfere with the virus cell fusion pathway has allowed the design of more potent peptide inhibitors by means of increasing the affinity of the peptide for the intermediate form of the viral protein involved in fusion (Lee et al., 2014),(Pessi et al., 2009).

It was shown that bovine and human lactoferrin (LF) specifically inhibited hepatitis C virus (HCV) infection in cultured non-neoplastic human hepatocyte-derived

PH5CH8 (Abe et al., 2007a). Moreover, it was also demonstrated that the main contributing factor to prevent of hepatitis C virus HCV infection, is the interaction of lactoferrin (LF) and the envelop 2 (E2) protein. Only part of lactoferrin is required for this activity. (Abe et al., 2007b). LF and a peptide derived from it have been shown also to inhibit herpes simplex HSV. A different peptide, from the lactoferrin N-terminal domain, has a high potency anti HSV peptide, blocking viral entry and stimulating the immune system. Interestingly, Lf synergises with acyclovir (ACV), is a potent inhibitor of HSV replication and is an apparent inactivator of the HSV DNA polymerase. Other researchers have targeted the requirement of HYSV to bind to heparan sulfate. They introduced a protease resistant arginine-rich peptide, called DG2 containing D-amino acids. DG2 is stable with respect to proteases, inhibits HSV-1 entry into cells and blocks all aspects of infection (Jenssen, 2005),(Jaishankar et al., 2015).

1.5.2 Peptides inhibiting influenza virus

There are a number of macromolecules and peptides shown to inhibit influenza virus. Some have been discovered through a process of structure-led screening and design. Others have been fortuitous discoveries.

1.5.2.1 Macromolecular inhibitors of influenza virus infectivity

Because HA binding to sialic acid is the first step in virus entry, blocking this interaction is considered to be a promising therapeutic route (Guo et al., 2002, Matrosovich and Klenk, 2003). Indeed, studies since the late 1940s have demonstrated that a variety of sialic acid-containing molecules isolated from different natural sources, ranging from serum, urine and meconium to egg white

and edible bird nests are inhibitors of influenza viruses (Krizanova and Rathova, 1969). Many sialic acid-containing polymers have been developed such as sialyloligosaccharides containing poly L-glutamic acid backbones, sialic acid-conjugated dendritic polymers and sialyllactose-carrying polystyrene (Reuter et al., 1999, Totani et al., 2003, Tsuchida et al., 1998). HA interaction with sialylglycoconjugates is also the target for a peptide identified by random library selection for sialic acid mimetics (Matsubara et al., 2010).

LF (Section 1.5.1) interacts not only with the viral influenza viral envelope, but also with viral haemagglutinin and blocks viral attachment. The relation of this to lactoferrin heparin-binding properties is now known (Pietrantoni et al., 2003).

'Phage display libraries have been screened for peptides that bind HA competitive with sialic acid and so would block HA interacting with the cell surface. Initial hits were improved by selection of expanded sublibraries. Analysis of the structure of the most effective peptide shows that it is a mimic of sialic acid. Other peptides have been derived from existing proteins, by analogy with, for example, the peptides derived from lactoferrin (Section 1.5.1). The Kα2-helix peptide from the viral FLICE-like inhibitor protein (vFLIP) of Kaposi's sarcoma-associated herpesvirus (KSHV) when fused to the TAT peptide inhibits influenza A virus replication and transmission in *vitro* and *in vivo*. It protected mice challenged with lethal doses of highly pathogenic influenza A H5N1 or H1N1 viruses (Moon et al., 2017). Moreover, the TAT-Kα2 peptide may have a broad antiviral activity spectrum as it is also effective vesicular Stomatitis Virus (VSV) and respiratory Syncytial Virus (RSV). The possible mechanism of action TAT-Kα2 peptide is the

destabilization of the viral membranes, depending on their lipid composition of the viral envelop (Matsubara et al., 2010, Moon et al., 2017).

1.5.2.2 Peptides derived from natural sources

There are a considerable number of peptides that inhibit influenza virus infectivity, at least *in vitro*. What follows is a brief summary of some of these.

Cyanovirin-n (CV-N) and related sequences showed highly potent antiviral activity against almost all strains of influenza A and B virus, including clinical isolates and a neuraminidase inhibitor-resistant strain (EC_{50} = 0.004 to 0.04 µg/ml). CV-N was inactive against rhinoviruses, human parainfluenza virus, respiratory syncytial virus, and enteric viruses, but was moderately active against some herpesvirus and hepatitis virus (bovine viral diarrhea virus) strains (50% effective concentration [EC_{50}] = ~1 µg/ml) while inactive against others. CV-N may act by binding certain high mannose oligosaccharide structures such as oligomannose-8 and oligomannose-9, which may account, at least in part, for the spectrum of its antiviral activity (O'Keefe et al., 2003).

A 20-amino-acid peptide (EB, for entry blocker) RRKKAAVALLPAVLLALLAP derived from the signal sequence of fibroblast growth factor 4, binds to the viral haemagglutinin, so inhibiting the attachment of virus to cellular receptors, preventing infection. EB peptide exhibited broad-spectrum antiviral activity against influenza viruses including the H5N1 subtype *in vitro* and in four- to six-week-old BALB/c mice (Jones et al., 2006a). Pretreatment of mice with EB provided 100% protection against numerous subtypes including the highly pathogenic H5N1 viruses (Jones et al., 2006b). Other entry blocker peptides include a 16 amino acid

peptide sequence, Flufirvitide, derived from the fusion initiation region of the HA, which is currently in clinical trials. This has shown effective inhibition of influenza virus infection by blocking binding of HA to sialic acid. The peptide also appears to modulate the immune system of the host by inducing the production of anti-inflammatory cytokines and chemokines, so increasing the activity of neutrophils, and improving phagocytosis of macrophages (Cederlund et al., 2011, Skalickova et al., 2015a).

The human genome encodes a viral envelope targeting peptides, cathelicidins hCAP-18, which are between 12 and 80 amino acids long (Puig-Basagoiti et al., 2016). These cationic antimicrobial peptides are able to destroy the viral envelope and induce a number of host protective mechanisms, including chemokine and cytokine production, promotion of barrier repairs, T-cell polarization and enhance viral dsRNA signalling via Toll-Like Receptor 3 (TLR3) (Choi and Mookherjee, 2012, Currie et al., 2016).

Like the cathelicidins the defensins are host defence antimicrobial peptides. One of their activities is to target viral envelopes, including that of influenza virus (Wilson et al., 2013, Shah and Chang, 2012). As well as a direct action on the viral envelope, defensins stimulate the innate immune response (Mohan et al., 2013). In this study they were able to inhibit the synthesis of viral RNA and proteins and increase the activity of mucosal epithelia (Salvatore et al., 2007).

`

1.5.2.3 'FluPep'

It was discovered that influenza A virus, including the H1N1 subtype, was strongly susceptible to a peptide called FluPep (Nicol et al., 2012b). FluPep was originally identified as a sequence in Tkip (tyrosine kinase inhibitor peptide), thought to act as a mimic of the suppressor of cytokine signalling (SOCS) protein that binds to the autophosphorylation site of tyrosine kinases. SOCS is often indispensable to virus replication, as it inhibits the activation of STAT transcription factors, which regulate the intensity of inflammatory cytokine responses involved in protecting the host. In initial work with poxvirus, Tkip protected against acute poxvirus infection and chronic autoimmune damage in the nervous system (Ahmed et al., 2009) and so its activity against other viruses, particularly 'flu virus was determined (Nicol et al., 2012b). FluPep and derived sequences inhibited a variety of influenza A virus subtypes (including H1N1, H3N2 and H5N1) at nanomolar concentrations in cell models. In 5–6-week-old BALB/c mice inoculated intranasally with mouse-adapted A/WSN/33 virus, pre-treatment with FluPep resulted in 100% survival of the mice, with no symptoms and loss of weight (Nicol et al, 2012a).

However, it transpired that this peptide derived from Tkip exerted its antiviral activity outside the cell, so independent of it blocking SOCS, which is actually inside the cell. Thus, the peptide was shown to prevent virus attachment to cells, by an ELISA type assay for virus (Nicol et al., 2012b). Using an ELISA with Flupep absorbed to the wells, HA was shown to bind the peptide and a minimal binding sequence of 6 amino acids was determined to be the core sequence responsible for this interaction. This peptide also inhibited virus infectivity, though with an IC_{50} in

the micromolar range. The conclusion was that FluPep's anti-viral activity occurred by means of it binding HA protein, so preventing 'flu virus binding to epithelial cells. However, there are some discrepancies in these data. The competition assay on the MDCK cells where peptide prevented virus binding does not show an obvious dose response. In addition, the concentrations of peptide required for the inhibition of virus binding and of virus infectivity in cells are different (Nicol et al., 2012a). It is, therefore, not given that the mechanism proposed by these authors whereby FluPep inhibits 'flu virus infectivity is indeed by binding HA.

1.6 Aims of the project

Although the FluPep has been shown to be effective *in vitro* and in *vivo*, peptides in general are not very stable in biological environments due to proteolysis, though this can be modulated by the incorporation of D-amino acids and/or non-amide bonds between amino acids (Nicol et al., 2012b). Peptides also often require organic solvents such as dimethyl sulfoxide (DMSO) to improve their solubility, which restricts their use in a clinical setting. Indeed, FluPep is extremely hydrophobic, which limits its solubility in water. Moreover, the mechanism of how peptides such as FluPep exert their antiviral activity is often poorly defined. This is partly due to a lack of high sensitivity probes that are readily quantifiable and easily conjugated to the peptide.

The objective of this thesis is to synthesise conjugates of FluPep and gold nanoparticles. The incorporation of FluPep into a nanoparticle may improve its solubility. In addition, the number of FluPeps per nanoparticles can be controlled (Levy et al., 2006a). So the effect of valency on antiviral activity can be explored.

Most importantly, gold nanoparticles also provide a ready means to quantify FluPep-nanoparticle conjugates. The aims of this thesis are:

A- To synthesise gold nanoparticle functionalised with FluPep and compare their antiviral activity to free peptide.

B- To determine if plurifunctionalisation of gold nanoparticles with FluPep increases the antiviral activity of the peptide.

C- To identify the mechanism of FluPep antiviral activity.

D- To use information relating to the mechanism to design a more potent FluPep.

This will be achieved by:

1- Determine if nanoparticle ligand shell could be designed with reduced non-specific interaction compared to the mix matrix ligand shell.

2- Functionalising and purifying FluPep-gold nanoparticle conjugates and determining their stability.

3- Characterise the anti-flu activity of FluPep-gold nanoparticle conjugates.

4- Characterise the interactions of FluPep-gold nanoparticle conjugates with influenza virus and cells.

5- Test in parallel the anti-viral activity of FluPep-silver nanoparticle conjugates.

6- Design modified FluPep sequences with enhanced activity.

`

Chapter 2

Gold nanoparticles passivation, functionalisation with FluPep and determination their antiviral activity

2.1 Introduction

Gold nanoparticles may be passivated successfully with a mix matrix (70% CVVVTol: 30% HS-$(CH_4)_{11}$-EG_4 both mole/mole) ligand shell (Sections 1.4.2, 1.4.6). They are stable in a variety of *in vitro* tests, including DTT ligand exchange and can be functionalised in a manner that provides control over the number of functional ligands incorporated into the ligand shell. Moreover, mix matrix passivated nanoparticles have low non-specific binding to cells (Duchesne et al., 2012), indicating that they would be suitable for experiments involving cultured mammalian cells. However, this is not the only ligand combination that is able to impart good stability to nanoparticles.

Thus, in previous work other ligand mixtures that produce robust ligand shells on gold nanoparticles were identified. Some of the ones imparting stability *in vitro* tests that was at least as good as the mix matrix ligand shell included a mixture of HS-$(CH_4)_{11}$-EG_4 with either the peptidols H-CAVLT-ol, H-CAVLTY-ol or H-CFFFY-ol (Chen et al., 2012). In this chapter, different ligand shell combinations were examined to see if any perform better than the standard mix matrix and would, therefore, be useful for probing FluPep function. This work was also driven by the early observation (Section 3.2.2) that the standard mix matrix ligand shell was quite hydrophobic; that is, nanoparticle passivated with this ligand shell bound to hydrophobic interactions columns. Since hydrophobic interaction chromatography would be one means to purify nanoparticles functionalised with FluPep ligand,

which is itself hydrophobic, identifying a less hydrophobic ligand shell was important. The ligands tested included the following:

1. CVT-ol
2. A peptidol with a charged group at position 3 (K or D)
3. A peptidol with a serine backbone (CSSSS-ol).
4. A peptidol with polar group at position 3 (CVNVT-ol)
5. A peptidol with a zwitterionic C- terminus (CVVVK-OH)
6. Standard peptide, so with an acidic C-terminus.

In addition various a combinations of the above were tested. The rational was as follows. Though counter intuitive from the point of view of ligand packing, peptidols such as (1) above, which are shorter than the eleven carbon alkane chain on the alkane thiol ethylene glycol ligand, were previously observed to impart greater stability of gold nanoparticles when part of a ligand mixture with HS-$(CH_4)_{11}$-EG_4 (Chen et al., 2012). The introduction of amino acids with charged or polar side chains (3-4 above) may result in the formation of salt bridges or extra H-bonds between ligands and so increase ligand shell stability. Whereas a peptide will impart a negative charge to the nanoparticle and in all likelihood cause non-specific binding to positively charged molecules in a biological experiment (Duchesne et al., 2008a), it was of interest to examine the stability of such peptides mixed with the alkane thiol ethylene glycol ligand. Peptides with a zwitterionic C-terminus were also tested, since they may form a ligand shell with no net charge. Finally, evidence was acquired to demonstrate that nanoparticles with a mix matrix ligand shell could be functionalised with FluPep ligand and purified by cation-exchange chromatography.

2.2 Materials and Methods

2.2.1 Buffers

10 x PBS (pH 7.4)

- 1.4 M NaCl
- 27 mM KCl
- 81 mM Na2PO4
- 15 mM KH2PO4

1 M Tris-HCl (pH 7.4)

- 121.14 g Tris Base
- 800 mL dH2O

Silver nanoparticles preparation (pH 7.4)

- 10 x (100 mM NaNO3)
- 10x(20 mM HEPES)

Enzyme preparation (pH 7.0)

- 100 mM sodium acetate
- 0.1 mM calcium acetate

2.2.2 Peptides and nanoparticles

Peptides (Table 2.1) were purchased from Peptide Protein Research (PPR Ltd, Hampshire, UK), with the exception of a small batch of FluPep, which was a gift of Prof. Tony Nash, University of Edinburgh. The peptide, synthesized by the School of Chemistry, University of Edinburgh was the same as used in Niccol et al., 2012 and allowed direct comparison of the commercial peptide used for most

of the work in the thesis. The alkethiol ethylene glycol ligand, HS-EC_{11}-EG_4, was purchased from Prochimia (ProChimia Surface Sp. z o.o., Sopot, Poland). Gold nanoparticles of 9 nm diameter stabilized in citrate buffer were purchased from British Biocell (BBInternational Ltd, UK) and silver nanoparticles of diameter 10 nm from nanoComposix Inc. (CA, USA). Nanosep filters 10 kDa cut off were from PALL (PALL Corp., Portsmouth, and Hants, UK). UV-Vis spectra (2 nm incremental steps) were measured using a SpectraMax Plus spectrophotometer (Molecular Devices, Wokingham, UK) and 384 well plates from Corning (Lowell, US) and the concentration of gold nanoparticles and of silver nanoparticles determined at 450 nm (Haiss et al., 2007) and 392 nm (Paramelle et al., 2014) respectively.

2.3 Nanoparticle synthesis

2.3.1 Mix Matrix Nanoparticle preparation (AuNPs or AgNPs)

Mix matrix ligands 70:30 (mole:mole) CVVVT-ol: HS-$(CH2)_{11}$-EG_4-OH were prepared as described (Duchesne et al., 2008a) by first diluting 35 µL CVVVT-ol (4 mM DMSO:H_2O) with 35 µL ddH_2O and 6 µL HS-C_{11}-EG_4-OH (2 mM) with 6 µL EtOH and 18 µL ddH_2O. Adding the two solutions together yielded a 2 mM ligand solution of 70% (mole/mole) CVVVT-ol and 30% (mole/mole) HS-C_{11}-EG_4-OH. The ligand mixture was added to 900 µL (gold or silver) nanoparticles and vortex mixed. Once mixed, 100 µL of x10 phosphate-buffered saline (PBS: 137 mM NaCl, 3 mM KCl l, 8 mM Na_2HPO_4, 15 mM KH_2PO_4) with Tween-20 (0.1 % v/v) pH 7.4 was added to gold nanoparticles (Duchesne et al., 2008a) and 10 x (100 mM $NaNO_3$, 20 mM HEPES (Free et al., 2012) with Tween-20 (0.1 % v/v) pH 7.4

to silver nanoparticles (Free et al., 2012), vortex mixed and the (gold or silver) nanoparticles placed on a rotating wheel for 24 h at room temperature. Nanoparticles were concentrated 10 x using 10 kDa Nanosep centrifugal filters (PALL Corp., Portsmouth, Hants, UK). Samples were centrifuged for 7 min at 10000 g (~12,000 x g) and the gold nanoparticles diluted with 1 x PBST (PBS 0.05% (v/v) Tween-20) and silver nanoparticles with 1x (100 mM $NaNO_3$, 20 mM HEPES). Other ligand shells (Chapter 3) were synthesised by the same method, by varying the ligand and the relative ratio of the ligands.

2.3.2 Chromatography

2.3.3 Gel filtration

Sephadex G25 was used to group separate AuNPs or AgNPs from small (<1000 Da) molecules and to buffer-exchange AuNPs or AgNPs. In general, AuNPs or AgNPs were applied in volume no greater than 3% of the column volume, e.g. 100 µL AuNPs or AgNPs on to a 3 mL Sephadex G25 column. The column was equilibrated in the required buffer and run in the same buffer. Columns were calibrated with blue dextran (elutes in V_0) and potassium dichromate (elutes in V_i). AuNPs or AgNPs were easily recovered in the void volume, since they are bright pink and yellow respectively.

2.3.4 Purification of functionalised (AuNPs or AgNPs)

FluPep functionalised gold nanoparticles should bind to carboxymethyl CM Sepharose as the net charge of the FluPep ligand sequence is +6 (Table 2.1). FluPep functionalised nanoparticles were eluted by increasing electrolyte concentrations (Table 2.2). Thus, the FluPep functionalised (AuNPs or AgNPs) ion-exchanged on

this chromatography support, which is, therefore, suitable for their purification. Gold nanoparticles were synthesised with a range of mole % of FluPep ligand. After application of the (AuNPs or AgNPs) to the column, the non-functionalised ones were collected in the flow through and the functionalised ones eluted with1 M NaCl

2.5 mM NaH2PO4. Quantification of the gold nanoparticles by UV-Vis spectrophotometry then allowed the relation of bound and unbound (AuNPs or AgNPs) to the mole % of FluPep in the original ligand mixture to be analysed. The data indicate that at 0.03% mole %, 10 % of the AuNPs bound the column and thus most (~95 %) of these (AuNPs or AgNPs) will possess just a single FluPep ligand (Levy et al., 2006a) At higher mole % the number of FluPep ligands per nanoparticle will increase. It is interesting to note that all the (AuNPs or AgNPs) were not observed to bind to the CM Sepharose column at higher mole % of FluPep ligand, something that has been observed previously with other functional peptides (Nieves et al., 2014, Paramelle et al., 2015). Nonetheless, the simple purification of the functionalised (AuNPs or AgNPs) means that the effects on influenza virus infectivity of mono- *versus* plurifunctionalisation can be determined. Moreover, since it is known that (AuNPs or AgNPs) passivated with the mix matrix (70:30 molar ratio of SH-$(CH_2)_{11}EG_4$ and CVVVT-ol) have an average of 1200 peptidols per nanoparticle (Duchesne et al., 2008a), it is possible to estimate the average number of FluPep ligands grafted on the gold nanoparticles by simply using their mole % in the ligand mixture.

`

2.3.5 Ion-exchange, hydrophobic and affinity chromatography

Ion-exchange, hydrophobic and affinity chromatography were performed on homemade micro columns of diethylaminoethyl (DEAE), carboxymethyl (CM), phenyland nickel- nitrilotriacetic acid (Ni-NTA) Separose and heparin agarose. The chromatography gel was packed into a white pipette tip (200µL) using half the filter as a frit at the bottom and equilibrated in the appropriate buffer (Table 2.2). Capped AuNPs or AgNPs were concentrated on a Nanosep filter and exchanged into the appropriate buffer. Then, the AuNPs or AgNPs were applied to the column, the unbound fraction was recovered. Columns were washed with the eluted with the appropriate buffer (Table 2.2). The concentration of AuNPs and AgNPs in the different fractions was determined by measuring absorbance at 450 nm (Haiss et al., 2007) and 410 nm (Paramelle et al., 2015), respectively.

Table 2.2 Chromatography buffers, pH 7.4

Chromatography gel	Equilibration buffer	Washing buffer	Elution buffer 1	Elutionbuffer 2
Diethylaminoethyl (DEAE) Sepharose	1 x PBS	1 x PBS	1 M NaCl in 2.5 mM NaH2PO4 pH 7.4	2 M NaCl 5 mM NaH2PO4 pH 7.4
Carboxymethyl (CM) Sepharose	1 x PBS	1 x PBS	1 M NaCl 2.5 mM NaH2PO4 pH 7.4	2 M NaCl 5 mM NaH2PO4 pH 7.4
Phenyl Sepharose	1 x PBS	1 x PBS	H_2O 0.1%(v/v) Triton-X-100 pH 7.4	H_2O 0.1%(v/v) Triton-X-100 pH 7.4
Ni-NTA Sepharose	20 mM Tris-Cl pH 7.4	20 mM Tris-Cl pH 7.4	1 M imidazole in 20 mM Tris-Cl pH 7.4	10 mM EDTA in 20 mM Tris-Cl pH 7.4
Heparin agarose	1 x PBS	1 x PBS	1M NaCl 2.5 mM NaH2PO4 pH 7.4	2M NaCl 5 mM NaH2PO4 pH 7.4

`

2.3.6 Sample and buffer flow considerations for microcolumns

Initially it proved difficult to bind functionalised AuNPs to ion exchange gels. It was subsequently found that this was due to the flow rate on the micro columns being too fast. Ideally such columns should be run under gravity flow, but they are too small for this. Therefore, samples and buffers must be loaded slowly using a pipette with a maximum flow rate ~ 100 µL/90s to ensure sufficient contact time between the nanoparticles and the column.

2.4 Direct functionalization of AuNPs and AgNPs

AuNPs and AgNPs were functionalised with antiviral peptides via two routes. Directly by using an antiviral peptide incorporating the standard mix matrix peptide sequence at the N- terminus. Indirectly by reaction of a thiol at the antiviral peptide N-terminus with a maleimide on the AuNPs ligand shell. The antiviral peptides are based on the published nomenclature (Nicol et al., 2012a). The sequence and nomenclature of the peptides used is described in (Table 2.1).

Table 2.1 Antiviral peptides names and their amino acid sequences. FP4 and FP2 sequences are from (Nicol et al., 2012a)

Peptide name	Amino acid sequence	MW
FluPep	WLVFFVIFYFFRRRKK	2252
RRKK FluPep	RRKKWLVFFVIFYFFR	2252
FluPep Δ RRKK	WLVFFVIFYFFR	1684
FP2	WLVFFVIAYFAR	1531
FluPep ligand	CVVVTAAAWLVFFVIFYFFRRRKK	2967
RRKK FluPep ligand	CVVVTAAARRKKWLVFFVIFYFFR	2967
FluPep ligand Δ RRKK	CVVVTAAAWLVFFVIFYFFR	2398
H6FluPep ligand	CVVVTAAAHHHHHHWLVFFVIFYFFRRRKK	3790
FluPep ligandH6	CVVVTAAAWLVFFVIFYFFRRRKKHHHHHH	3790
Super FluPep 1	CVVVTAAARRPKGRGKRRREKQRWLVFFVIFYFF	4345
Super FluPep 2	CVVVTAAARGAPRRGQRTRRKNKWLVFFVIFYFFR	4218

`

2.4.1 Functionalization with FluPep ligands

To functionalise AuNPs and AgNPs directly with FluPep and its variants (Table 2.1) were included in the ligand mix. The ligand shell was prepared as stated previously (Section 2.2), but the initial ligand mixture included the functionalised peptide at the mole % indicated in the figure legends. Then AuNPs from the rotating wheel were concentrated to ~ 100 µL with 10 kDa Nanosep centrifugal filters, by centrifugation for 7 min 10000 g. The AuNPs were diluted to 500 µL and the centrifugation repeated. As the functional peptides have a higher molecular weight than the Vi cut off of Sephadex G25, this process was repeated 6 to 7 times to remove excess functional peptide. The grafting number of CVVVT-ol peptides for 2 mM Mix matrix capped 10 nm AuNPs is around 1200 per nanoparticle (Duchesne et al., 2008a). The proportion of functional peptide in solution is assumed equal to the proportion of functional peptide on the AuNPs (Levy et al., 2006b). So to prepare AuNPs with different average numbers of FluPep, the mole % of FluPep in the ligand mix was varied.

2.4.2 Indirect Functionalization of AuNPs

A considerable amount of work was done on indirect functionalisation of nanoparticles, due to the initial inability to get functionalised nanoparticles to bind to chromatography supports (cation-exchange and affinity). However, as this issue was related to flow rate (Section 2.2.4) it was abandoned. The method is reported here, since it may be of use in the future.

Mix matrix ligand were prepared as stated previously (Section 2.2) and included with peptides possessing both azide and 6xH functions ($CVVVTHHHHHHN_3$,

CVVVT N_3 HHHHHH), and left on the rotating wheel overnight. As with the FluPep ligands, the molecular weight of these functionalised peptides (> 1000 Da) meant they could not be removed by gel filtration of G25. Instead, AuNPs were subjected to at least 5 cycles of concentration to 100 µL and diluted to 500 µL in a 10 KDa cut-off Nanosep filter (7 min centrifugation at 10000 g).The AuNPs were then subjected to nickel- affinity chromatography (Section 2.3) and their concentration determined. This was also used to demonstrate successful functionalization. The azide functionalised AuNPs were then reacted with a maleimide functionalised cyclooctyne (DIBO-Mal). Samples were left overnight in dark on a rotating wheel to yield maleimide functionalised gold nanoparticles. The resulting maleimide AuNPs were reacted with molecules containing a thiol group, FGF2 was used as a positive control (Nieves et al., 2014). Then AuNPs were coupled to FluPep ligand.

Maleimide has a double bond which reacts with thiols to form a covalent thioether linkage. This is known as thiol-Michael addition. FGF2 was added in a 35-fold molar excess to increase the reaction yield. In the case of reaction with FluPep, it was important to remove any excess, unreacted FluPep, which might confound subsequent measurements of antiviral activity of AuNPs. Consequently, after reaction with FluPep, the reaction mixture was subjected to 6 to 7 cycles of concentration and dilution from 100 µL to 500 µL in 10 kDa cut-off Nanosep filters.

2.5 UV-Visible spectrophotometry and nanoparticle quantification

Absorption spectra of AuNPs and AgNPs were recorded using a Spectra Max spectrophotometer (Molecular Devices, Wokingham, UK), between 450 nm and

700 nm for gold nanoparticles and 410 nm to 600 for silver nanoparticles with 2 nm incremental steps.

2.6 Dithiothreitol (DTT) ligand exchange

2.6.1 Ligand exchange assay

A one molar DTT stock solution was prepared. The stock solution was further diluted to give concentrations ranging from 0.05 to 500 mM. Purified ligand capped AuNPs or AgNP 57µL, 33 µL 10x PBS and 10 µL DTT solutions) at different concentrations (or milliQ water when the required concentration of DTT was 0 mM) were added to a 384 well plate. A blank well, which only contained 100 µL of milliQ water, was used as reference. All samples were in assayed in duplicate.

2.6.2 Calculation of Aggregation Parameter (AP)

The surface plasmon absorption peak of 8.8 nm diameter gold nanoparticles is at 520 nm. When gold nanoparticles are aggregated, their surface plasmons couple causing a red shift in their plasmon absorbance to nearly 650 nm. The aggregation parameter (AP) was defined as ($A_{650\ nm} - A_{ref\ 650\ nm}$)/ ($A_{520\ nm} - A_{ref\ 520}$), where $A_{650\ nm}$ and $A_{520\ nm}$ are the absorbance of gold nanoparticles at 650 nm and 520 nm, respectively, and $A_{ref650nm}$ and A_{ref520} are the absorbance of water at 650 nm and 520 nm, respectively (Chen et al., 2012). For comparison of results, this primary stability parameter was normalised by dividing the AP value of control ligand capped AuNPs measured in milli Q water where [DTT] = 0.

For silver nanoparticles diameter ~10 nm with a ligand shell the surface plasmon absorption peak is at 410 nm. Consequently, the AP for silver nanoparticle was

defined as ($A_{600\ nm}$-$A_{ref\ 600\ nm}$)/ ($A_{410\ nm}$-$A_{ref\ 410}$), where $A_{600\ nm}$ and $A_{410\ nm}$ are the absorbance of Ag nanoparticles at 600 nm and 410 nm, respectively and $A_{ref\ 600\ nm}$ and $A_{ref\ 410}$ are the absorbance of water at 600 nm and 410 nm, respectively.

2.7 Tissue culture

2.7.1 Cell culture

Madin-Darby canine kidney epithelial cells (MDCK) were grown in Dulbecco's Modified Eagle's Medium supplemented with 5% (v/v) bovine serum, 1% (v/v) of 200 mM L-Glutamine, 1% (v/v) 100 U/mL penicillin and 1% (v/v) 100 µg/mL streptomycin and incubated at 37°C under 5% (v/v) CO_2 atmosphere. Cells were passaged with 0.05% (v/v) trypsin along with the chelating agent, 1x Versene-EDTA (Gibco, life technologies, UK).

2.7.2 Cell freezing and thawing

The cells were released from the cell dish by trypsin digestion (Section 2.6.1) and 9 mL cell culture medium was added. The cells were counted, placed in a 20 mL universal tube and collected by centrifugation at 800 g for 5 minutes. The supernatant was discarded and the cell pellet was resuspended in freezing medium (14.5 mL Dulbecco's modified Eagle's medium (DMEM, Life technologies), 1.5 mL dimethyl sulfoxide and 4 mL FCS to obtain the desired cell concentration (1~1.5 x 10^6 cells/mL). The cells (1 mL) in freezing medium were placed in 1.5 mL cryotubes and transferred to a -80^{o}C freezer. The frozen cells were stored in a -140^{o}C freezer. The cells taken out from freezer were thawed at 37^{o}C in a water bath. Then, the cells were transferred into a universal tube and 20 mL thawing medium (16 mL DMEM medium and 4 mL FCS) was slowly added. The cells in the thawing

medium were collected by centrifugation at 800 g for 5 minutes and 10 mL cell culture medium was added to resuspend cells, which were then placed into a 10 cm dish and transferred to the 37 ^{o}C incubator.

2.7.3 Cell counting

There are two methods for cell counting, both of which were used, depending on availability.

- Coulter counter method, detached cells (0.5 mL) were diluted to 20 mL with coulter Isoton II diluent (Beckman Coulter). The cells were counted in a Coulter Electronics particle counter. Cells from each dish were counted three times.
- Hemocytometer:

- Using a pipette, take 100 μL of trypan blue-treated cell suspension and apply to the hemocytometer. Very gently fill both chambers underneath the coverslip, allowing the cell suspension to be drawn out by capillary action.
- Using a microscope, focus on the grid lines of the hemocytometer with a 10X objective.

- Using a hand tally counter, count the live, unstained cells (live cells do not take up trypan blue) in one set of 16 squares. When counting, employ a system whereby cells are only counted when they are within a square or on the right-hand or bottom boundary line. Following the same guidelines, dead cells stained with trypan blue can be also be counted for a viability estimate if required.

- Move the hemocytometer to the next set of 16 corner squares and carry on counting until all four sets of 16 corner squares are counted.

2.8 Influenza virus preparation

2.8.1 Preparation of influenza virus stock

To infect a T25 flask of MDCK cells, cells were grown to 90% confluence, which corresponds to 7 x 10^6 cells. Then, the cell monolayer was washed with 2 x 5 mL PBS. Then, virus was added to the cells at a multiplicity of infection (MOI) (Section 1.3.1) of 0.001 in 2 mL DMEM, made up by adding 7 µL virus stock to 1993 µL DMEM. Cells were incubated with virus for 1 h at 37 ^{0}C on a rocking platform or flasks were manually rocked every 10 mins. A stock of 2.5 µg/mL N-acetyl trypsin was prepared by adding 125 uL from the original stock (100 µg/mL) to 4875 uL DMEM. Virus containing medium was removed and the cell monolayer washed with 2 x 5 Ml DMEM. The N-acetyl trypsin in DMEM was added to the flask and cells were incubated 24 – 48 h at 37^{0}C until the cytopathic effect (CPE) had developed to a point where the cells were lifting from the flask surface. Medium was removed and centrifuged for 5 min at 2500 g to remove cell debris and this viral stock was stored at -80^{0}C.

2.8.2 Determination of influenza virus titre by plaque assay

Serial dilution of the virus was prepared by pipetting 990 µL of DMEM (containing Pen/Strep and L-Glutamine) in a 5 mL bijoux and 10 µL of stock virus to give a 100-fold dilution followed by serial 10-fold dilutions. This was repeated down to 10^{-8}. Virus (400 µL) from each bijoux was added to duplicate wells, and the number of plaques determined (Section 2.7.3).

`

2.8.3 Anti-viral activity of AuNPs incorporated with FluPep

The purified nanoparticles functionalised with the appropriate FluPep at different mole % (Section 2.3) were diluted in PBS as appropriate and mixed with virus. The mixture of virus and AuNPs was then added to the cells (Section 2.7.5).

2.8.4 Influenza virus plaque assay

Two days prior to infection, six well plates were set up with 0.5 x 10^6 MDCK cells per well. When the cells were confluent, medium was removed and wells were washed with PBS twice prior to infection. The monolayers of MDCK cells were then infected with a dilution of 'flu virus stock (A/WSN/33 H1N1 subtype, Section 2.7.1) required to obtain around 100 plaques per well.

2.8.5 Infection with flu viruses

Serial dilutions of the virus were prepared by pipetting 990 µL serum free DMEM (containing Pen/Strep and L-Glutamine) in a bijoux with 10 µL of stock virus to give a first 10^{-2} dilution followed by serial 10-fold dilutions. This was repeated down to 10^{-8}. 400 µL from each bijoux was added to the corresponding wells in duplicates. Plates were then placed in the 37 ^{o}C incubator and rock every 10 minutes for 1 hr.

2.8.6 Gel agarose overlay

Low melting agarose (2% w/v) was melted in sterile distilled water and kept at 55 ^{0}C in a water bath prior to use. To make the overlay medium, 50 mL 10 x MEM medium was mixed with 10 µL of a 10 mg/mL stock of N-acetyl trypsin bovine pancreas type V-S was added to give a final concentration of 2 µg/mL. This was

then divided into two 25 mL volumes and kept at 37 ^{0}C. After 1 h of infection with virus, the medium was removed from the culture dishes. Then, 25 mL of the 2 % (w/v) agarose was quickly added to one of the 25 mL aliquots of 2x MEM medium. This was mixed and 2 mL added to each well, left for 15 minutes to set, and then plates were inverted and placed back in the incubator for 3 days.

2.8.7 Fixing and staining of cells

After approximately three days post-infection, cells were fixed with 4 mL 10% (v/v) neutral buffered formalin (Leica Biosystems Peterbrough Ltd, Bretton Peterborough, Cambridgeshire for 1 hr. Then the 10% (v/v) neutral buffered formalin was removed, the agarose overlay was discarded and plates were stained with 0.1% (w/v) toluidine blue in water or 20 minutes, washed with water and left to dry before counting plaques.

2.8.8 Determination of IC_{50}

A dose-response curve describes the relationship between increasing the concentration of the compound and the change in response that is measured in the biological system. In this Thesis compounds are peptides and nanoparticles and the response is the number of plaques caused by 'flu virus in MDCK cells. In the case of inhibitors, the concentration at which half the biological response is inhibited is the IC_{50}. This provides a convenient way to compare different experiments with different compounds. IC_{50} was calculated using Prism and a step-by-step example is given to guide Prism users through constructing sigmoidal curves from dose–response data. The steps in this example are outlined here:

`

- Enter data – Create a data table for dose-response data.
- Transform X values to log form – Alter the number format of the X values.
- Normalize the Y values – Express Y values from different data sets on a common scale.
- Nonlinear regression – Use an equation defined in Prism to determine specific parameter values for your data.
- Compare the curves statistically – Use Prism to determine whether two curves are statistically different.
- Review the graph – Check that the data and the analysis agree.
- Review the results – View and interpret the results of the analysis.

2.9 Results

2.9.1 Resistance of mix matrix nanoparticles to DTT ligand exchange

Standard mix matrix nanoparticles with 70% CVVVT-ol and 30% HS-$(CH_2)_{11}EG_4$ (both mole/mole) were synthesized (Section 2.2.1). After purification of the nanoparticles from excess ligands on Sephadex G25, they were subjected to a DTT-ligand exchange stability test (Section 2.5.1). The normalised aggregation parameter of the mix matrix didn't change up to 10 mM DTT, even after 24 h incubation. However, at 5 mM DTT after 48 h there was some evidence for ligand exchange, as the aggregation parameter was above 1.0 and at 10 mM DTT the ligand shell was clearly compromised at this time (Fig. 3.1) Therefore, these nanoparticles were similar in terms of their resistance to ligand-exchange to those made previously by others (Chen et al., 2012).

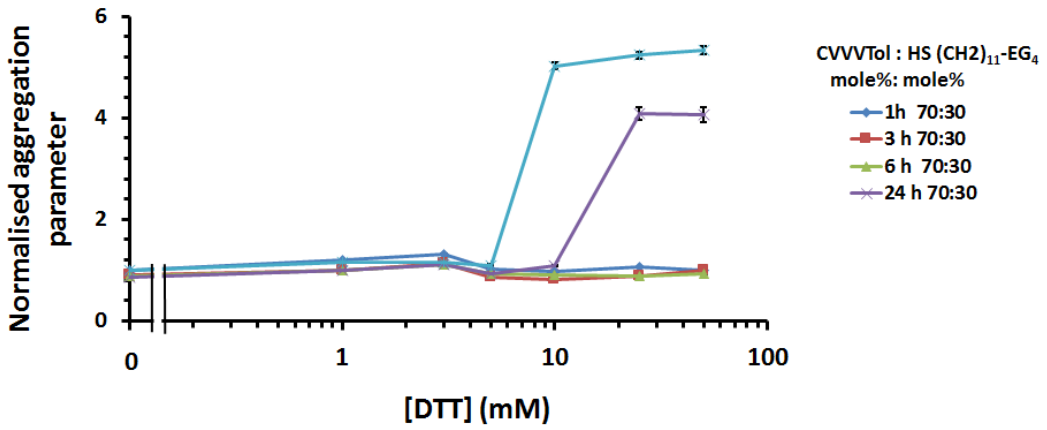

Fig. 2.1. Stability of mix matrix gold nanoparticles to DTT ligand exchange Time and dose-dependence of DTT ligand exchange for mix matrix gold nanoparticles. The molar ratios of the ligands are indicated in the legend. Results are the mean ± SD (n=3).

As noted in (Section 3.1), there is evidence that combinations of ligands other than the standard mix matrix may be more stable, at least with respect to ligand exchange (Duchesne et al., 2008a, Chen et al., 2012). To explore this, a selection of different peptidols were used in combination with the alkane thiol ethylene glycol HS-$(CH_2)_{11}EG_4$, as well as some peptides on their own. However, since Flupep ligand was considered to have the potential to alter the chromatography of nanoparticles, the interaction of Flupep ligand functionalised nanoparticles with different chromatography matrices was first determined.

2.9.2 Functionalisation of gold nanoparticles with FluPep and their interaction with chromatography matrices

The mix matrix ligand shell of 70:30 (mole/mole) peptidol and alkanethiol ethylene glycol assembled on gold nanoparticles has well characterised stability with respect to ligand exchange and non-specific binding (Duchesne et al., 2008a, Chen et al., 2012). In all cases the nanoparticles capped by the standard mix matrix ligand shell did not bind to either CM Sepharose or DEAE Sepharose in 20 mM Tris-Cl, pH 7.2 (Fig 3.2). This is consistent with previously published data (Duchesne et al., 2008a) and indicates that these nanoparticles do not have a non-specific interaction with Sepharose, DEAE or CM groups. However, when gold nanoparticles with this ligand shell were applied to a phenyl Sepharose column they all bound (Fig. 3.2C). This indicates that the mix matrix ligand shell results in a fairly hydrophobic nanoparticle. Indeed, attempts at eluting the mix matrix nanoparticles from the column with 1 % (v/v) Triton-X-100 were unsuccessful.

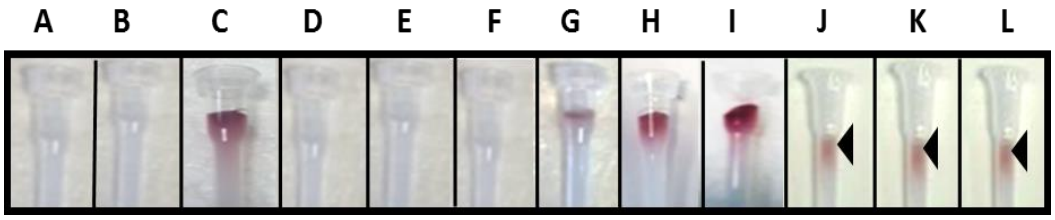

Fig. 2.2. CM, DEAE and phenyl Sepharose HIC column chromatography of purified gold nanoparticles with a mix matrix ligand shell. Homemade mini columns were prepared (Section 2.2.5) and equilibrated in 20 mM Tris HCl (pH7.2). Nanoparticles, in some cases functionalised with FluPep ligand (Section 2.3) were applied to the column and if bound, elution was attempted with a suitable buffer. (A) Mix matrix gold nanoparticles applied to DEAE Sepharose. (B) Mix matrix gold nanoparticles applied to CM Sepharose. (C) Mix matrix gold nanoparticles applied to phenyl Sepharose. Mix matrix gold nanoparticles functionalised with 0.1% (D), 3% (E) and 5 % (F) FluPep ligand (all mole/mole) were applied to DEAE Sepharose. (G) Mix matrix gold nanoparticles functionalised with 0.1% (G), 3% (H) and 5% (I) FluPep ligand (all mole/mole) were applied to CM Sepharose. (J) Mix matrix gold nanoparticles functionalised with 0.1% (J), 3% (K) and 5% (L) gold nanoparticles- FluPep ligand applied to a phenyl Sepharose column. The arrow indicates the reddish/pink band where nanoparticles have bound to the column.

Gold nanoparticles were then functionalised with different mole % of FluPep ligand and purified from excess ligand using size-exclusion chromatography on Sephadex G25 and filtration on a 10 kDa cut off filter (Section 2.2.4). FluPep ligand functionalised nanoparticles did not bind to DEAE Sepharose (Figs 2.2 D-E), so FluPep ligand in itself does not bind to Sepharose or DEAE. FluPep ligand when incorporated into a ligand shell will have a net charge of +6. Not surprisingly, when purified FluPep ligand functionalised gold nanoparticles were applied to a CM Sepharose they bound (Figs 2.2 G-I). FluPep ligand is quite hydrophobic and gold nanoparticles functionalised with it bound to phenyl Sepharose (Figs 2.2 J-L). However, the underlying hydrophobicity of the mix matrix ligand shell (Fig. 2.2C)

means that hydrophobic interaction chromatography cannot be used to separate FluPep ligand functionalised gold nanoparticles from non-functionalised ones.

2.9.3 Stability of gold nanoparticles functionalised with different peptidols

2.9.3.1 Overview

Different peptidols were combined with the alkane thiol ethylene glycol (Table 2.3) to test various hypotheses regarding how the stability of the standard mix matrix nanoparticles might be improved. Another motivation was the observation that mix matrix nanoparticles are quite hydrophobic and bind strongly to phenyl Sepharose (Fig. 3.2). This property does not lead to substantial non-specific binding on cells (Duchesne et al., 2012). However, it precludes advantage being taken of the hydrophobicity of FluPep for the purification of FluPep ligand functionalised nanoparticles (Fig. 2.2). Thus, reducing the hydrophobicity of the ligand shell would allow the use of hydrophobic interaction chromatography for the purification of the functionalised nanoparticles.

CVT-ol was used because it has been reported that shortening the peptidol enhances stability (Chen et al., 2012). This is counterintuitive, since the pentapeptidol CVVVT-ol is roughly the same length as the alkane unit of the alkane thiol ethylene glycol. Then, a series of peptidols with charged or polar groups in the stem between the cysteine and the C-terminal threoninol were used, to see if the supplementary H-bonding capacity might increase the stability of the ligand shell. Finally, peptidols alone, without the alkane thiol ethylene glycol, and a peptide with a zwitterionic C-terminus were tested, as these might provide high stability, but not interact non-specifically with charged macromolecules.

Table 2.3. Ligand shell types and the sequences of the peptidol and peptide ligands

Ligand shell type	Ligand shell sequence
Short peptidol	CVT-ol
charged group position 3 (K or D)	CVKVTol, CVDVTol
serine backbone	CSSSS-ol
polar group at position 3	CVNVT-ol
zwitter ionic C- terminus	CVVVK-OH
Mix of all above	CVNVTol+CVDVTol CVNVTol+CVKVTol CVNVTol+CSSSSol CVDVTol+CVKVTol
peptides with a terminal carboxylic acid	CALNN-OH
peptidols with an amine	CVVVK-ol

2.9.3.2 CVT-ol

Published data indicated that shortening the peptidol would enhance the stability of the nanoparticles, so CVT-ol was used in a ligand mixture as 70 % CVT-ol : 30 % HS-$(CH_2)_{11}EG_4$ (both mole/mole) to passivate gold nanoparticles. The stability of the nanoparticles passivated with this ligand shell against DTT ligand exchange was determined. The results showed that the normalised aggregation parameter was unchanged up to 25 mM DTT after 24 h. However, at 5 mM after 48 h, the

normalised aggregation parameter started to rise above 1, and at 10 mM after 48 h the normalised aggregation parameter showed clearly that the nanoparticles had aggregated and so had undergone substantial ligand exchange (Fig 2.2 A). The proportion of CVT-ol peptidol in the Mix matrix was varied from the standard (70:30, 50:50 and 30:70) and compared to HS-EC_{11}-EG_4. The normalised aggregation parameter is shown for the 48 h time point. The normalised aggregation parameter for 50:50 (mole/mole) varied similarly to the 70:30 (mole/mole) mixture (Figs 2.3 A, B). However, the 30:70 (mole/mole) mixture of CVTol and HS-EC_{11}-EG_4 was more stable since at 48 h the aggregation parameter remained at 1 up to 10 mM DTT and only increased at 25 mM DTT (Fig 2.3 B). This is consistent with the high stability of the HS-EC_{11}-EG_4 ligand shell (Fig. 2.3 B).

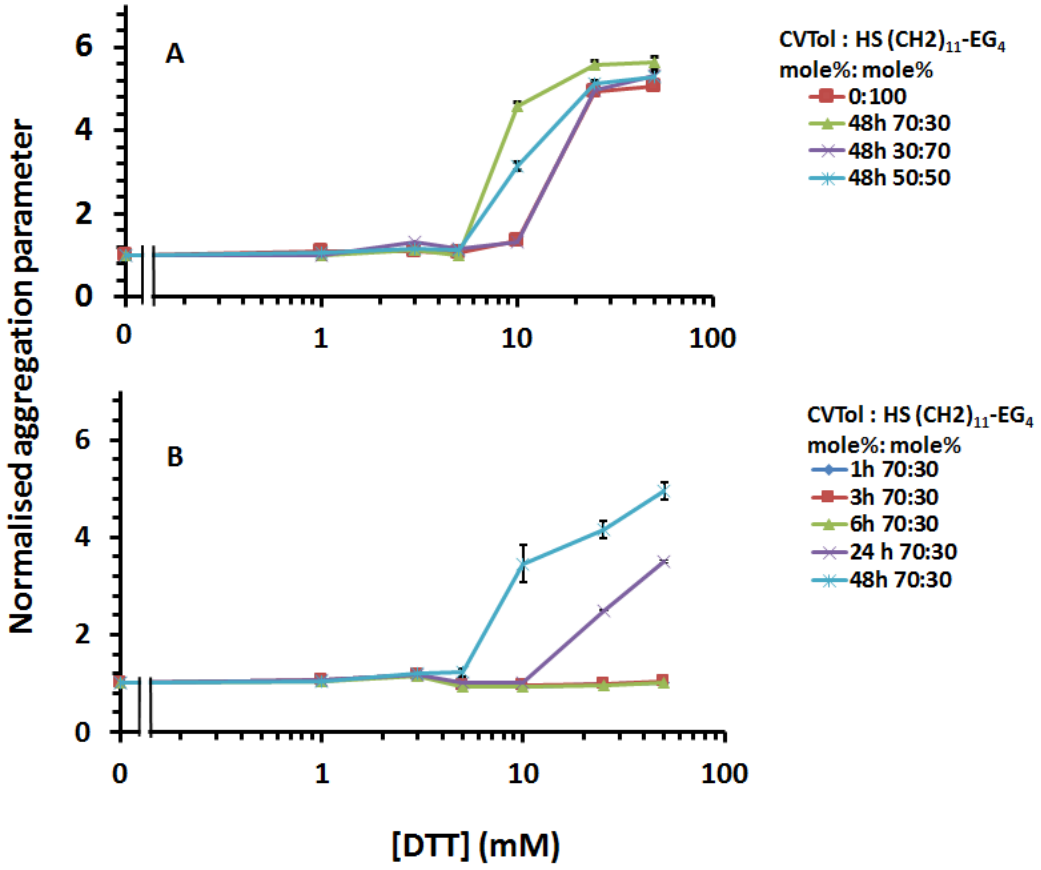

Fig. 2.3. Stability of gold nanoparticles capped with CVT-ol and HS-EC$_{11}$-EG$_4$ to DTT ligand exchange (A) Time and concentration dependence of DTT ligand exchange for gold nanoparticles with a ligand shell of 70% CVT-ol: 30% HS-EC$_{11}$-EG$_4$ (both mole/mole). (B) Concentration-dependence of DTT ligand exchange of nanoparticles capped with different mole% of CVT-ol and HS-EC$_{11}$-EG$_4$. The molar ratios of the ligands are indicated in the legend. Results are the mean ± SD (n=3).

2.9.3.3 Effect of a charged amino acid side chain at position 3 in the peptidol

The effect of either charged amino acids K or D at position 3 were investigated by synthesising nanoparticle ligand shells with different mole % of CVDVTol and CVKVTol and the alkane thiol ethylene glycol ligand (70:30, 50:50 and 30:70).

The results shown that after 24 h the aggregation parameter for CVDVTol and CVKVTol 70:30 and 50:50 was unchanged up to 10 mM DTT, while at 25 mM DTT this increased to ~ 4.6 for CVDVTol and ~4 CVKVTol, indicating nanoparticle aggregation. However, for 30:70 nanoparticles with either CVDVTol or CVKVTol the aggregation parameter unchanged until 25 mM and at 50 mM the aggregation parameter reached about 4.6 (Fig 2.4 A).

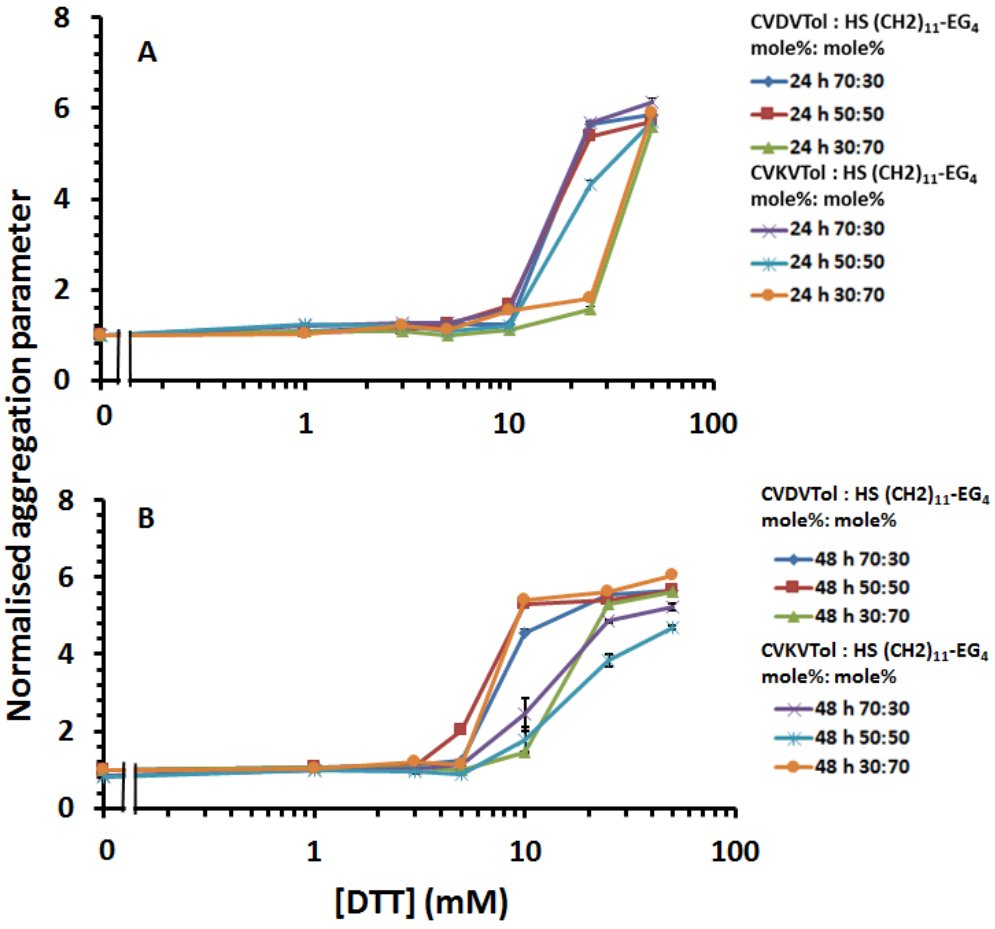

Fig. 2.4. Stability of mix matrix gold nanoparticles to DTT ligand exchange A Time and dose-dependence of DTT ligand exchange for mix matrix gold nanoparticles for CVDVTol and CVKVTol ligand shell after 24 h. B after 48 h. The molar ratios of the ligands are indicated in the legend. Results are the mean ± SD (n=3).

However, after 48 h the relative stability of the different formulations of the ligand shells changed for CVKVTol. Thus, for ligand shells comprising CVDVTol and the alkane thiol ethylene glycol, the rank order of stability remained the same as at 24 h: increasing the proportion of alkane thiol ethylene glycol to 70% (mole/mole) increased the resistance of the nanoparticles to DTT ligand exchange. However, for ligand shells with CVKVTol the nanoparticles with 70 % (mole/mole) alkane thiol ethylene glycol were less stable than those with a lesser mole % of this ligand in the mixture (Fig 2.4 B). Compared to the standard mix matrix (Fig. 2.1), incorporating a charged amino acid at position 3 either had no effect on the stability of the nanoparticles to ligand exchange or it increased it by a factor of around two. This suggests that increasing the H-bonding capacity of the peptidol in the ligand shell may increase the stability of that ligand shell to ligand-exchange.

2.9.3.4 Effect of polar amino acids

The effect of polar amino acids S and N were investigated by synthesising ligand shells with different mole % of CVNVTol and CSSSSol (70:30, 50:50 and 30:70) and alkane thiol ethylene glycol. It was expected that these would also be able to form additional H-bonds within the ligand shell. Interestingly, ligand shells with these peptides were either less resistant to ligand exchange with DTT than the standard mix matrix (CVNVT-ol, 70 % mole/mole) or similar Fig. 2.5). Thus, it would appear that incorporating a basic or acidic amino acid in the middle of the peptidol (Fig. 2.4) is more effective than an amide or using an entirely polar peptidol (Fig. 3.4).

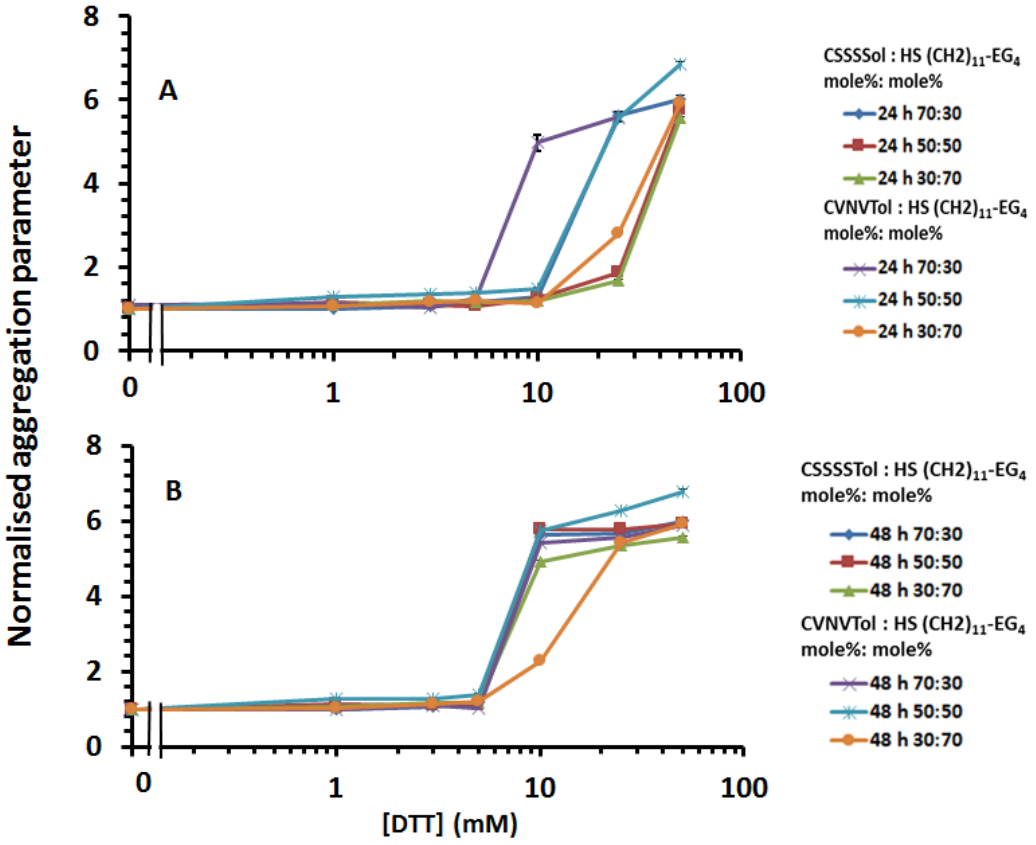

Fig. 2.5. Stability of gold nanoparticles capped with mixtures of polar peptidols and alkane thiol ethylene glycol ligands to DTT ligand exchange (A) Ligand exchange after 24 h incubation with different concentrations of DTT for gold nanoparticles capped with CVNVTol or CSSSSol and alkane thiol ethylene glycol ligands after 24 h and (B) after 48 h. The molar ratios of the ligands are indicated in the legend. Results are the mean ± SD (n=3).

2.9.3.5 Effect of combining different peptidols

The effect of combining of different peptidols which might enhance mix matrix stability was investigated by synthesising ligand shells form mixtures with different mole % of peptidols with a polar or charged amino acid at position 3: CVNVTol+CVDVTol and CVNVTol+CVKVTol with the alkane thiol ethylene glycol ligand at rations of 70:30, 50:50 and 30:70. It would appear that the presence of the asparagine at position 3 has a greater impact on the resistance of the

nanoparticles to ligand exchange than either of the two charged residues (Fig. 2.6). That is the stability against DTT ligand exchange of these nanoparticles resembles most that of the nanoparticles with a ligand shell comprising CVNVTol and the alkane thiol ethylene glycol (Figs 2.6A, B).

When the peptidols CSSSS-ol and CVNVT-ol were incorporated into mixed ligand shells they did not enhance the stability of the nanoparticles in ligand exchange tests (Figs 2.6 C). Thus, the incorporation of polar residues into the peptidol at best did not improve the resistance of the nanoparticle ligand shell to exchange with DTT, but in some cases reduced stability, with respect to the standard mix matrix ligand shell (Fig. 2.1)

The two peptidols with a charged residue were also combined, on the grounds that these may form a salt bridge in the ligand shell. Again these pairs were used with the alkane thiol ethylene glycol at different molar ratios of total peptidol (70:30, 50:50 and 30:70). These combinations were at least as resistant to ligand exchange with DTT (Figs 2.6 C, D) as the mix matrix ligand shell (Fig. 2.1) and in some cases more stable, but they did not impart greater stability that when used alone with the alkane thiol ethylene glycol (Fig. 2.4).

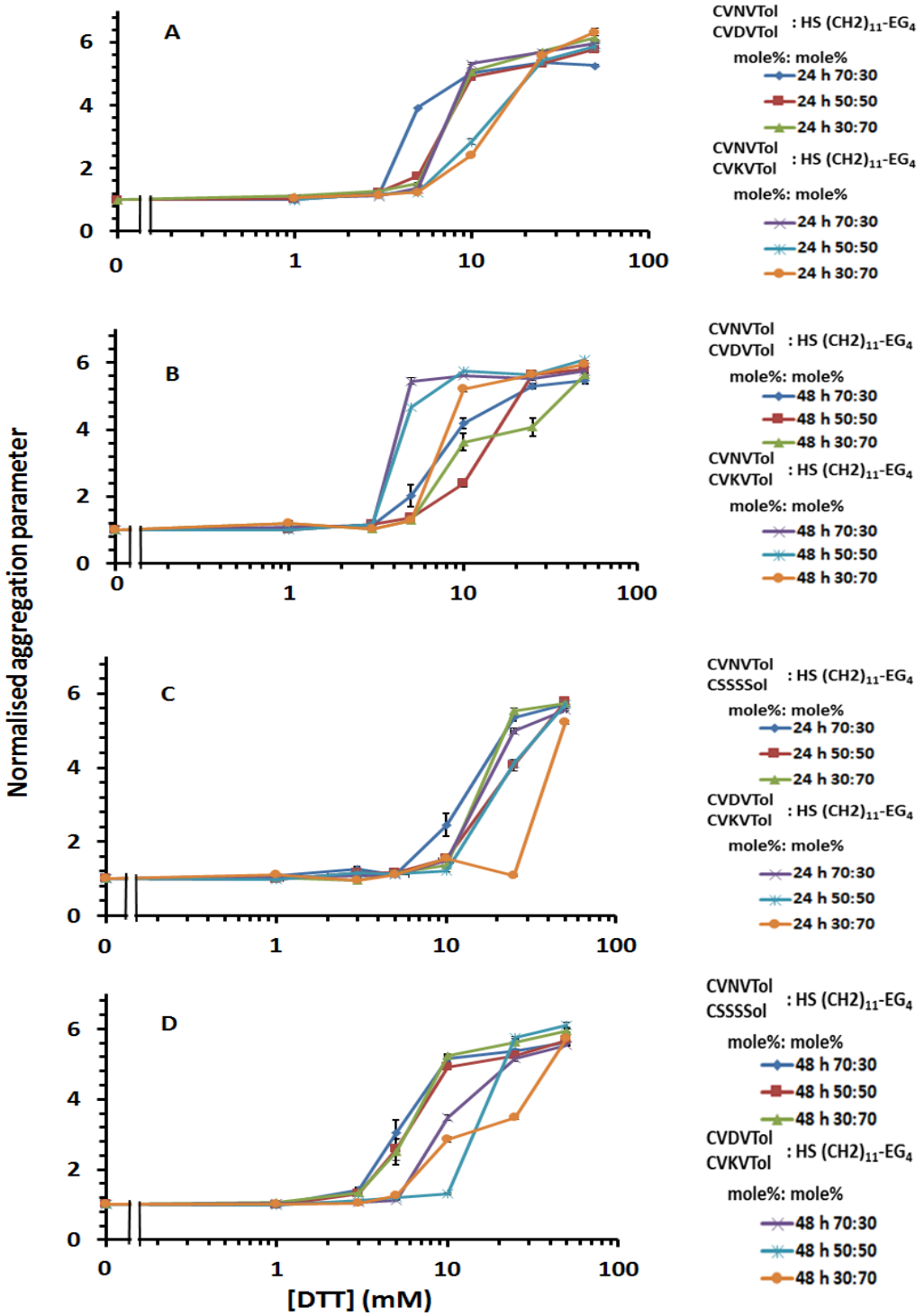

Fig. 2.6. Stability of combining different peptidols mix matrix gold nanoparticles to DTT ligand exchange A Time and dose-dependence of DTT ligand exchange for of polar amino acids peptidols + charged amino acids CVNVTol+CVDVTol and CVNVTol+CVKVTol mix matrix gold nanoparticles after 24 h. B after 48 h. C. Time and dose-dependence of DTT ligand exchange for polar and charged amino acids CVNVTol+CSSSSol and CVDVTol+CVKVTol after 24 h. D after 48 h. The molar ratios of the ligands are indicated in the legend. Results are the mean ± SD (n=3).

`

2.9.3.6 Effect of charge at the C-terminus

The introduction of charge at the C-terminus of the peptide would in principle reduce the hydrophobicity of the ligand shell, particularly if this was sufficiently stable to reduce and even omit the alkane thiol ethylene glycol, which will contribute to the hydrophobicity of the ligand shell. However, this is known to reduce the stability of the nanoparticles to ligand exchange (Chen et al., 2012, Duchesne et al., 2008a). The effect of charge at the C-terminus was investigated by synthesising ligand shells of CVVVKOH (C-terminal zwitterion) or CVVVKol (C-terminal amine) with the alkane thiol ethylene glycol at molar rations of 70:30, 50:50 and 30:70. Although little aggregation was apparent at 24 h (Fig. 3.7 A), at 48 h the 70:30 molar ratio ligand shells were as susceptible to ligand exchange as the control mix matrix (Figs 2.1 and 2.7 B).

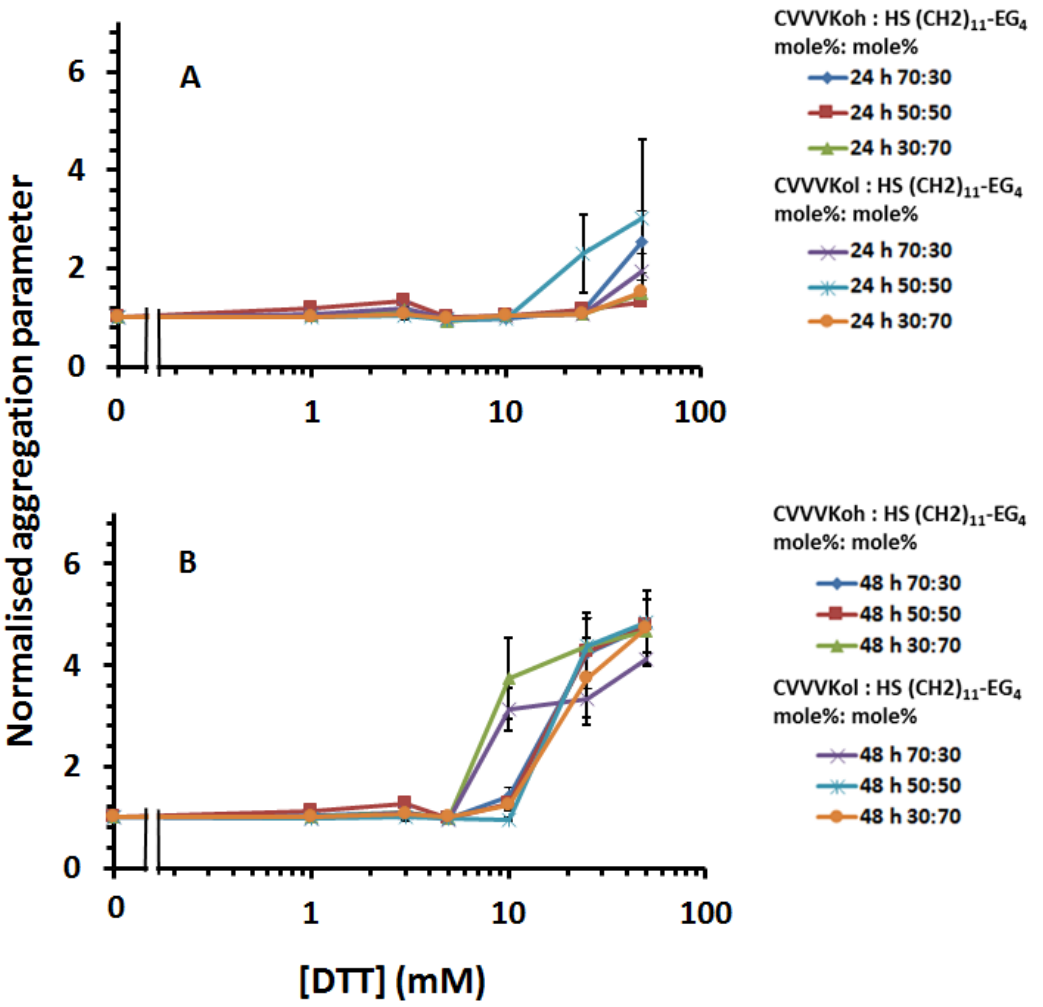

Fig. 2.7. Stability of charge at the C-terminus mix matrix gold nanoparticles to DTT ligand exchange A time and dose-dependence of DTT ligand exchange for mix matrix gold nanoparticles for CVVVKOH and CVVVKol ligand shell after 24 h. B after 48 h. The molar ratios of the ligands are indicated in the legend. Results are the mean ± SD (n=3).

Further experiments were performed with the peptide that had a C-terminal zwitterion, (CVVVK-OH, which was compared to a peptide with a terminal carboxylic acid (CALNN-OH). These were in some experiments mixed with the alkane thiol ethylene glycol. Neither CVVVK-OH nor CALNN-OH alone was able to prevent DDT mediated ligand exchange after 1 h (Fig. 2.8A). The relative

instability of the CALNN ligand shell in this assay has been noted previously(Chen et al., 2012) and the zwitterion terminated peptide was no more stable. Addition of even a small mole % of the alkane thiol ethylene glycol increased the resistance of the ligand shell to ligand exchange (Figs 2.8A-C). However, where their stability was greater than the standard mix matrix ligand shell (Fig. 2.1) this can be attributed by an increased mole % of the alkane thiol ethylene glycol ligand.

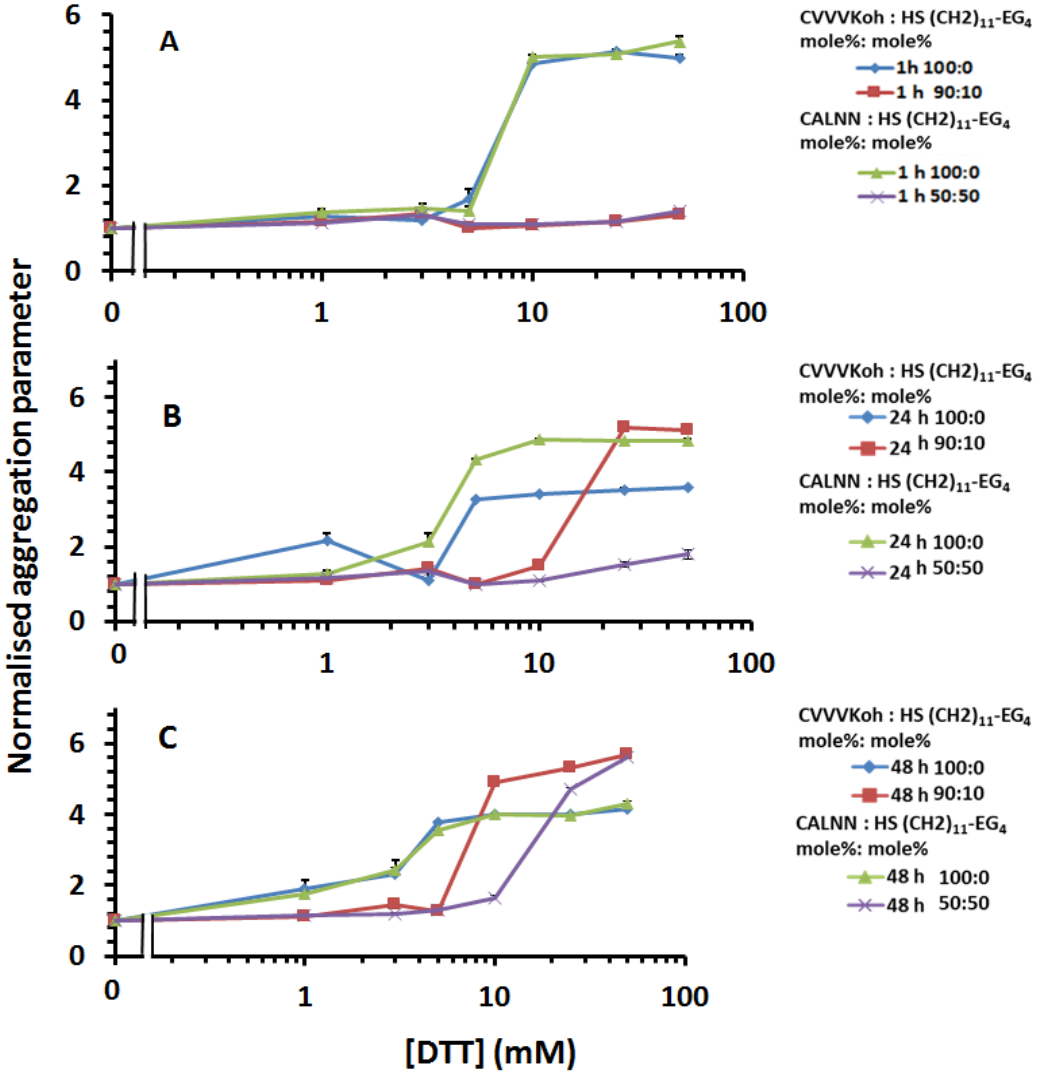

Fig. 2.8. Stability of A zwitterion of (CVVVK-OH), peptides with a terminal carboxylic acid (CALNN-OH) mix matrix gold nanoparticles to DTT ligand exchange A Time and dose-dependence of DTT ligand exchange for mix matrix gold nanoparticles for CVVVKOH and CALNN ligand shell after 1h. B 24 h. C after 48 h. The molar ratios of the ligands are indicated in the legend. Results are the mean ± SD (n=3)

`

2.9.4 Discussion

The planned work with ‘flu virus (Chapters 3 and 4) will entail incubating live cells in culture medium with nanoparticles for around three days, since this is the time required for the formation of plaques (Section 2.7.4). Previous work with functionalised mix matrix nanoparticles has only involved much shorter contact time of the nanoparticle with the culture medium and the cell (Duchesne et al., 2012, Nieves et al., 2015)). Resistance of the nanoparticle ligand shell to ligand exchange by small thiols will be very important, since cell culture medium contains ~ 1 mM cysteine, which though less effective than DTT, does cause ligand exchange (Chen et al., 2012), and this may be more pronounced over three days in the presence of the many other medium components. Consequently, ligand shells that were not as resistant as the mix matrix one were considered to be too high risk to use. Moreover, since the mix matrix ligand shell is well established for using nanoparticles as probes with cells, it was decided that a substantial improvement in resistance to DTT ligand exchange (~10-fold) would be necessary for the ligand shell to be changed with confidence.

Mix matrix gold nanoparticles were synthesized that had the same resistance to ligand exchange (Fig. 2.1) and absence of binding to Sephadex, Sepharose, carboxylic acids and amines (Fig. 2.2) as in previous work (Chen et al., 2012). However, these nanoparticles were observed to be very hydrophobic (Fig. 2.2), which was surprising, since they had been shown to exhibit little non-specific binding to cells (Duchesne et al., 2012, Nieves et al., 2015). However, it should be noted that hydrophobicity had never been examined before. As there were

indications in previous work that there may be more stable ligand shells, attempts were made to build on these data to design a more stable ligand shell, and also to determine whether a less hydrophobic, but equally stable one could be identified. The results were mixed. Some combinations of ligands were a little more resistant to ligand exchange, but the difference compared to the mix matrix was not considered to be large enough to pursue. This is because of the demonstration by others that the mix matrix ligand shell performs well in the context of living cells (Duchesne et al., 2012, Nieves et al., 2015). Changing the ligand shell on the grounds of an incremental increase *in vitro* stability was thought to be too high a risk. The ligand shells with a terminal charge, including those synthesised with zwitterionic ligands were considered to have reduced the stability of the nanoparticle to too great an extent to be useful in the planned work with 'flu virus.

On a more positive note, FluPep ligand functionalised nanoparticles were shown to bind to CM-Sepharose, but not DEAE-Sepharose. Since the control nanoparticles did not do so and mix matrix nanoparticles are stable in high electrolyte concentrations (Duchesne et al., 2012), these data mean that FluPep ligand functionalised nanoparticles should be easily purified from non-functional ones by cation-exchange chromatography. The principle of purification of functionalised nanoparticles by ion-exchange chromatography is demonstrated by the successful of purification of mix matrix nanoparticles functionalised with an acidic peptide on DEAE Sepharose (Paramelle et al., 2015). Therefore, the purification of FluPep ligand nanoparticles on CM-Sepharose was considered to be the method of choice for this step.

`

2.9.5 Conclusion

Gold nanoparticles were passivated successfully with a ligand shell called mix matrix, composed of 70% of CVVVTol:30% HS-EC_{11}-EG_4 (both mole/mole), which provided protection against non-specific binding to DEAE and CM Sepharose, Sephadex, and stability against electrolyte induced aggregation. However, nanoparticles passivated with the mix matrix bound to phenyl Sepharose indicating a high degree of hydrophobicity. Many attempts were made to reduce the hydrophobicity of the ligand shell. The results identified ligand mixtures that in some instances enhanced stability a little, but without a major effect on the hydrophobicity. Thus, it was decided that these ligand shell were not, from an experimental point of view, substantially better than the original mix matrix. Consequently, the remainder of the work in this thesis used the mix matrix ligand shell to passivated gold and silver nanoparticles. Gold nanoparticles were functionalised with different mole % of FluPep. FluPep functionalisation did not alter the stability of the nanoparticles, but did allow the nanoparticles to bind to CM Sepharose in an electrolyte-dependent manner, due to the RRKK C-terminal sequence on FluPep.

Aplaque assay demonstrated that the gold nanoparticles functionalised with FluPep inhibited ‘flu virus infectivity. Thus FluPep conjugated to gold nanoparticles retained its antiviral activities.

Chapter 3

3.1 Introduction

FluPep WLVFFVIFYFFRRRKK is potentially a new treatment for ‘flu virus infection; it was demonstrated by (Nicol et al., 2012b) that influenza A virus, including the H1N1 subtype, was strongly susceptible to inhibition by FluPep in cell and animal models (Section 1.5.2.3). This was promising, but there remains important questions regarding the mechanism of action of FluPep. To elucidate this question requires a sensitive probe to be attached to FluPep. Gold and silver nanoparticles were used due to their optical properties (Sections 1.4.2 and 1.4.5), which means these have the highest extinction coefficient and can be detected by UV-Vis spectroscopy at very low concentration. Moreover, photothermal microscopy, an optical technique, and transmission electron microscopy enable single nanoparticle detection, the latter at the subcellular scale, should this be required. The high density of these noble metal nanoparticles also enables easy separation. In Chapter 2 it was established that the mix matrix ligand shell of 70 % peptidol and 30 % (both mole/mole) is suitable for the synthesis of FluPep functionalised gold nanoparticles. In this chapter, the synthesis and purification of FluPep ligand functionalised gold and silver nanoparticles is described. The stability of the nanoparticle-FluPep conjugates *in vitro* has been determined and their anti-viral activity established. This work lays the foundation for the subsequent analysis of the mechanism of action of FluPep and the design of more effective peptides in Chapter 4.

`

3.2 Enhanced inhibition of influenza virus infection by peptide-nanoparticle conjugates

Section 3.2 is based on a preprint ref. https://www.biorxiv.org/content/early/2018/05/17/324939

3.2.1 Materials & methods

3.2.1.1 Materials

3.2.1.2 Peptides and nanoparticles

Peptides FluPep WLVFFVIFYFFRRRKK, FluPep ligand CVVVTAAAWLVFFVIFYFFRRRKK and the ligand shell matrix peptidol CVVVT-ol were purchased from Peptide Protein Research (PPR Ltd, Hampshire, UK). The alkethiol ethylene glycol ligand, HS-EC_{11}-EG_4, was purchased from Prochimia (ProChimia Surface Sp. z o.o., Sopot, Poland). Gold nanoparticles of 9 nm diameter stabilized in citrate buffer were purchased from British Biocell (BBInternational Ltd, UK) and silver nanoparticles of ~10 nm diameter from nanoComposix Inc. (CA, USA). Nanosep filters 10 kDa cut off were from PALL (PALL Corp., Portsmouth, and Hants, UK). UV-Vis spectra (2 nm incremental steps) were measured using a SpectraMax Plus spectrophotometer (Molecular Devices, Wokingham, UK) and 384 well plates from Corning (Lowell, US) and the concentration of gold nanoparticles and of silver nanoparticles determined at 450 nm (Haiss et al., 2007) and 392 nm (Paramelle et al., 2014), respectively.

3.2.2 Nanoparticle synthesis

3.2.2.1 Synthesis of FluPep functionalised nanoparticles

Mix matrix ligands 70:30 (mole:mole) CVVVT-ol: HS-$(CH2)_{11}$-EG_4-OH were prepared as described (Duchesne et al., 2008a) by first diluting 35 µL CVVVT-ol

(4 mM DMSO:H_2O) with 35 µL ddH_2O and 6 µL HS-C_{11}-EG_4-OH (2 mM) with 6 µL EtOH and 18 µL ddH_2O. Adding the two solutions together yielded a 2 mM ligand solution of 70% (mole/mole) CVVVT-ol and 30% (mole/mole) HS-C_{11}-EG_4-OH. The ligand mixture was added to 900 µL (gold or silver) nanoparticles and vortex-mixed. Once mixed, 100 µL of 10 x phosphate-buffered saline (PBS: 137 mM NaCl, 3 mM KCl l, 8 mM Na_2HPO_4, 15 mM KH_2PO_4) with Tween-20 (0.1 % v/v) pH 7.4 was added to gold nanoparticles (Duchesne et al., 2008a) and 10 x (100 mM $NaNO_3$, 20 mM HEPES (Free et al., 2012) with Tween-20 (0.1 % v/v) pH 7.4 to silver nanoparticles (Free et al., 2012), vortex mixed and the (gold or silver) nanoparticles placed on a rotating wheel for 24 h. Nanoparticles were concentrated 10-fold using 10 kDa Nanosep centrifugal filters (PALL Corp., Portsmouth, Hants, UK). Samples were then centrifuged for 7 min at 10000 rpm (~12,000 x g) and the gold nanoparticles diluted with 1 x PBST (PBS 0.05% (v/v) Tween-20) and silver nanoparticles with 1x (100 mM $NaNO_3$, 20 mM HEPES). The nanoparticles were then further separated from excess ligands by applying them (100 µL) to a 5 mL Sephadex G25 gel filtration column with PBS as a mobile phase.

To functionalise the nanoparticles with FluPep ligand, this was incorporated into the initial ligand mix at the mole % indicated in the figure legends. However, the separation of free FluPep ligand (Mw 2967 Da) required, in addition to the final gel-filtration on Sephadex G25, six washes, each wash involving a 10-fold dilution of the nanoparticles on a 10 kDa cut off Nanosep filter.

The concentration of FluPep ligand in a nanoparticle preparation was estimated in two ways: for low mole % of FluPep ligand, where the majority of the nanoparticles are determined to be functionalised with a single FluPep ligand, the nanoparticle

concentration was used as a proxy for FluPep ligand concentration, at higher mole % FluPep ligand, the number of peptidols incorporated into a 70:30 (mole/mole) mix matrix ligand shell of 8.8 nm gold nanoparticles (measured previously, 1200 peptidols, Duchense et al., 2008) was then multiplied by the mole % of FluPep ligand and by 1200. This latter estimate will deviate from actual concentration by the fraction of non-functionalised nanoparticles, since the functionalised nanoparticles are purified from the latter.

3.2.2.2 Ion-exchange chromatography

Ion-exchange chromatography were performed on homemade mini columns of diethylaminoethyl (DEAE) and carboxymethyl (CM) Sepharose (GE Healthcare Bio-Sciences AB, Sweden). The chromatography gel slurry was packed into a white pipette tip (200 µL) using half the filter as a frit and equilibrated in PBS. Capped nanoparticles were concentrated and exchanged into the appropriate buffer using a a 10 kDa cut off Nanosep centrifugal filter. The nanoparticles were then applied to the column, the unbound fraction was recovered. Columns were washed with PBS and eluted with 1 M NaCl and then 2 M NaCl in 8 mM Na_2HPO_4, 15 mM KH_2PO_4, pH 7.4.

3.2.2.3 Calculation of the aggregation parameter (AP)

The surface plasmon absorption peak of 8.8 nm diameter gold nanoparticles is at 520 nm. When gold nanoparticles are aggregated, their surface plasmons couple causing a red shift in their plasmon absorbance to approximately 650 nm. The aggregation parameter (AP) was defined as ($A_{650\ nm}$-$A_{ref\ 650nm}$)/ (A_{520nm}-$A_{ref\ 520}$), where A_{650nm} and A_{520nm} are the absorbance of gold nanoparticles at 650 nm and

520 nm, respectively, and $A_{ref650nm}$ and A_{ref520} are the absorbance of water at 650 nm and 520 nm, respectively (Chen et al., 2012). For comparison of results, this primary stability parameter was normalised by dividing the AP value of control ligand capped gold nanoparticles measured in milli Q water where [DTT] = 0.

For silver nanoparticles diameter of approximately 10 nm, the surface plasmon absorption peak with a mix matrix ligand shell is at 410 nm. The AP for silver nanoparticle was defined as $(A_{600\ nm}-A_{ref\ 600nm})/ (A_{410\ nm}-A_{ref\ 410})$, where A_{600nm} and A_{410nm} are the absorbance of Ag nanoparticles at 600 nm and 410 nm, respectively and $A_{ref\ 600nm}$ and $A_{ref\ 410}$ are the absorbance of water at 600 nm and 410 nm, respectively.

`

3.2.3 Results and Discussion

3.2.3.1 Stability of FluPep functionalised gold nanoparticles

The mix matrix ligand shell of 70:30 mole/mole peptidol and alkanethiol ethylene glycol assembled on gold nanoparticles has well characterised stability with respect to ligand exchange and non-specific binding (Duchesne et al., 2008a, Chen et al., 2012), but the effect of incorporating the FluPep amino acid sequence at the C-terminus of the CVVVT matrix sequence is unknown. Since the molecular weight of FluPep ligand (2967 Da) is greater than that required for group separation on Sephadex G25 (1000 Da) additional purification by means of washes on a 10 kDa cut off Nanosep filter were included to ensure removal of any free FluPep ligand. When up to 5% (mole/mole) FluPep ligand was incorporated in the ligand matrix, the gold nanoparticles still eluted in the void volume of the Sephadex G25 column, so did not bind non-specifically to this chromatography matrix and their UV-Vis spectrum in PBS was indistinguishable from that of control mix matrix gold nanoparticles (Fig. 3.1A). This indicates that the FluPep sequence did not reduce the stability of the gold nanoparticles under these standard conditions. A more stressful test is ligand exchange with small thiols (Chen et al., 2012, Duchesne et al., 2008a, Schulz et al., 2016, Schulz et al., 2013). Ligand-exchange results in a ligand shell that is unable to prevent electrolyte-induced aggregation of the nanoparticles, demonstrated by a decrease in the plasmon absorption at 520 nm.

Gold nanoparticles with a ligand shell incorporating 5% (mole/mole) FluPep ligand had a very similar resistance to ligand exchange with DTT as the control mix matrix protected gold nanoparticles. Thus, their aggregation parameter was unchanged up

to 5 mM DTT, even after 48 h incubation (Figs 3.1 B, C). At 10 mM DTT after 48 h there was some evidence for ligand exchange, as the aggregation parameter was above 1.0 and at 25 mM DTT the ligand shell was clearly compromised. Nanoparticles incorporating lesser amounts of FluPep ligand (0.1% to 3 % mole/mole) were no less stable (Figs S1A-F). Consequently, the incorporation up to 5% (mole/mole) FluPep ligand in the ligand mixture did not reduce the stability of the gold nanoparticles with respect to ligand exchange and such nanoparticles could be used in cell culture medium.

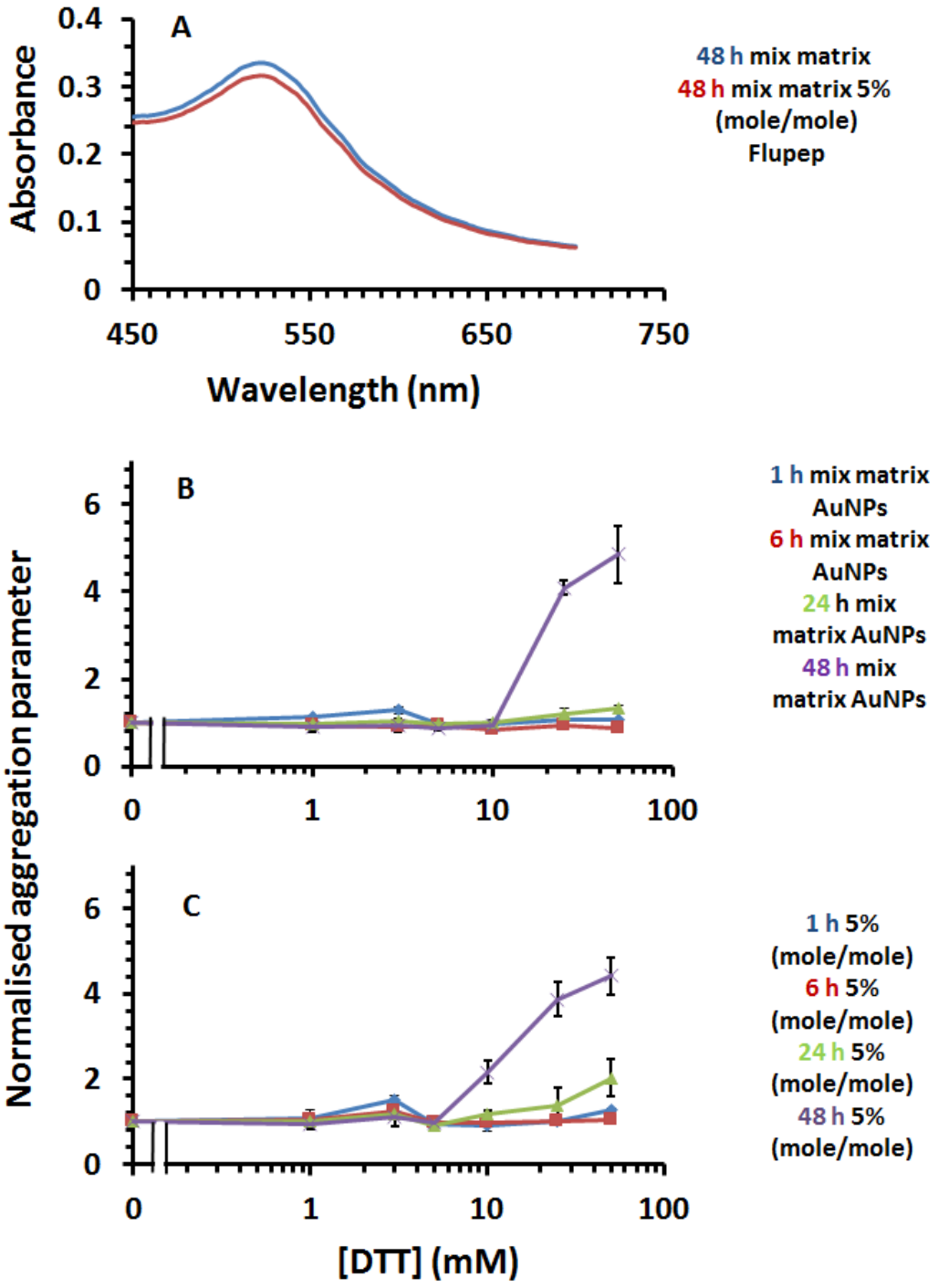

Fig. 3.1. Stability of gold nanoparticles to DTT ligand exchange (A) UV-Vis spectra of mix matrix capped gold nanoparticles and mix matrix capped gold nanoparticles incorporating 5% (mole/mole) Flu|Pep ligand in PBS. Time and dose-dependence of DTT ligand exchange for (B) mix matrix gold nanoparticles and for gold nanoparticles with a ligand shell incorporating 5% (mole/mole) FluPep ligand. Results in (b) and (C) are the mean ± SD (n=3).

`

3.2.3.2 Purification of functionalised gold nanoparticles

To functionalise the nanoparticles, the peptide FluPep ligand was included in the ligand mix, its mole % in relation to the matrix ligand reflects its grafting density on the gold nanoparticles (Levy et al., 2006a, Duchesne et al., 2008a, Duchesne et al., 2012, Free et al., 2012, Paramelle et al., 2015, Nieves et al., 2014). This can be determined by chromatography targeting specifically the grafted function, which also provides a means to purify the functionalised gold nanoparticles from those not functionalised, when the mole % of the functional ligand is low. Thus, when 10% of the functionalised gold nanoparticles bind to the chromatography column, most of these (95 %) will possess just one grafted functional ligand (Levy et al., 2006a, Duchesne et al., 2008a). Since FluPep ligand, like FluPep, has a net charge at pH 7.4 of +6, cation-exchange chromatography was used to purify functionalised gold nanoparticles. Parallel chromatography was performed on the anion-exchanger DEAE-Sepharose to control for possible non-specific binding of FluPep ligand to Sepharose.

Mix matrix gold nanoparticles did not to bind to either CM Sepharose or DEAE Sepharose (Fig. S2), as described previously (Duchesne et al., 2008a). Similarly, when FluPep ligand was incorporated in the ligand shell there was no binding to DEAE Sepharose, indicating an absence of non-specific interactions with the chromatography resin (Fig. S2). In contrast, the FluPep functionalised gold nanoparticles bound to CM Sepharose and were eluted by increasing electrolyte concentrations (Fig. 3.2). Thus, the FluPep functionalised gold nanoparticles ion-exchanged on this chromatography support, which is, therefore, suitable for their

purification. Gold nanoparticles were synthesised with a range of mole % of FluPep ligand. After application of the gold nanoparticles to the column, the non-functionalised gold nanoparticles were collected in the flow through and the functionalised ones eluted. Quantification of the gold nanoparticles by UV-Vis spectrophotometry then allowed the relation of bound and unbound gold nanoparticles to the mole % of FluPep in the original ligand mixture to be analysed. The data indicate that at 0.03 mole %, 10 % of the gold nanoparticles bound the column and thus most (~95 %) of these gold nanoparticles will possess just a single FluPep ligand (Levy et al., 2006a). At higher mole % the number of FluPep ligands per nanoparticle will increase. It is interesting to note that not all gold nanoparticles were observed to bind to the CM Sepharose column at higher mole % of FluPep ligand, something that has been observed previously with other functional peptides (Nieves et al., 2014, Paramelle et al., 2015).

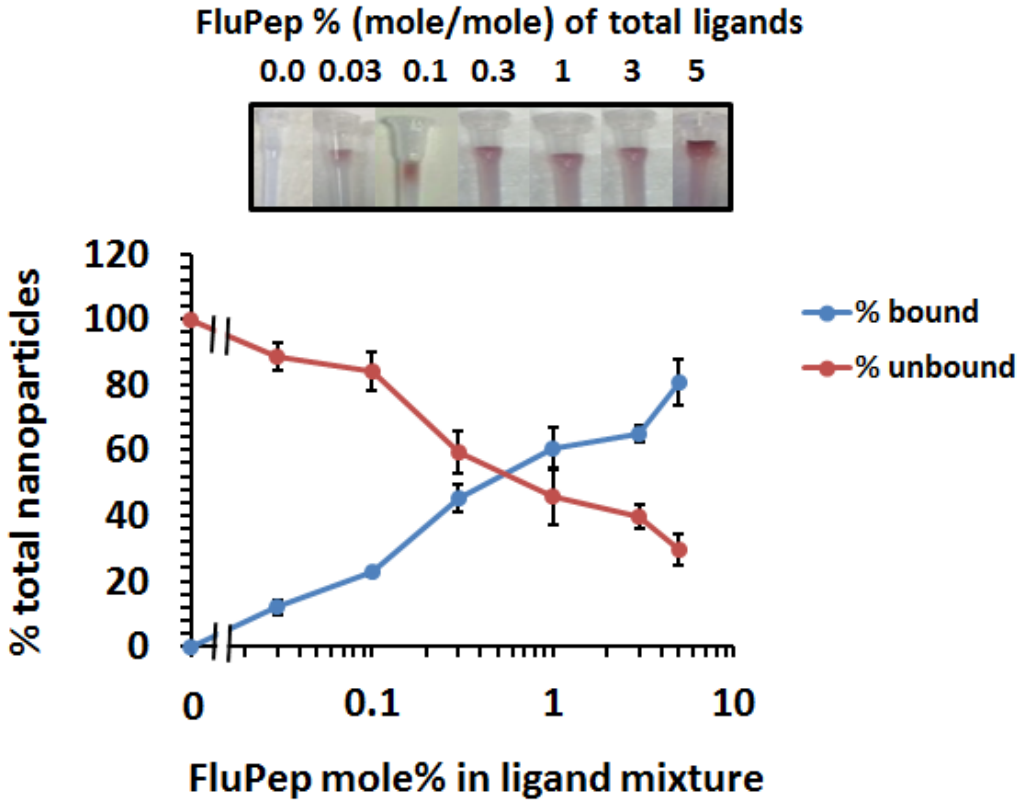

Fig. 3.2. Purification of FluPep ligand functionalised gold nanoparticles by CM-Sepharose cation-exchange chromatography. Gold nanoparticles functionalised with different mole % FluPep ligand were subjected to chromatography on CM-Sepharose. Top, images of columns after loading and washing with PBS. Bottom, quantification by absorption at 450 nm (Haiss et al., 2007) of unbound (through and PBS wash fractions) and bound (eluted with 2 M NaCl) fractions. Results are the mean ± SD (n=3).

3.2.3.3 Anti-flu activity of FluPep and FluPep ligand

The MDCK are susceptible to both influenza type A and B viruses and are routinely used to measure 'flu virus infectivity. The principle is that following virus binding, virus will infect a cell, reproduce and lyse that cell; released virus then infects neighbouring cells, the overlay preventing long-range diffusion of virus. After three days, the area of lysed cells is visualised as a plaque that does not stain with toluidine blue. In control (no virus) and vehicle (DMSO) treated cells, the cell

monolayer in the well was evenly stained (Fig. S3). In the presence of virus, there were substantial areas where cells had lysed and there was no staining. Virus titre was adjusted so that the cleared lysed cell areas corresponded to individual plaques, i.e., clear circles that could be distinguished from one another and so counted (corresponding to ~100 plaques/well). In the presence of FluPep there was a reduction in the number of plaques and this was concentration-dependent (Fig 3.4, A). Counting plaques in multiple experiments allowed the determination of the dose-response and the IC_{50}. In these experiments the IC_{50} of the original FluPep sequence was found to be of the order of 140 pM (Fig. 3.3). This is less potent than described in the original publication, where an IC_{50} of 14 pM was measured. The source of this discrepancy is unknown, but more than likely relate to differences in cells such as passage number, and/or virus preparations. The FluPep ligand, used to functionalise gold nanoparticles was slightly less potent, with an IC_{50} of around 210 pM, suggesting that the N-terminal extension CVVVTAA reduced the antiviral activity somewhat (Fig 3.3 and Table 3.1).

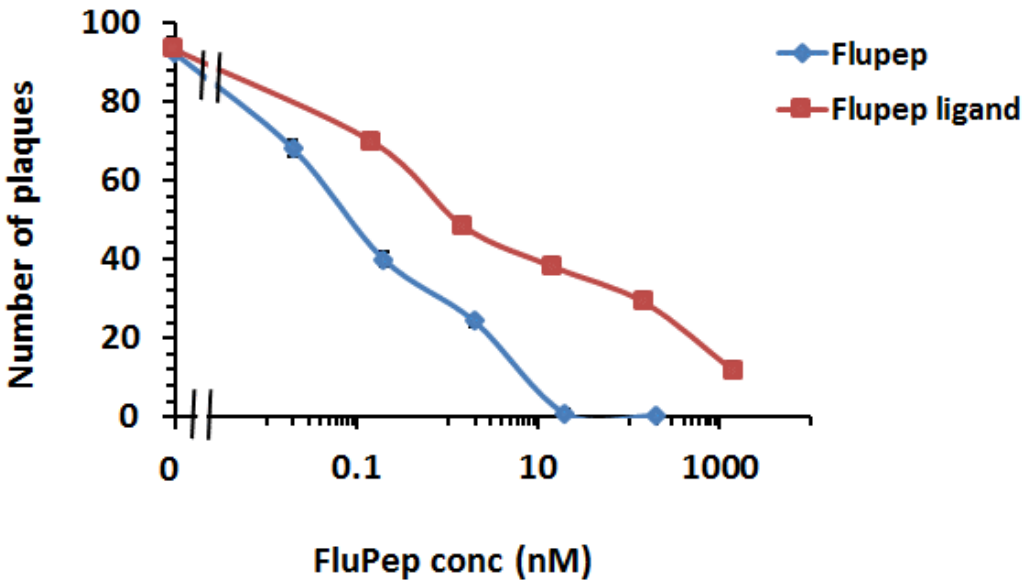

Fig. 3.3: Determination of the half maximal inhibitory concentration (IC_{50}) of FluPep and and FluPep ligand in a plaque assay. Results, demonstrated that FluPep IC_{50} less than FluPep ligand, this might be due to the incorporation of the CVVVTAAA- extension.Results are the mean ±SD (n=3).

Table 3.1: (IC_{50}) of FluPep and FluPep ligand.

FluPep	**IC_{50} nM**
FluPep	0.14
FluPep ligand	2.1

3.2.3.4 Anti-flu activity of FluPep functionalised gold nanoparticles

The addition of control mix matrix passivated nanoparticles had no detrimental effect on viral infectivity, since their addition to the cells did not change the number of plaques (Fig. 3.4A). However, when purified mix matrix capped gold nanoparticles functionalised with 5 % (mole/mole) FluPep ligand were added, there

was a marked decrease in the number of plaques, i.e. reduced virus infectivity (Fig. 3.4A). Thus, FluPep ligand antiviral activity was maintained when it was conjugated to gold nanoparticles.

For gold nanoparticles functionalised with 0.03% (mole/mole) FluPep ligand, the number of plaques started to decrease at 20 pM gold nanoparticles and reached a minimum of approximately two to eight plaques at 200 pM (Fig. 3.4B). As the grafting density of FluPep ligand was increased, so did the antiviral activity, to reach a maximum at 5 % (mole/mole) FluPep (Fig. 3.4B). This is reflected by the decreased IC_{50}, which shows a 4.5-fold greater potency of nanoparticles functionalised with 5 % (mole/mole) FluPep ligand, when compared to nanoparticles functionalised with just 0.03 % (mole/mol) FluPep ligand (Table 3.2). The nanoparticles were always purified by cation-exchange chromatography (Fig. 3.2), so in all cases nanoparticles had at least one FluPep ligand. When most nanoparticles have just a single FluPep ligand (0.03 % and 0.1 % mole/mole, Fig. 3.2), the nanoparticle concentration is a reasonable proxy for FluPep ligand concentration. Taken together, these data indicate that the potency of FluPep ligand on the nanoparticles is greater than that of free FluPep and of the native FluPep peptide (Tables 3.1 and 3.2).

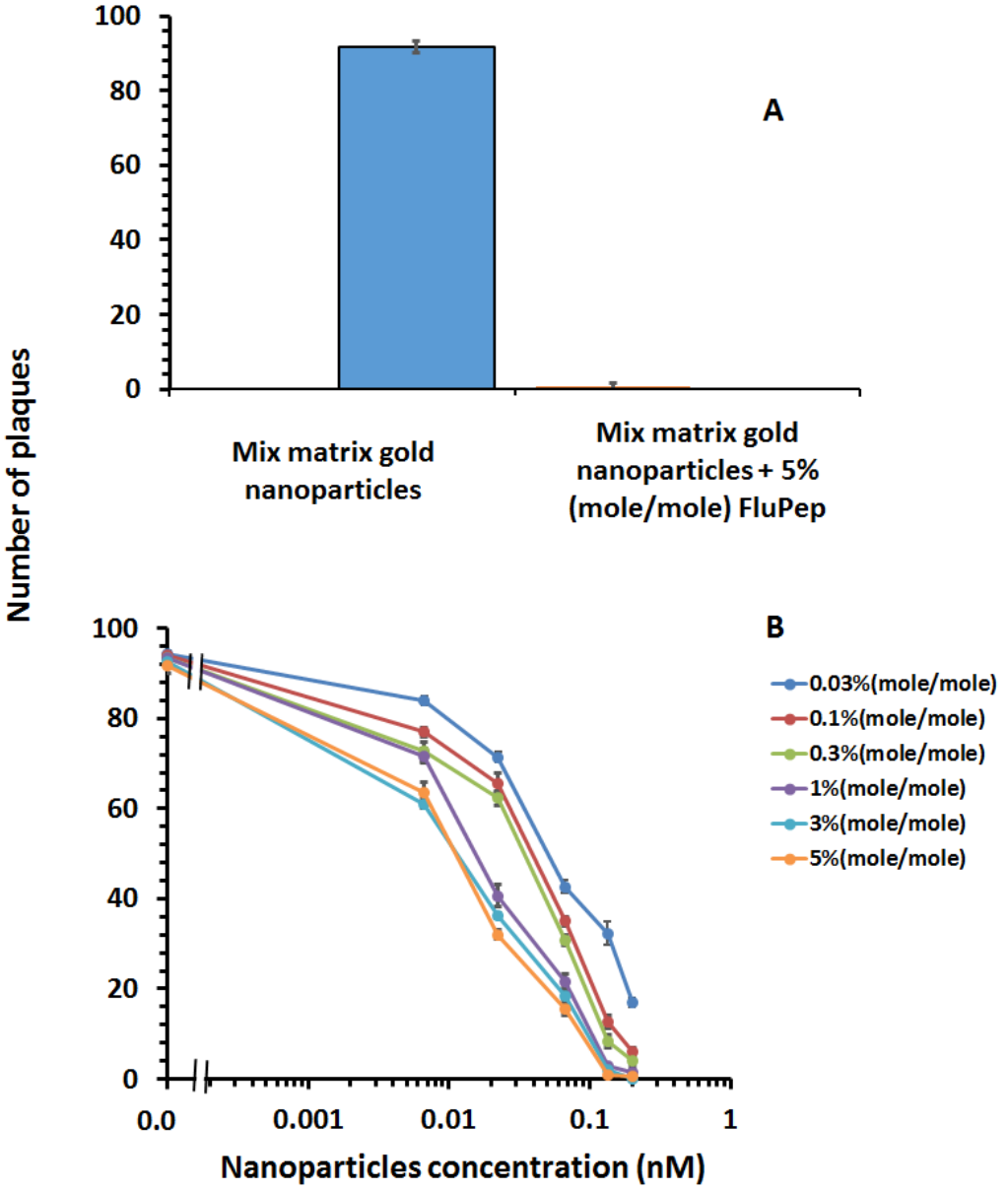

Fig. 3.4. Effect of gold nanoparticles functionalised with FluPep ligand on influenza virus plaque formation. (A) Number of plaques observed in the presence of mix matrix control gold nanoparticles and gold nanoparticles functionalised with 5 % (mole/mole) FluPep ligand. (B) Dependence of inhibition of plaque formation on the concentration of gold nanoparticles and the % (mole/mole) of FluPep ligand. Results and the mean ±SD (n=3). Error bars may be smaller than the symbol

Table 3.2: (IC_{50}) of different mole% of FluPep ligand with respect to gold nanoparticle concentration.

Mole % FluPep ligand	**IC_{50} nM**
0.03	0.073
0.1	0.068
0.3	0.058
1	0.023
3	0.016
5	0.015

3.2.3.5 Stability of FluPep functionalised silver nanoparticles

Silver has well-established anti-microbial properties. It was of interest to determine whether FluPep functionalised silver nanoparticles possessed a similar anti-flu activity to their gold counterparts. The mix matrix ligand shell has been shown to impart good stability to silver nanoparticles (Free et al., 2012). First, the effect of incorporating FluPep into the ligand shell on nanoparticle stability was measured. As for gold nanoparticles, up to 5% (mole/mole) FluPep ligand incorporated into the ligand matrix had no discernible effect on the handling and purification of the silver nanoparticles: the silver nanoparticles did not bind non-specifically to Sephadex G25, as they eluted in the void volume and their UV-Vis spectrum in PBS was indistinguishable from that of control mix matrix silver nanoparticles (Fig. 3.5A). When challenged by a small thiol, DTT, the silver nanoparticles passivated

by the mix matrix ligand shell were somewhat more prone to ligand exchange than their gold counterparts. Thus, after 3 h and 6 h in 50 mM DTT a small increase in aggregation parameter was apparent (Fig. 3.5B). After 24 h and 48 h, the aggregation parameter started to rise at 3 mM DTT, which was most pronounced at 48 h. Importantly, the inclusion of 5% (mole/mole) FluPep ligand in their ligand shell did not change the stability of the silver nanoparticles with respect to DTT-mediated ligand exchange (Fig. 3.5C).

Purification of the FluPep functionalised silver nanoparticles was achieved by cation-exchange chromatography on CM-Sepharose. As the percentage of FluPep incroprated into the ligand shell increased, so did the percentage of nanoparticles bound to CM-Sepharose (Fig. 3.6). This suggests that the mole % FluPep ligand in the initial mixture of ligands added to the nanoparticles reflects its incorporation into the ligand shell (Levy et al., 2006a, Duchesne et al., 2008a). Thus, as for gold nanoparticles, when 10 % of the total nanoparticle preparation bound to the CM-Sepharose column, ~95% of the bound nanoparticles will possess a single FluPep ligand (Levy et al., 2006a); at higher mole % of FluPep ligand and increasing proportion of the silver nanoparticles will incorporate more than one FluPep ligand.

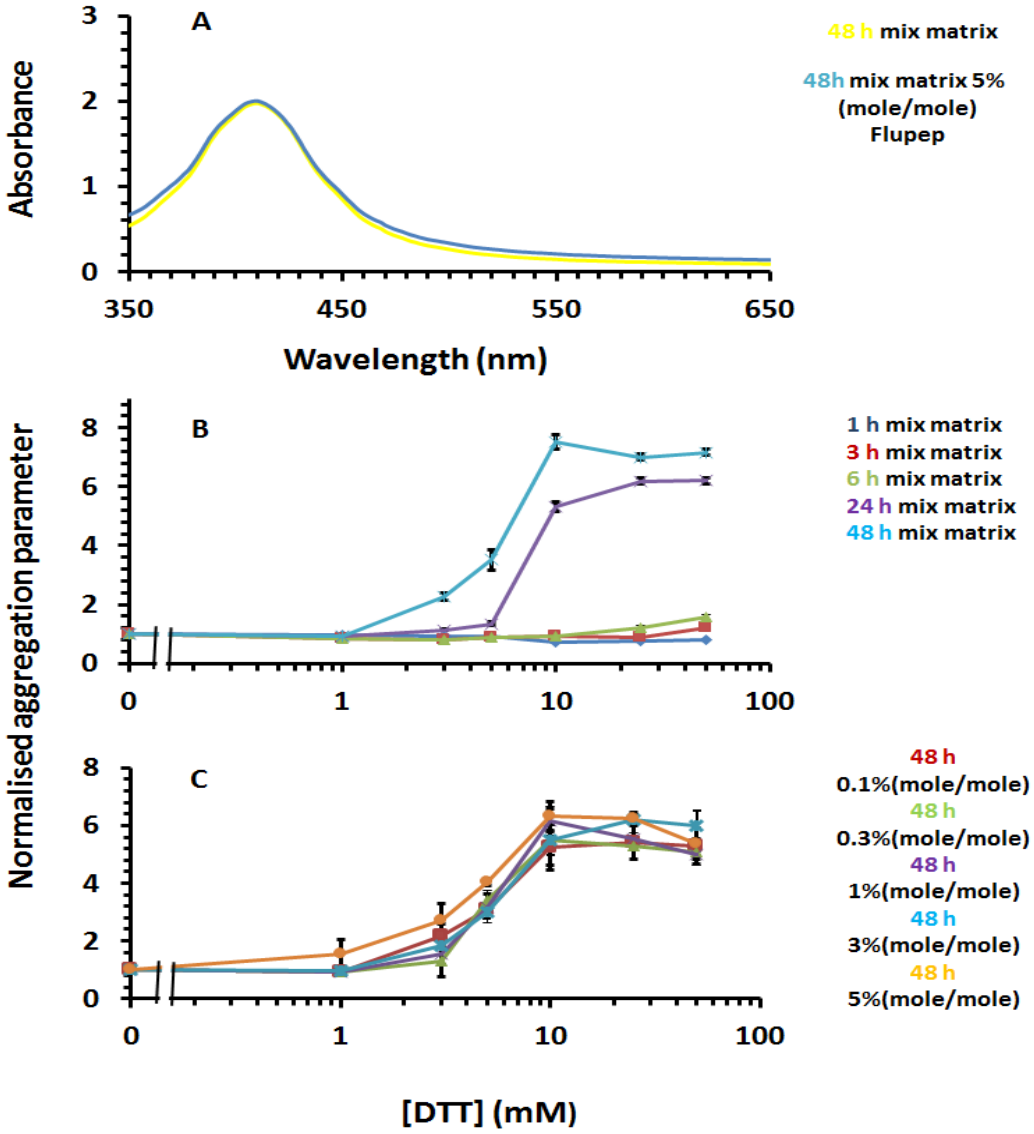

Fig. 3.5. Stability of silver nanoparticles to DTT ligand exchange. (A) UV-Vis spectra of mix matrix capped silver nanoparticles and mix matrix capped silver nanoparticles incorporating 5% (mole/mole) Flu|Pep ligand in PBS. Time and dose-dependence of DTT ligand exchange for (B) mix matrix silver nanoparticles and (C) silver nanoparticles incorporating different mole % FluPep ligand. Results are the mean ± SD (n=3).

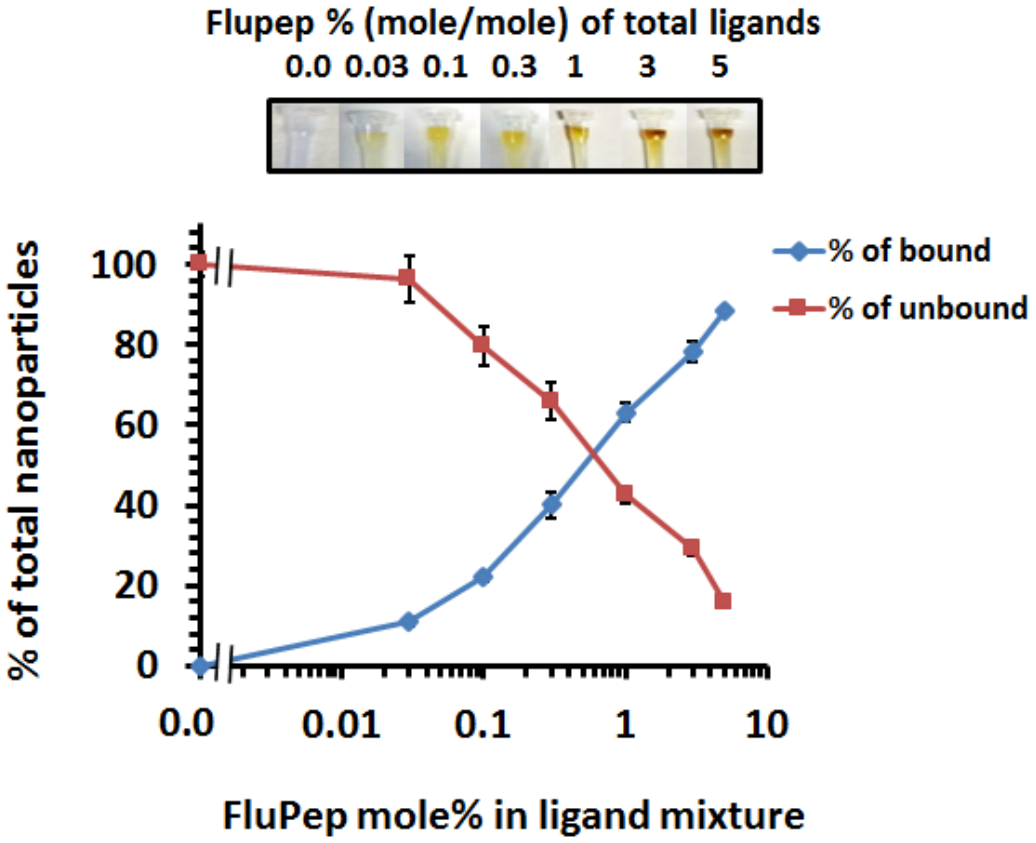

Fig. 3.6. Purification of FluPep ligand functionalised silver nanoparticles by CM-Sepharose cation-exchange chromatography. Silver nanoparticles functionalised with different mole % FluPep ligand were subjected to chromatography on CM-Sepharose. Top, images of columns after loading and washing with PBS. Bottom, quantification of unbound (through and PBS wash fractions) and bound (eluted with 2 M NaCl) fractions. Results are the mean ± SD (n=3).

3.2.3.6 Anti-flu activity of FluPep ligand incorporated to silver nanoparticles

Control mix matrix passivated silver nanoparticles had no effect on viral infectivity (Fig. 7). It is the silver (Ag^{+}) ions that exert anti-microbial activity (Hsueh et al., 2015). Thus, this result indicates that there is not a substantial release of Ag^{+} ions from the silver nanoparticles during the experiment. This concurs well with our data (Fig. 3.5) and previously reported observations (Free et al., 2012) demonstrating

that the mix matrix ligand shell imparts good stability to the silver nanoparticles. Incorporation of FluPep ligand into the mix matrix ligand shell caused a marked reduction in number of plaques (Fig. 3.7). As the mole % of FluPep ligand in the ligand shell increased, so did the antiviral activity of these particles (Fig. 3.7 and Table 3.4). Around 10% of silver nanoparticles functionalised with 0.03 % (mole/mole) FluPep ligand bind to the CM-Sepharose column, indicating that the majority of these will carry just a single FluPep ligand (Fig. 3.6), so the nanoparticle concentration will equate to the FluPep ligand concentration. These nanoparticles are as potent as free FluPep and more potent than free FluPep ligand (Tables 3.1 and 3.3). However, FluPep ligand functionalised silver nanoparticles were less effective at inhibiting influenza virus infectivity than the corresponding gold nanoparticles (Tables 2 and 4). At higher mole % FluPep ligand (≥0.1 % mole/mole) many, if not all nanoparticles, will be functionalised with two or more FluPep ligands. As for gold nanoparticles, the nanoparticle concentration will no longer equate to the FluPep ligand concentration.

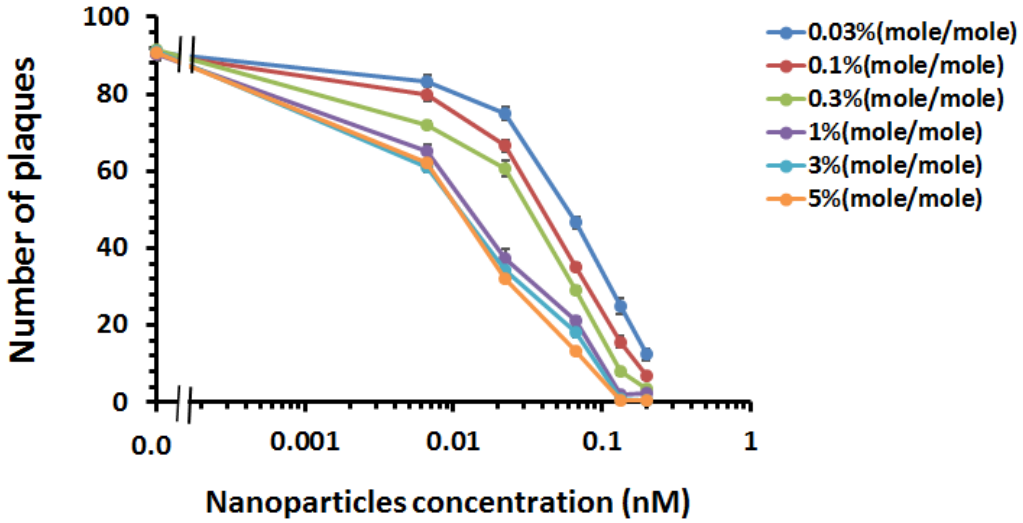

Fig. 3.7. Determination of the half maximal inhibitory concentration (IC_{50}) of silver nanoparticles functionalised with FluPep ligand. Dependence of inhibition of plaque formation on the concentration of silver nanoparticles and the % (mole/mole) of FluPep ligand. Results and the mean ±SD (n=3).

Table 3.3: (IC_{50}) of silver nanoparticles functionalised with different mole % FluPep ligand.

Mole % FluPep ligand	**IC_{50} nM**
0.03	0.14
0.1	0.077
0.3	0.056
1	0.019
3	0.016
5	0.015

`

3.2.4 Conclusion

Influenza viruses pose a substantial danger to global health, because of susceptibility of these viruses to rapid mutations in their genomes, ease of transmission via the respiratory route, and availability of animal reservoirs. Currently, the preventative and remedial therapies against these viruses are inadequate. In the current study, we have functionalised nanoparticles with FluPep, a peptide demonstrated to inhibit influenza A virus subtypes, including H1N1, H3N2 and H5N1(Nicol et al., 2012b). Monofunctionalised nanoparticles-FluPep were more active that free peptide. These data highlight that a nanoparticle formulation of such peptide inhibitors of 'flu virus may be particularly effective. Purification of the functionalised nanoparticles by cation-exchange chromatography indicated that the FluPep ligand sequence was exposed to solvent, rather than associated with the mix matrix ligand shell, a conclusion supported by the observation that the gold and silver nanoparticle FluPep ligand conjugates possessed antiviral activity. At low stoichiometries of FluPep ligand: nanoparticle conjugation, the potency of the FluPep ligand is enhanced compared to that of the free peptide. The FluPep amino acid sequence is hydrophobic and its solubilisation requires dimethyl sulfoxide (DMSO). Although a useful solvent, its use in therapies is problematic due to DMSO potential adverse reactions in some individuals such as a sensation of burning, vesiculation, dryness of skin and local allergic reactions (Cavaletti et al., 2000, Delatorre et al., 1981, Worthley and Schott, 1969). Thus, conjugation to nanoparticles may provide a means to deliver effectively and safely FluPep ligand with enhanced activity in a solvent-free formulation. Though the mix matrix ligand shell prevents the dissolution of the silver, its modification will reduce

its effectiveness (Free et al., 2012). Thus, it will be possible to design silver nanoparticles that act through FluPep ligand and released Ag^+ ions. The pulmonary route to deliver drugs against respiratory infections is well established, therefore, delivery of functionalised nanoparticles against ‘flu viruses is highly feasible. In conclusion, nanoparticle formation of FluPep ligand or analogous peptides offers a route to new treatments for ‘flu and other respiratory pathogens.

`

3.2.5 Supplementary information

Table of contents **Page**

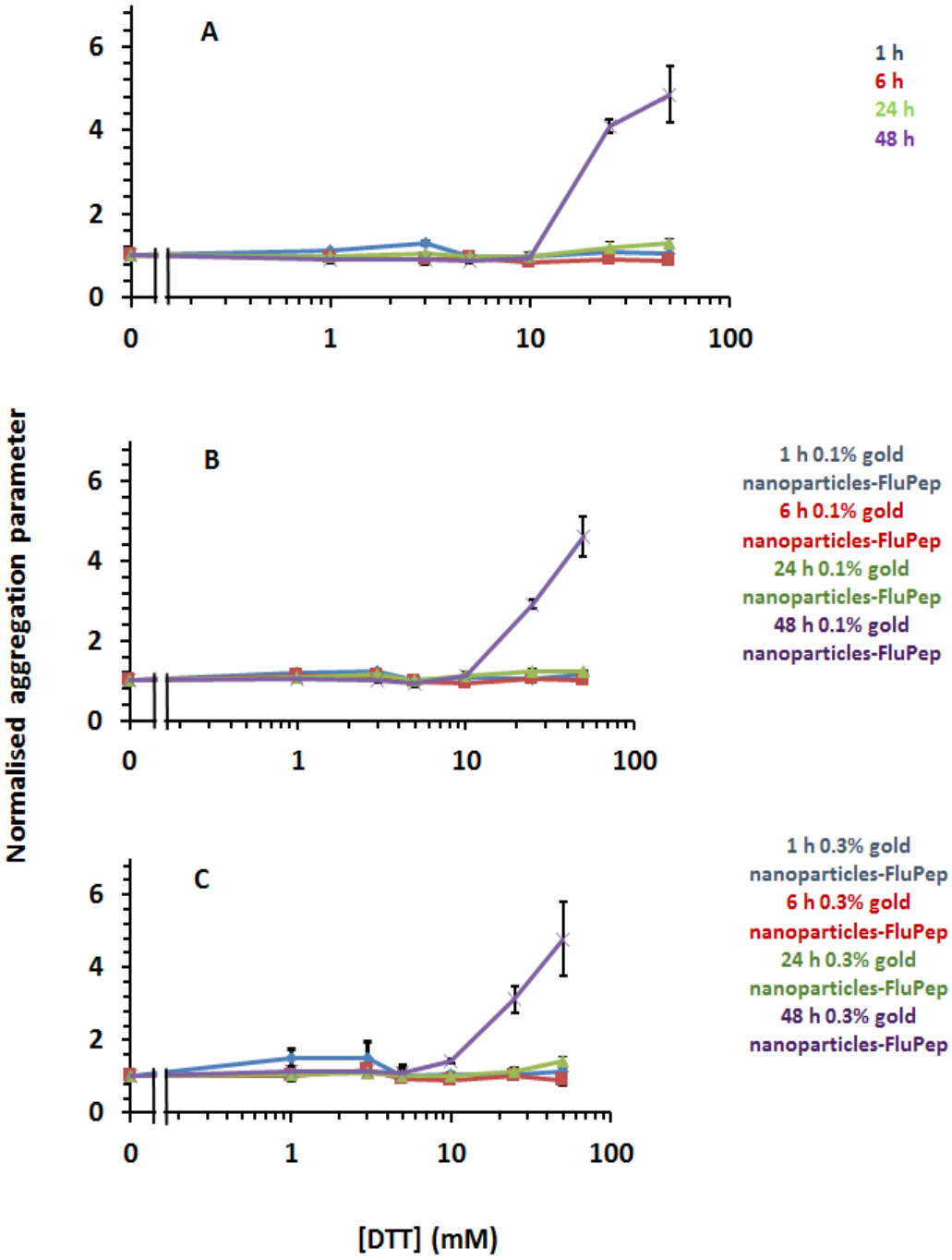
A
B
C
Normalised aggregation parameter
[DTT] (mM)
0
2
4
6
0
1
10
100
1 h
6 h
24 h
48 h
1 h 0.1% gold nanoparticles-FluPep
6 h 0.1% gold nanoparticles-FluPep
24 h 0.1% gold nanoparticles-FluPep
48 h 0.1% gold nanoparticles-FluPep
1 h 0.3% gold nanoparticles-FluPep
6 h 0.3% gold nanoparticles-FluPep
24 h 0.3% gold nanoparticles-FluPep
48 h 0.3% gold nanoparticles-FluPep

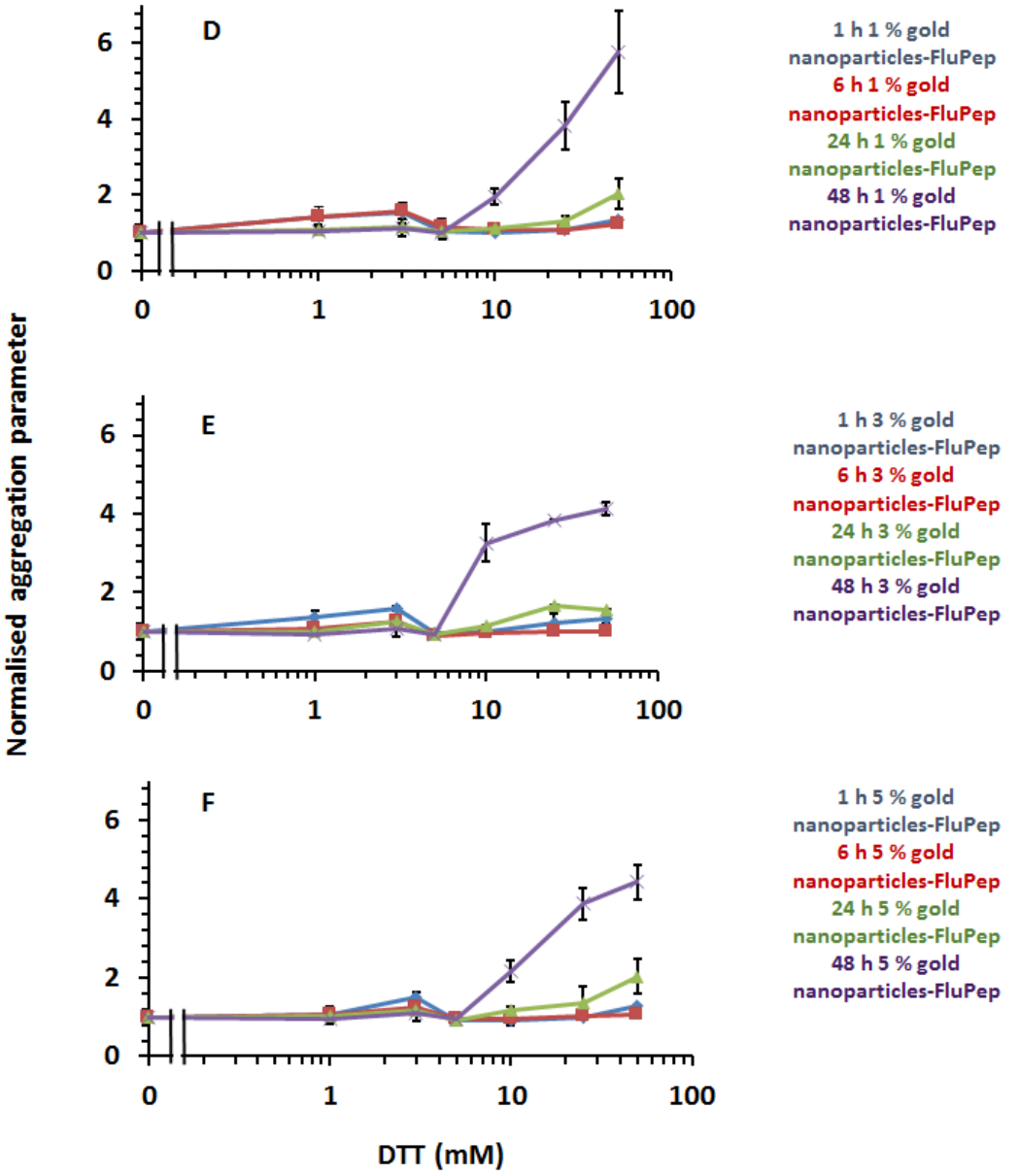

Fig. S1. Stability of gold nanoparticles functionalised with FluPep ligand. Gold nanoparticles incorporating different % (mole/mole) FluPep ligand in their ligand shell were incubated in varying concentrations of DTT for different times and the normalised aggregation parameter was calculated. A 70:30 CVVVT-ol HS-$(CH2)_{11}$-EG_4-OH mix matrix gold nanoparticles. B 0.1% (mole/mole) FluPep ligand functionalised gold nanoparticles. C 0.3% (mole/mole) FluPep ligand functionalised Gold nanoparticles. D 1 %(mole/mole) FluPep ligand functionalised gold nanoparticles. E 3% (mole/mole) FluPep ligand functionalised gold nanoparticles. F 5 % (mole/mole) FluPep ligand functionalised gold nanoparticles. Results are the mean ± SD (n=3).

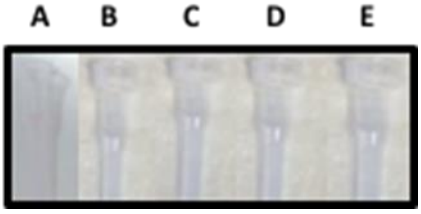

Fig. S 2. CM-Sepharose and DEAE-Sepharose chromatography of gold nanoparticles. Gold nanoparticles were applied to mini columns of CM- and DEAE-Sepharose, as described in Materials and Methods in 20 mM Tris HCl (pH7.2) and the column washed with PBS. (A) Mix matrix gold nanoparticles applied to DEAE Sepharose. (B) Mix matrix gold nanoparticles applied to CM Sepharose. (C) Mix matrix gold nanoparticles functionalised with 0.3% (mole/mole) FluPep ligand applied to DEAE Sepharose (D) Mix matrix gold nanoparticles functionalised with 3% (mole/mole) FluPep ligand applied to DEAE Sepharose. (E) Mix matrix gold nanoparticles functionalised with 5% (mole/mole) FluPep ligand applied to DEAE Sepharose. In all cases the nanoparticles failed to bind to the ion-exchange column. This demonstrates that mix matrix passivated nanoparticles do not bind to CM- or DEAE-Sepharose and that when these nanoparticles are functionalised with FluPep ligand, they fail to bind to DEAE-Sepharose.

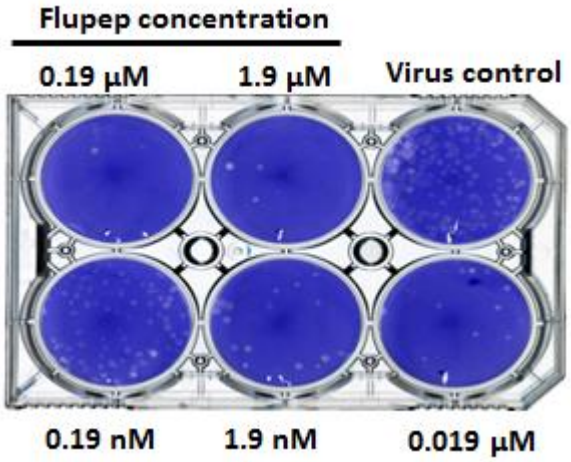

Fig. S 3: Example of a plaque assay. A confluent monolayer of MDCK cells was infected with influenza virus at varying dilutions and covered with an agarose overlay, to prevent the virus infection from spreading indiscriminately, as described in Materials and Methods. Virus plaques are the cleared circles, e.g., arrow. A viral plaque is formed when a virus infects a cell within the fixed cell monolayer. The virus infected cell will lyse and spread the infection to adjacent cells where the infection-to-lysis cycle is repeated. Here, the ability of FluPep to inhibit replication of WSN virus (~100 plaques per well in control) was determined. Assays were carried out with virus in the presence of vehicle (DMSO, 1.5% final concentration), or virus in the presence of increasing concentrations of FluPep. Concentrations of FluPep are shown.

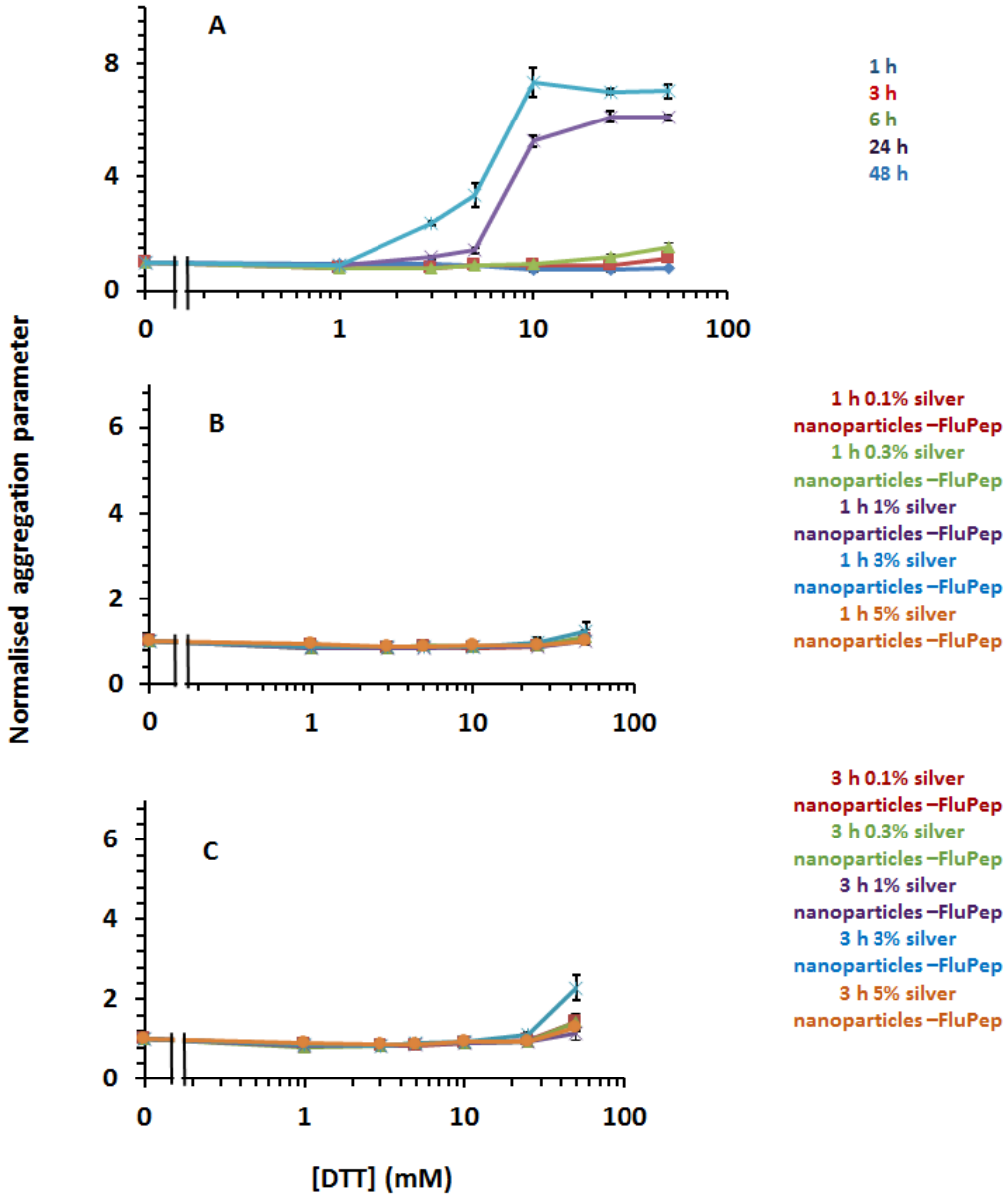
A
B
C
Normalised aggregation parameter
[DTT] (mM)
1 h
3 h
6 h
24 h
48 h
1 h 0.1% silver nanoparticles –FluPep
1 h 0.3% silver nanoparticles –FluPep
1 h 1% silver nanoparticles –FluPep
1 h 3% silver nanoparticles –FluPep
1 h 5% silver nanoparticles –FluPep
3 h 0.1% silver nanoparticles –FluPep
3 h 0.3% silver nanoparticles –FluPep
3 h 1% silver nanoparticles –FluPep
3 h 3% silver nanoparticles –FluPep
3 h 5% silver nanoparticles –FluPep

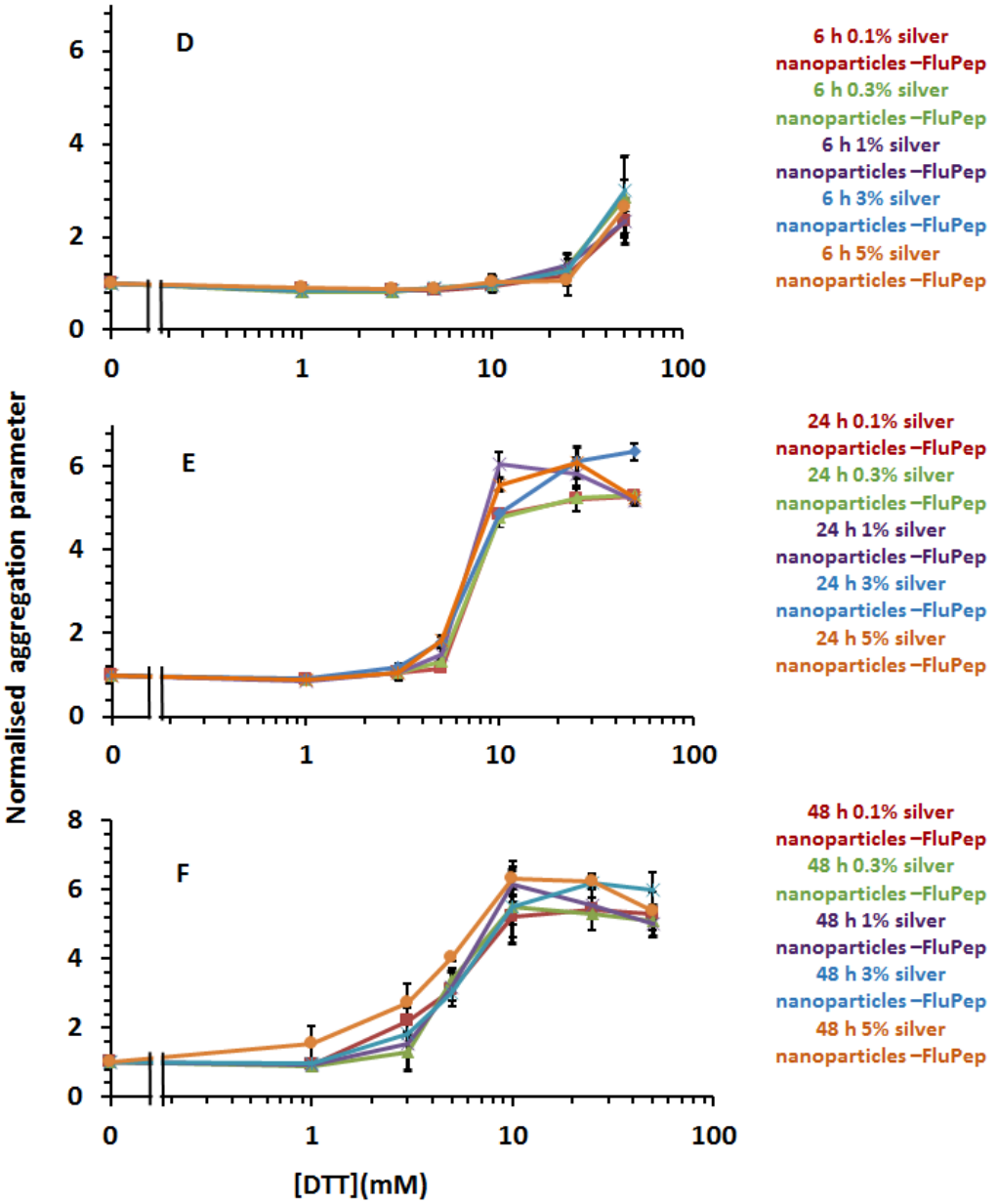

Fig. S 4: Stability of silver nanoparticles functionalised with FluPep ligand. Silver nanoparticles incorporating different % mole/mole FluPep ligand in their ligand shell were incubated in varying concentrations of DTT for different times and the normalised aggregation parameter was calculated. A 70:30 CVVVT-ol HS-$(CH2)_{11}$-EG_4-OH mix matrix silver nanoparticles. B 0.1% (mole/mole) FluPep ligand functionalised silver nanoparticles. C 0.3% (mole/mole) FluPep ligand functionalised silver nanoparticles. D 1 % (mole/mole) FluPep ligand functionalised silver nanoparticles. E 3% (mole/mole) FluPep ligand functionalised silver nanoparticles. F 5 % (mole/mole) FluPep ligand functionalised silver nanoparticles. Results are the mean ± SD (n=3).

`

3.3 Positive control for gold nanoparticles functionalisation

FluPep and FluPep ligand are effective at very low concentrations (Table 3.1). There is a high concentration of Flupep ligand in the ligand mixture (Section 2.3.1). Therefore, it was important to demonstrate that the purification of FlupPep ligand functionalised nanoparticles from free ligand (Section 2.2.4) not incorporated into the ligand shell was effective. Gold nanoparticles with 5% (mole/mole) FluPep ligand and in parallel a mock reaction control of 5% (mole/mole) FluPep ligand mixed with the standard mix matrix 70% CVVVTol: 30% HS-$(CH2)_{11}EG_4$ in the absence of gold nanoparticles were prepared. These were subjected to the standard purification procedure (Section 2.2.4). Then the antiviral activity of the retentate was measured. In the case of the FluPep ligand functionalised nanoparticles, the antiviral activity of the retentate was considerable, as expected (Fig. 3.3). However, for the mock reaction control, the number of plaque remained nearly the same as the viral control untreated with FluPep ligand which is about ~ 87 plaques (Fig. 3.3). The ligand only mixture was not subjected to Sephadex G25 chromatography, which will remove some of the Flupep ligand. Thus, any residual activity in this sample represents the upper limit for a contribution to the inhibitory activity in the nanoparticle sample form free FluPep ligand. These results demonstrate that the antiviral activity observed with FluPep functionalised nanoparticles is indeed due to Flupep ligand conjugated to the nanoparticles rather than free FluPep ligand carried over from the ligand hell synthesis step.

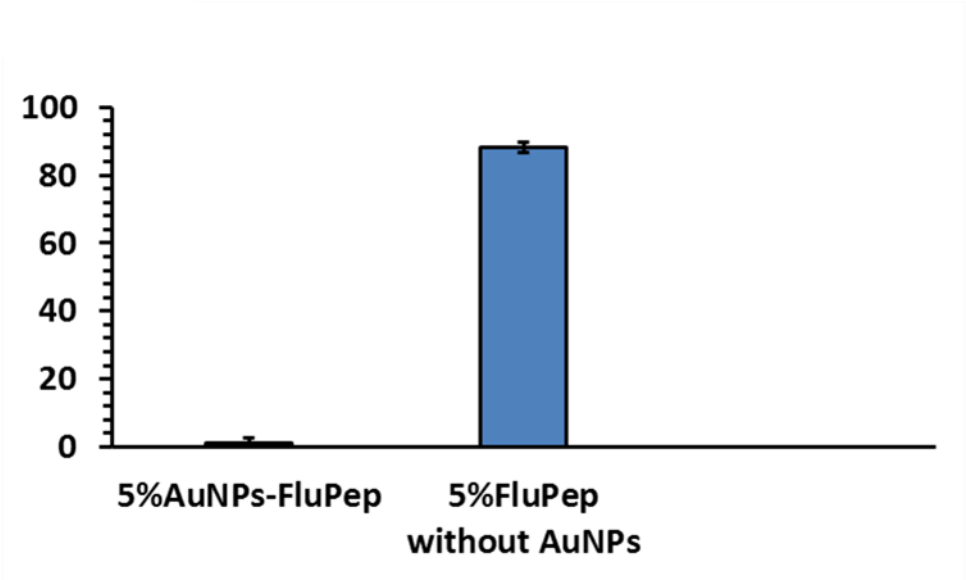

Fig. 3.3: Measurement of the effectiveness of the separation of free Flupep ligand from gold nanoparticles. Gold nanoparticles were functionalised with 5% (mol/mole) FluPep ligand and a mock functionalisation, containing ligands but no nanoparticles were subjected to purification by centrifugation on a 10 kDa nanosep filter. The antiviral activity of the retentates was measured. Results are the mean ±SD of three measurements.

3.4 Discussion

It was demonstrated by (Nicol et al., 2012b), that FluPep inhibited influenza virus infectivity in cell and animal models (Section 1.5.2.3). In this chapter gold and silver nanoparticles were functionalised with Flupep ligand and some of their properties measured. As described in this section, the incorporation of up to 5% mole/mole Flupep ligand in the nanoparticles does not affect their stability, measured by non-specific interaction with Sephadex and Sepharose, DEAE and ligand exchange with DTT. When incorporated into the nanoparticle ligand shell. FluPep ligand retains its anti-viral activity.

The nanoparticle probe appears to have no effect on viral infectivity. Thus, the observation that nanoparticles functionalised with FluPep retain the antiviral activity of the peptide means that such nanoparticle can be used to probe the mechanism of action of FluPep. This opens the way to use a similar approach for other antiviral peptides. As noted in (Section 1.5.2.3) for Flupep the experiments that led to the conclusion that it interact with HA are not entirely convincing. This relates to a simple problem: how to detect a peptide at low concentration in a biological system. Nanoparticles provide one means to achieve this (Section 1.4). Consequently, the work in this chapter provides a strategy to the wider community engaged in the identification and functional analysis of peptides that inhibit virus infectivity, some of which were described in (Sections 1.5.1 and 1.5.2.1).

3.5 Conclusion

Gold and silver nanoparticles were passivated with mix matrix and functionalised with FluPep. Purification and stability assays demonstrated that FluPep didn't alter the stability of the gold and silver gold nanoparticles. However, silver nanoparticles were somewhat less stable than gold ones. Only nanoparticles functionalised with FluPep showed antiviral activity. Moreover, conjugation to nanoparticles enhanced considerably the antiviral activity of FluPep.

`

Chapter 4

4.1 Introduction

In Chapter 3, the successful incorporation of FluPep into the ligand shell of gold and silver nanoparticles was demonstrated and these nanoparticles possessed strong antiviral activity. There remains an important question relating to FluPep: what is the mechanism of its antiviral action? Knowing its molecular targets would allow hypotheses to be tested and potentially the design of novel peptides with even greater antiviral activity. Gold nanoparticles can be detected with high sensitivity by a variety of means, due to their plasmon resonance (Section 1.4.2). In this chapter advantage is taken of detection of the gold nanoparticles by UV-Vis spectrometry to establish what the target of FluPep may be: virus, cell surface molecule or both. In this way the association of the gold nanoparticle-peptide conjugates with cells was measured directly, by UV-Vis spectrophotometry, and indirectly as the antiviral activity with the plaque assay. This is complemented by selective treatments of cells to identify the classes of molecules that FluPep binds to. Finally, the importance of the association of FluPep with extracellular anionic polysaccharides was tested by using peptides with a FluPep sequence and a variety of extensions, designed to increase interactions with extracellular matrix polysaccharides.

4.2

An anti-‘flu peptide that interacts with sulfated glycosaminoglycans

Section 3.2 is a manuscript in preparation

`

4.2.1 Materials & methods

4.2.1.1 Materials

4.2.1.2 Peptides and gold nanoparticles

Peptides FluPep WLVFFVIFYFFRRRKK, FluPep ligand CVVVTAAAWLVFFVIFYFFRRRKK, super FluPep 1 CVVVTAAARRPKGRGKRRREKQRWLVFFVIFYFFR, super FluPep 2 CVVVTAAARGAPRRGQRTRRKNKWLVFFVIFYFFR, CVVVTAAARRKK, and the ligand shell matrix peptidol CVVVT-ol were purchased from Peptide Protein Research (PPR Ltd, Hampshire, UK) (Table 4.1). The alkethiol ethylene glycol ligand, HS-EC_{11}-EG_4, was purchased from Prochimia (ProChimia Surface Sp. z o.o., Sopot, Poland). Gold nanoparticles of 9 nm diameter stabilized in citrate buffer were purchased from British Biocell (BBInternational Ltd, UK). Nanosep filters 10 kDa cut off were from PALL (PALL Corp., Portsmouth, Hants, UK). UV-Vis spectra (2 nm incremental steps) were measured using a SpectraMax Plus spectrophotometer (Molecular Devices, Wokingham, UK) and 384 well plates from Corning (Lowell, US) and the concentration of gold nanoparticles was determined at 450 nm (Haiss et al., 2007).

`

Table 4.1. Peptide names, amino acid sequences and their molecular weight

Peptide name	Amino acid sequence	MW (Da)
FluPep	NH_2WLVFFVIFYFFRRRKK-OH	2252
RRKKFluPep	NH_2RRKKWLVFFVIFYFFR-OH	2252
FluPepΔ RRKK	NH_2WLVFFVIFYFFR-OH	1684
FluPep ligand	NH_2CVVVTAAAWLVFFVIFYFFRRRKK-OH	2967
RRKK FluPep ligand	NH_2CVVVTAAARRKKWLVFFVIFYFFR-OH	2967
FluPep ligandΔRRKK	NH_2CVVVTAAAWLVFFVIFYFFR-OH	2398
Super FluPep1	NH_2CVVVTAAARRPKGRGKRRREKQRWLVFFVIFYFFR-OH	4345
Super FluPep2	NH_2CVVVTAAARGAPRRGQRTRRKNKWLVFFVIFYFFR-OH	4218

4.2.2 Synthesis of FluPep functionalised nanoparticles

Mix matrix ligands 70:30 (mole:mole) CVVVT-ol: HS-$(CH2)_{11}$-EG_4-OH were prepared as described (Duchesne et al., 2008a) by first diluting 35 µL CVVVT-ol (4 mM DMSO:H_2O) with 35 µL ddH_2O and 6 µL HS-C_{11}-EG_4-OH (2 mM) with 6 µL EtOH and 18 µL ddH_2O. Adding the two solutions together yielded a 2 mM ligand solution of 70% (mole/mole) CVVVT-ol and 30% (mole/mole) HS-C_{11}-EG_4-OH. The ligand mixture was added to 900 µL gold nanoparticles and vortex mixed. Once mixed, 100 µL of x10 phosphate-buffered saline (PBS: 137 mM NaCl, 3 mM KCl l, 8 mM Na_2HPO_4, 15 mM KH_2PO_4) with Tween-20 (0.1 % v/v) pH 7.4 was

added to gold nanoparticles (Duchesne et al., 2008a) vortex mixed and the gold nanoparticles placed on a rotating wheel for 24 h. Nanoparticles were concentrated 10 x using 10 kDa Nanosep centrifugal filters (PALL Corp., Portsmouth, Hants, UK). Samples were centrifuged for 7 min at 10000 rpm (~12,000 x g) and the gold nanoparticles diluted with 1 x PBST (PBS 0.05% (v/v) Tween-20). The nanoparticles were then further separated from excess ligands by applying them (100 µL) to a 5 mL Sephadex G25 gel filtration column with PBS as a mobile phase.

To functionalise the nanoparticles with functional peptide ligands such as FluPep ligand, these were incorporated into the initial ligand mix at the mole % indicated in the figure legends. However, the separation of these ligands (Mw > 1000 Da) required in addition to gel-filtration on Sephadex G25 six washes, each involving a 10-fold dilution of the nanoparticles on a 10 kDa cut off Nanosep filter.

The concentration of functional peptide ligand in a nanoparticle preparation was estimated in two ways. For low mole % of functional peptide ligand, where the majority of the nanoparticles are determined to be grafted with a single functional ligand, the nanoparticle concentration was used as a proxy for functional ligand concentration. At higher mole % functional ligand, the number of peptidols incorporated into a 70:30 (mole/mole) mix matrix ligand shell of 8.8 nm gold nanoparticles (measured previously, 1200 peptidols, Duchense et al., 2008) was then multiplied by the mole % of functional ligand and by 1200. Since the functionalised nanoparticles are purified, this latter estimate will not reflect that actual concentration. However, the error can be estimated from the fraction of nanoparticles functionalised.

`

4.2.2.1 Purification of functionalised gold nanoparticles

Ion-exchange, and heparin affinity chromatography were performed on homemade micro columns of diethylaminoethyl (DEAE), carboxymethyl (CM) and heparin agarose. The chromatography gel was packed into a white pipette tip (200µL) using half the filter as a frit at the bottle and equilibrated PBS. Capped GNPs were concentrated by Nanosep and exchanged into PBS. Then, the GNPs were applied to the column, the unbound fraction was recovered. Columns were washed with PBS and eluted stepwise with 1 M NaCl and 2 M NaCl in1x PBS pH 7.2. The concentration of GNPs in the different fractions was determined by measuring absorbance at 450 nm (Haiss et al., 2007). Quantification of the gold nanoparticles then allowed the relation of bound and unbound gold nanoparticles to the mole % of functional ligand in the original ligand mixture to be analysed. The data indicate that at 0.03% (mole/mole) functional ligand, 10 % of the gold nanoparticles bound the column and thus most (~95 %) of these gold nanoparticles will possess just a single functional ligand, as determined previously (Levy et al., 2006a). At higher mole % the number of functional ligands per nanoparticle will increase. Thus, the purification of the functionalised gold nanoparticles means that the effects on influenza virus infectivity of mono- *versus* plurifunctionalisation can be determined.

4.2.2.2 Separation of influenza virus from gold nanoparticles by filtration

WSN/H1N1 virus stock (10 µL) was mixed with 10 µL gold nanoparticles and left for one hour on a rocking platform at 37 °C and then 980 µL phosphate-buffered saline (PBS) was added. The mixture of influenza virus and gold nanoparticles were

centrifuged on a nanosep filter of 100 kDa cut off (PALL Corporation, 600 south Wanger Road. Ann Arbor ,Michigan) with approximate pore size of ~ 10 nm for one minute at 10000 g. Following resuspension of the residual ~100 µL retentate in PBS, this was repeated 4-5 times. The concentration of gold nanoparticles in the retentate and filtrate was measured at 450 nm (Haiss et al., 2007).

4.2.2.3 Pretreatment of MDCK cells with peptides and functionalised gold nanoparticles

The medium from confluent monolayers of MDCK cells was removed and 10 µL of different gold nanoparticles functionalised with different mole % of FluPep ligand or free peptide mixed with 440 µL of DMEM was added and incubated at 37 ^{0}C for one hour. After removing this solution the cell monolayers were washed with different solutions as indicated in the figure legends. Then a viral plaque assay was performed to determine the degree to which the antiviral activity of the gold nanoparticles functionalised with different mole % of FluPep ligand or free peptide was retained.

4.2.3 Measurement of association of nanoparticles with virus and cells

4.2.3.1 Filtration method to separate virus and nanoparticles

WSN/H1N1 virus stock (10 µL) was mixed with 10 µL of ~10 nm gold or silver nanoparticles functionalised with a defined mole % of FluPep ligand in a 1.5 mL Eppendorf tube and then 300 µL PBS was added. After one hour in a tissue culture incubator (37 °C) a further700 µL PBS was added and the mixture placed in a 100 kDa cut off nanosep filter unit (PALL), which has an approximate pore size of ~ 10 nm. Following centrifugation for one minute at 10000 g, the ~100 µL retentate (care

being taken not to centrifuge to dryness) was diluted with 700 µL PBS and the process repeated 4-5. The final retentate and filtrate were then subjected to analysis by UV-Vis spectroscopy to quantify nanoparticles (Section 2.5) and SDS-PAGE to identify proteins.

4.2.3.2 Association of nanoparticles with cells

MDCK cells were cultured in six well plates as for the viral plaque assay (Section 2.8.4). Cell monolayers then incubated for one hour at 37 ^{0}C with gold nanoparticles, as described in the figure legends. In some experiments a competitor was included with the nanoparticles. Then the culture medium was removed and the cell monolayers were washed twice with 3 mL PBS to remove any residual free nanoparticles. Various washes and extracts from the cells, detailed in the figure legends, were collected and the nanoparticle content quantified by measuring the absorption at 520 nm.

In some experiments peptides or nanoparticles after the washes with PBS or with PBS and 2 M NaCl the activity of virus was measured by the plaque assay (Section 2.8.4)

4.2.3.3 Treatment of MDCK cells with glycosidases

Following fixation (Section 2.8.7) the fixed cells were washed with PBS three times and then incubated with 2 mL PBS containing 25 mM Glycine to block any remaining partially active fixative. The blocking medium was discarded after 15 min and cells were washed with 3x PBS to remove any remaining blocking medium. Cells were then incubated with the following enzymes:

(i) To degrade heparan sulfate 400 µL heparinase II and III (100 µL heparinase II and 200 µL heparinise and 100 µL of 100 mM sodium acetate and 0.1 mM calcium acetate, pH 7.0; gift from Dr. Edwin Yates, University of Liverpool).

(ii) To degrade chondroitin sulfate (including dermatan sulfate) 1 mL chondroitinase ABC (Sigma-Aldrich; 1.25 mU in PBS with x mg/mL bovine serum albumin) was added to the cells. The inclusion of bovine serum albumin is essential with these enzymes, as they contain traces of protease; the bovine serum albumin ensures cell proteins are not degraded.

(iii) To degrade sialic acid, neuraminidase 200 µL neuraminidase + 800 µL of 50 mM sodium acetate 4 mM $CaCl_2$ 100 µg/mL BSA, pH 7.4

In all cases, cells were incubated with the enzymes overnight at 37 ^{0}C.

4.2.4 SDS-PAGE and silver staining

4.2.4.1 SDS-PAGE

To prepare samples for SDS-PAGE, sample (30 µL) was mixed with 10 µL 4x SDS-PAGE loading buffer (50 % (v/v) glycerol, 10 % (w/v) SDS, 25 % (v/v) 2-mercaptoethanol in 0.3 M Tris-Cl, pH 6.8 and coloured with bromophenol blue), and then heated at 95°C for 10 min. Ten µL of the samples along with 10 µL SDS-PAGE markers (SDS7-1VL, Sigma) were loaded onto a 12 % (w/v) SDS-polyacrylamide gel (Table 2.3) and the gels were run at 30 mA (per gel), 200 V for 50 min with running buffer (50 mM Tris-Cl, 192 mM glycine and 0.1 % (w/v) SDS).

Table 4.2: SDS-PAGE Gel preparation

SDS-PAGE Resolving Gel (ingredients for 12 % gel – 2 gels)	Total 10 mL
Acrylamide/ bis-acrylamide stock (30 %, w/v)	4.0 mL
Tris-HCl (3 M), pH 8.85	2.5 mL
DD- Water	3.5 mL
10 % Sodium dodecyl sulfate (SDS) w/v	100 µL
TEMED(N, N, N', N', Tetramethylethylene diamine)	10 µL
Ammonium persulphate 50 mg/mL (freshly made)	100 µL

SDS-PAGE Stacking Gel (ingredients for 12 % gel – 2 gels)	Total 5 mL
Acrylamide/ bis-acrylamide stock (30 %, w/v)	650 µL
Tris-Cl (1.25 M), pH 6.8	500 µL
DD- Water	3.5 mL
10 % Sodium dodecyl sulfate (SDS) w/v	50 µL
TEMED (N, N, N', N', Tetramethylethylene diamine)	10 µL
Ammonium persulphate 50 mg/mL (freshly made)	50 µL

4.2.4.2 Coomassie Staining and Destaining

The gels were incubated in Coomassie stain (50 % (v/v) methanol v/v, 10 % (v/v) acetic acid, 0.25 % (w/v) CBB R-250)(ThermoFisher, UK) for 60 min, then soaked in de-staining buffer (40 % (v/v) methanol, 10 % (v/v) acetic acid) until the bands became clear.

`

4.2.4.3 Silver staining

After electrophoresis, the gels were soaked in fixative (40 % (v/v) ethanol, 10 % (v/v) acetic acid) for 1 hour following by soaking twice in 10 % (v/v) ethanol (5 min/each) and washing in RO water three times, each for 5 min.

Following incubation in 0.2 % (w/v) silver nitrate for 30 min, the gels were washed with water for 15 s and then dipped in freshly made developer solution (2.5 % (w/v) Na_2CO_3, 0.03 % (v/v) formaldehyde) until the solution went brown. New developer was then used to further stain the gel until bands were stained to the required intensity. Stop solution (1 % v/v acetic acid) was used to stop the reaction between silver and formaldehyde. The gels were then washed with water six times for 5 min each. Freshly made reducer (0.6 % w/v sodium thiosulphate, 0.3 % w/v potassium ferricyanide, 0.1 % w/v sodium carbonate) was used to remove the excess silver and clear the background. The gels were then quickly washed with a large volume of water and followed by five washes with water (5 min/each). When required, gels were re-stained to increase the sensitivity of detection, starting by the addition of 0.2 % (v/v) silver nitrate for 30 min.

`

4.2.5 Results and Discussion

4.2.5.1 Binding of nanoparticle-FluPep ligand conjugates to virus

FluPep may interact with the influenza virus envelope, components of the cell surface or both. Initial experiments aimed to determine which of these was the physical target of FluPep was. Advantage was taken of the exceptionally high extinction coefficient of the gold nanoparticles, which allows sensitive detection by UV-Vis spectrophotometry (Haiss et al., 2007) and the difference in size between the nanoparticle-FluPep ligand conjugate (diameter ~10 nm) and the virus (diameter ~100 nm). Virus and FluPep ligand -conjugated gold nanoparticles were incubated at 37 °C for 30 min, as in a plaque assay (section 3). The gold nanoparticles were then separated from virus with a centrifugal filter with a cut-off of 10 nm. The results demonstrated that the gold nanoparticle-FluPep ligand conjugate was recovered in the filtrate and not in the retentate. (Fig.4.1A). The presence of virus was determined by detection of viral protein. SDS-PAGE demonstrates that the retentate, but not the filtrate, contains bands corresponding to the expected size of HA protein (Fig. 4.1B). These data demonstrate that the FluPep ligand does not interact directly with the virus, since virus and FluPep functionalised nanoparticles are effectively separated by the filtration step.

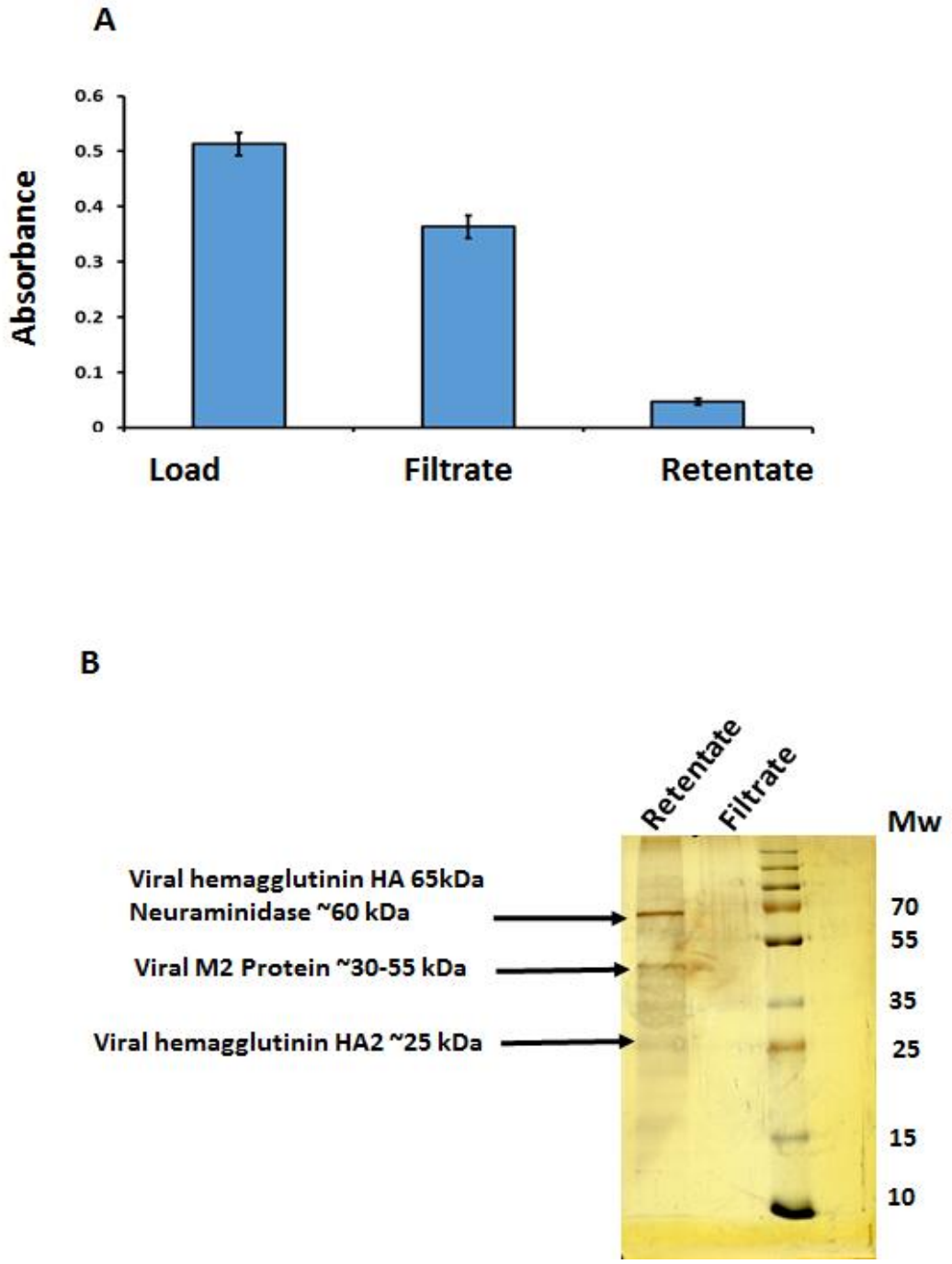

Fig. 4.1. Measurement of binding of FluPep functionalised nanoparticles to virus by filtration. (A) Following incubation of FluPep functionalised nanoparticles, the mixture was subjected to filtration on a 100 kDa cut-off centrifugal filter (Materials and Methods). The absorbance in the retentate and the filtrate was measured to determine the presence of nanoparticles. Results are the mean ± SD (n=3). (B) SDS-PAGE of the fractions from (A), the bands corresponding to major viral proteins are only present in the retentate and indicated by arrows.

`

4.2.5.2 Binding of nanoparticle-FluPep ligand conjugates to cells

To determine if the gold-nanoparticle-FluPep ligand conjugate bound to cells, these were incubated at 37°C for 30 min with the conjugate in the same conditions as for a plaque assay (Chapter 3). Following incubation, the nanoparticles released by various treatments were quantified. The PBS wash fractions contained virtually no detectable gold nanoparticles, indicating that there were no gold nanoparticles loosely associated with the cell surface. The absorbance of cells collected by scraping could not be read directly, due to scattering by cell clumps, so instead, cells were released by trypsin treatment. After trypsinisation the cells were found to contain a large amount of gold nanoparticles functionalised with either 3% (mole/mole) or 5% (mole/mole) FluPep ligand (Fig. 4.2A). The recovery of nanoparticles functionalised with 3% (mole/mole) and 5% (mole/mole) FluPep ligand 0.53 and 0.54, respectively in the cells represents ~60% of the gold nanoparticle FluPep ligand conjugate added. This demonstrates that not only are the FluPep ligand conjugated gold nanoparticles associated with the cells, but that their binding site(s) has a high capacity and reasonably fast kinetics. To determine whether the interaction of the gold nanoparticle-FluPep ligand conjugate with its cellular target(s) involved ionic bonding, cells were washed with PBS and then with 2 M NaCl. The results showed that NaCl released 32% of the gold nanoparticles added to the cells, which is a little over half of the amount of the total cell-associated FluPep ligand -conjugated nanoparticles (Fig. 4.2B).

Thus, around half of the cell bound gold nanoparticle-FluPep ligand conjugate are associated with an anionic component. The remainder may also be associated with

such components, but may have other interactions (H-bonding, van der Walls bonding) preventing release by high concentrations of electrolytes or have been internalised, so no longer accessible to the 2 M NaCl.

To determine whether internalisation of the FluPep ligand -nanoparticle conjugates was occurring the experiment was repeated, but at 4°C. Initially the effect of temperature on the level of binding was determined, since reactions are slower at 4°C. At the lower temperature, the PBS wash still failed to remove bound gold nanoparticle-FluPep ligand conjugate, a little more gold nanoparticle-FluPep ligand conjugate was recovered in the 2 M NaCl wash as the absorption of this wash was ~ 0.36. Following trypsinization, the absorption of 3% (mole/mole) or 5% (mole/mole) FluPep ligand was 0.64 and 0.67 respectively, which corresponded to ~ 69% of the FluPep ligand-gold nanoparticles originally added to the cells. This is slightly more than at 37°C (~ 56%) (Fig.4.2C). This indicates that at the lower temperature binding will have reached near maximal levels within the 30 min incubation. Next, following trypsinisation, the cells were mixed with fetal calf serum (FCS) to block trypsin and centrifuged to allow quantification of FluPep ligand-nanoparticles associated with trypsin-sensitive molecules on the cell surface and those that have been internalised. The results showed that the PBS wash did not remove any detectable bound gold nanoparticles-FluPep ligand conjugates. However, the supernatant of the trypsinised cells incubated with 3% and 5% (mole/mole) gold nanoparticles FluPep ligand at 37°C had an absorption of 0.06 and 0.08, respectively, while the corresponding supernatant of the cells incubated with 3% and 5% (mole/mole) gold nanoparticles FluPep ligand at 4°C had a higher absorption of 0.11 and 0.17, respectively (Fig. 4.2E). In contrast, the absorption of

the pellet of the cells incubated with 3% and 5% (mole/mole) gold nanoparticles FluPep ligand at 37°C was 0.22 and 0.42, respectively, while the absorption of the pellet of the cells incubated with 3% and 5% (mole/mole) gold nanoparticles FluPep ligand at 4°C was 0.13 and 0.2 respectively (Fig. 4.2F).

Thus, at 37 °C, most of the FluPep ligand-nanoparticle conjugate is associated with a trypsin resistant compartment; at 4 °C, this fraction decreases by around 40 % to 50 %. One interpretation of these data is that the FluPep ligand-nanoparticle conjugate is internalised. However, the fraction of FluPep ligand nanoparticles released by washing the cells with 2 M NaCl is less than that associated with the trypsin-sensitive compartment. The former will release FluPep ligand nanoparticle conjugates associated with anionic components on the cell surface. The difference between the two fractions may be due to steric hindrance by the nanoparticle, or of the protein it is associated with, preventing trypsin from cleaving the proteins.

It appears that the nanoparticle-FluPep ligand conjugate binds to extracellular components, at least some of which are anionic, and does not readily dissociate into the bulk medium. This is reminiscent of how growth factors, and other protein ligands involved in paracrine signalling interact with sulfated glycosaminoglycans of the extracellular and pericellular matrix (Duchesne et al., 2012, Sun et al., 2016). To determine if FluPep ligand might interact with sulfated glycosaminoglycans competitions were performed. FluPep ligand itself at 100 µM reduced the binding of gold nanoparticle-FluPep ligand conjugates by ~ 80%, whereas heparin at 100 µM reduced the binding by 90% (Fig. 4.2D). The strong, but incomplete competition by FluPep ligand and heparin may reflect the multivalency of the gold nanoparticle-FluPep ligand conjugate, the very high capacity of its cell binding sites

or interactions with multiple and distinct cellular components. Nevertheless, these data demonstrate the specificity of the interaction of the FluPep ligand-nanoparticle conjugate and that it binds to anionic cellular components, which can be competed with heparin.

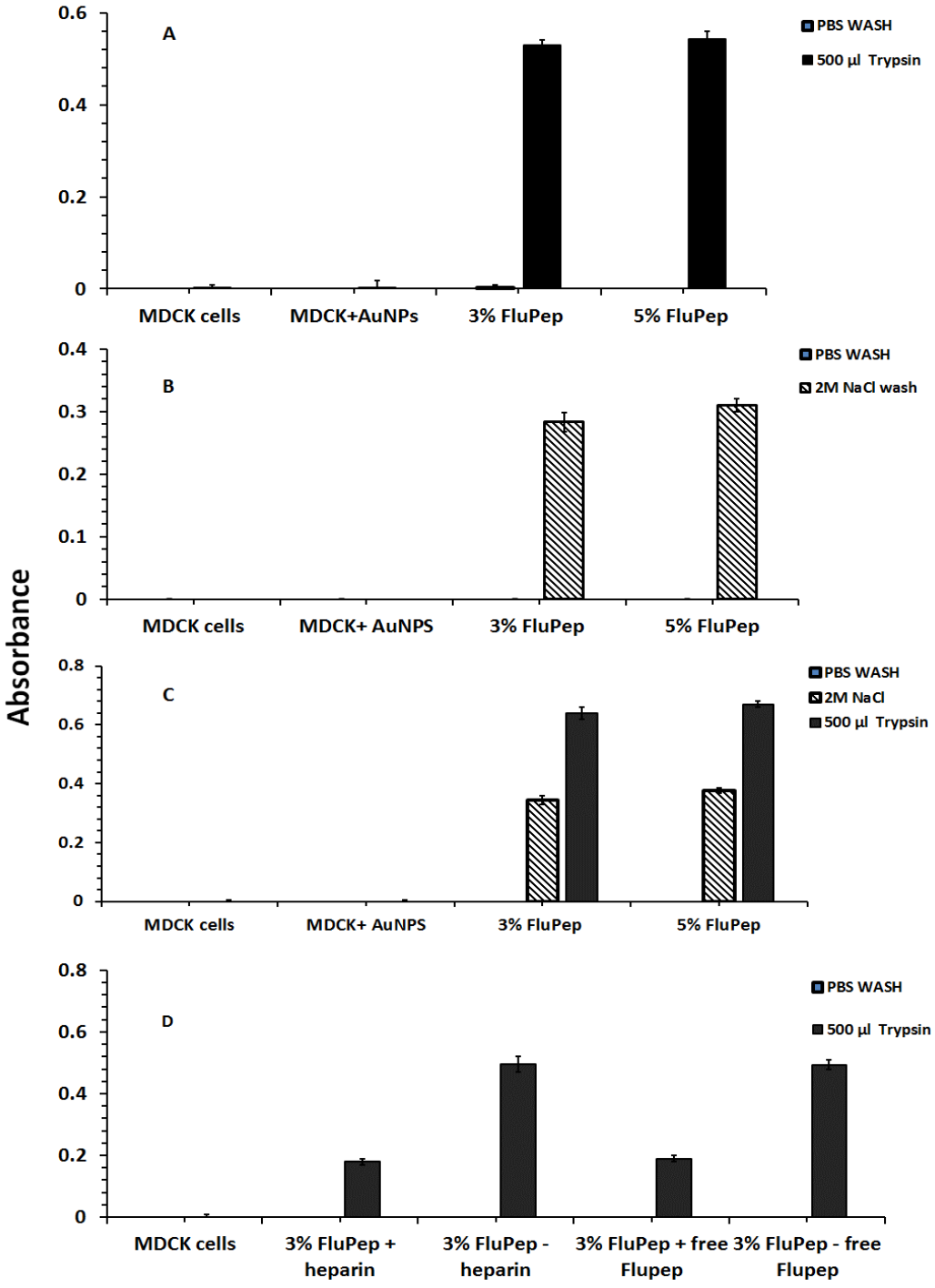

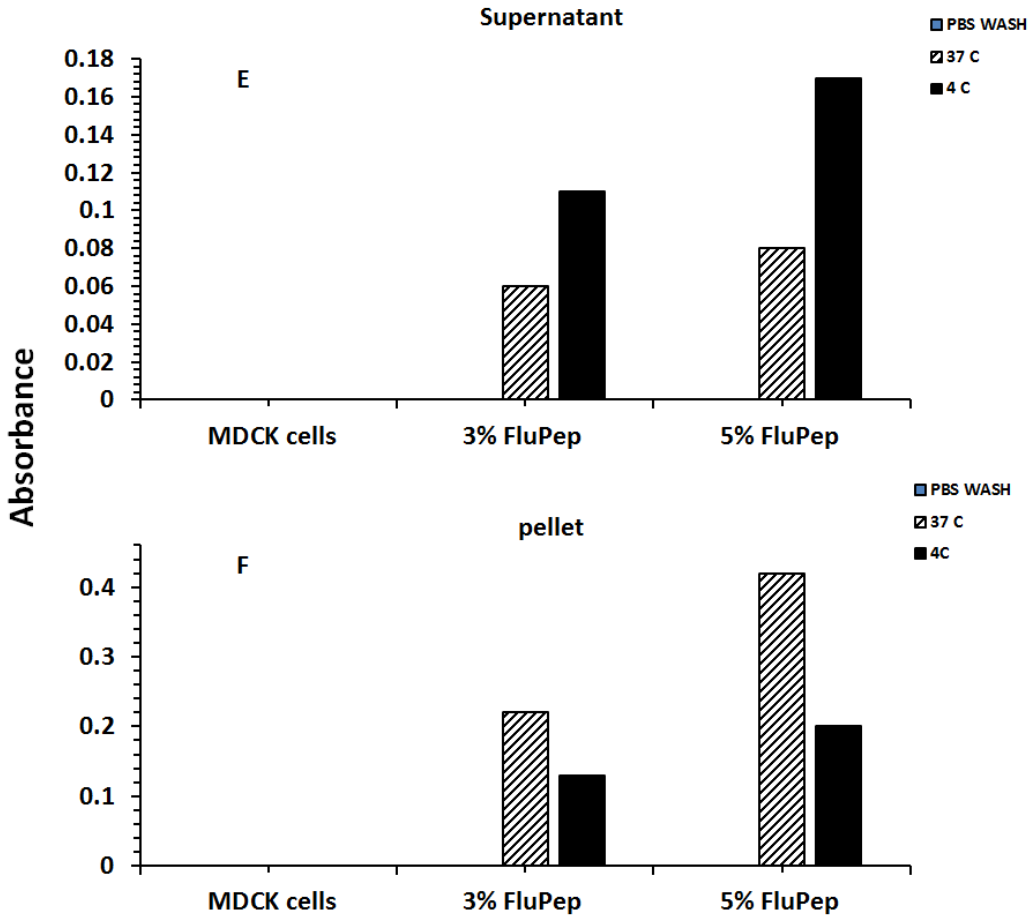

Fig. 4.2. Association of gold nanoparticles-FluPep ligand with MDCK cells. A. MDCK cells were treated with mix matrix gold nanoparticles, different mole % of gold nanoparticles -FluPep ligand and MDCK cells only, then incubated for one hour at 37 ^{0}C, thereafter unbound mix matrix gold nanoparticles and gold nanoparticle-FluPep ligand conjugates were removed and the cells washed with 1x PBS. The cells were then trypsinised to facilitate measurement of the absorbtion of the nanoparticles at 520 nm. B. Cells were washed with 1x PBS and then with 2 M NaCl, these fractions were collected and absorption measured at 520 nm. C. The previous steps were done in sequence in the cold room with fixed cells; washed with PBS, 2 M NaCl then trypsinised. D. competitions by including 100 µL heparin (100 µM) or free FluPep (100 µM). E and F measuring the contribution of internalisation to the association of nanoparticles funciotnalised by FluPep ligand to the cells. Binding of the nanoparticles functionalised with FluPep was performed at 37 °C or 4 °C. Following a wash with PBS, cells were trypsinised and centrifuged for 1 min at 10000 g and the absorbance of the nanoparticles at 520 nm measured. Results are the mean ± SD (n=3).

The gold nanoparticle-FluPep ligand conjugate has previously been shown to bind to CM-Sepharose, which is used to purify these nanoparticles (Chapter 3). Since the nanoparticle-FluPep ligand conjugates bound to cellular anionic components, it was of interest to determine if they would also bind to a heparin affinity matrix. The results showed that gold nanoparticles FluPep ligand conjugates, regardless of the mole/mole % functionalisation bound to a heparin affinity column. This binding was due to the FluPep ligand, since as the mole % of FluPep ligand increased, so did the percentage of gold nanoparticles binding to the column (Fig. 3). Moreover, as the mole % of FluPep ligand increased, so did the concentration of NaCl required for elution (Fig. 4.3).

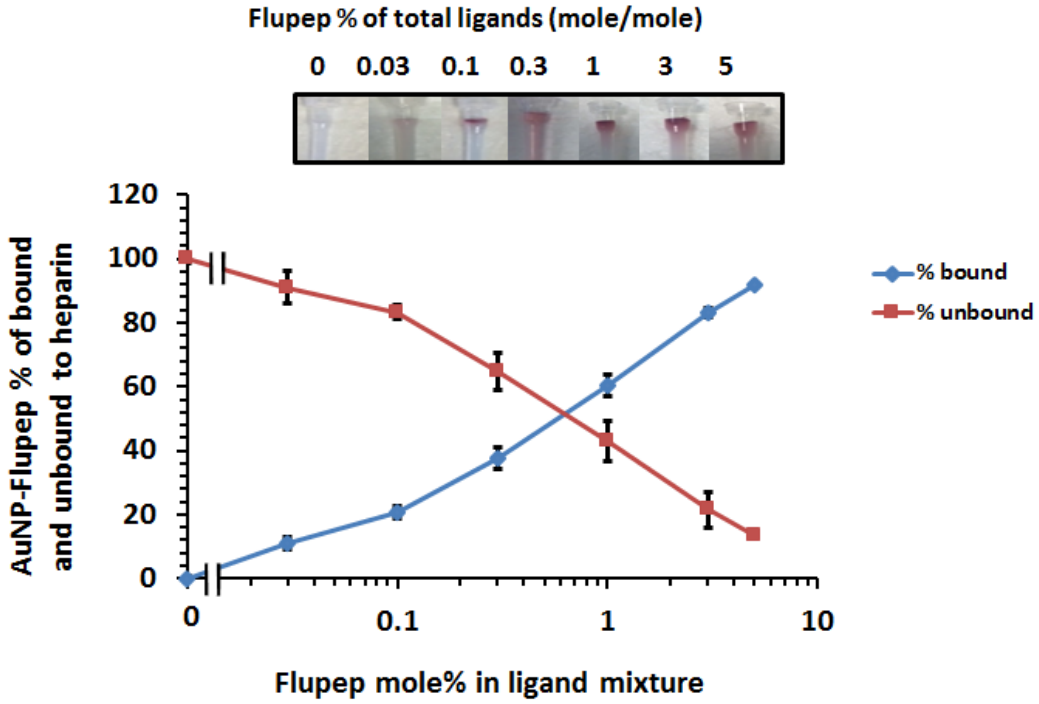

Fig. 4.3. Binding of gold nanoparticles functionalised with FluPep ligand to heparin affinity columns. (A) Image of columns following loading of gold nanoparticles functionalised with different mole % FluPep ligand and washing the columns with PBS. The pink colour represents bound nanoparticles. (B) Quantification of the % of nanoparticles unbound and eluted with 2 M NaCl from heparin affinity columns in terms of the mole % of FluPep ligand in the ligand mixture used to functionalise the nanoparticles. Results are the mean ± SD (n=3).

`

4.2.5.3 Binding of gold nanoparticle-FluPep ligand conjugates to fixed and enzyme-treated MDCK cells

To define better the anionic component(s) on the cells the gold nanoparticle-FluPep ligand conjugates interact with, cells were subjected to various enzyme treatments prior to measuring binding of the nanoparticles. To avoid the effect of the continuous biosynthesis of such molecules by cells and any acute effects due to the stimulation of a cell signalling pathways, fixed cells were employed. First the effects of fixation on the binding of the gold nanoparticle-FluPep ligand conjugates were determined. Following fixation, the amount of bound gold nanoparticle-FluPep ligand conjugate was determined for fixed and live cells. MDCK cells were incubated with 10 µL nanoparticles functionalized with 5% (mole/mole) FluPep ligand in 440 µL PBS for 1 hour at 37 0C and then washed with PBS. Trypsinisation with 500 µL trypsin for 15 mins was used as before to enable quantification of cell-associated nanoparticles. The results demonstrated that fixation did not affect the amount of FluPep ligand functionalised gold nanoparticles bound to the cells (Fig. 4.4).

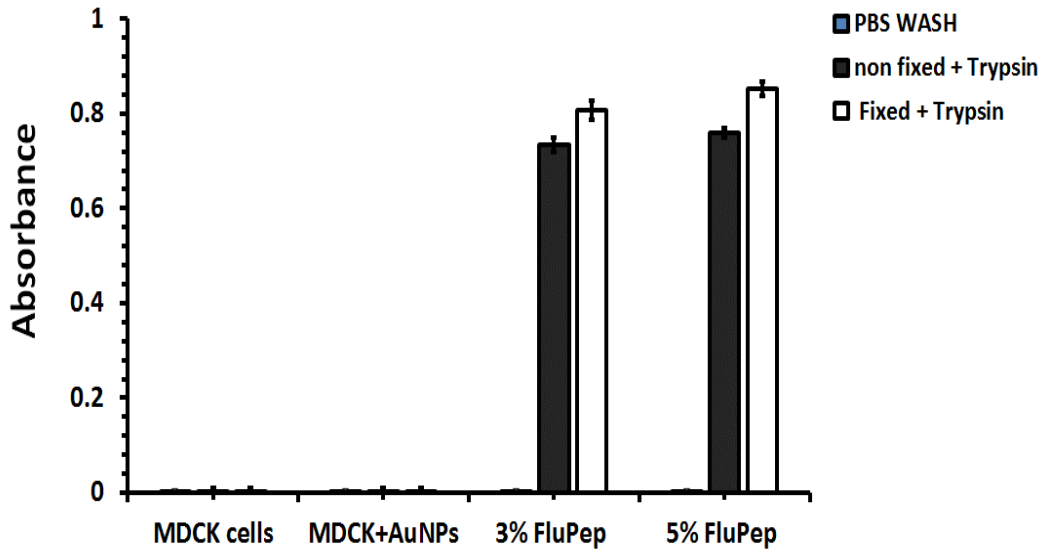

Fig. 4.4. Comparison of binding of FluPep functionalised nanoparticles to live and fixed MDCK cells. Cells (live and fixed were incubated with mix matrix gold nanoparticles, some functionalised with FluPep ligand, and the cell-associated nanoparticles quantified in a PBS wash and the trypsinised cells. Results are the mean ± SD of 3 experiments.

A series of enzyme digestion experiments with neuraminidase (sialidase), heparinase and chondroitinase ABC were then used to determine what FluPep ligand was binding to in the pericellular matrix of MDCK cells. Following 24 h digestion of fixed cells, they were incubated with gold nanoparticles functionalised with 3% and 5% (both mole/mole) FluPep ligand 1 hour at 37 0C. Cell-associated gold nanoparticles were quantified by measuring the absorption at 520 nm of trypsinised cells. In untreated cells, the absorption of the trypsinate was between 0.47 and 0.52. In neuraminidase treated wells the absorption was reduced to 0.13-0.14, a ~70% decrease (Fig. 4.5A). Similarly, treatment of the cells with heparinase reduced the amount of bound FluPep ligand functionalised gold nanoparticles by ~ 80%, whereas chondroitinase ABC digestion had no effect on the absorption at 520 nm of the trypsinate (Fig. 4.5B). These data demonstrate that the FluPep ligand functionalised gold nanoparticles bind to sialic acid-containing glycans and to

heparan sulfate, the latter being consistent with the in vitro binding of the nanoparticles to a heparin-affinity column (Fig. 4.3). It is interesting to note the selectivity of FluPep ligand binding, since no chondroitinase ABC sensitive interaction was detected; it is important to note that the inclusion of BSA with the chondroitinase was important to block the small amount of contaminating protease that is often in commercially sourced enzymes. Neuraminidase and heparinase, reduced, but did not abolish the binding of the FluPep ligand-functionalised gold nanoparticles. However, when cells were digested with both enzymes the amount of bound FluPep ligand functionalisd gold nanoparticles was reduced by ~96% (Fig. 4.5C). These data indicate that sialic acid containing glycans and heparan sulfate represent the major binding sites of FluPep ligand on cells. Thus, it is likely that it is through these interactions that FluPep ligand exerts its effect, directly or indirectly.

In the original work, RRKK was added to either the N or C termini of the peptide derived from the sequence of TKIP, in order to improve solubility in aqueous solution (Nicol et al., 2012). We reasoned that this basic tract of amino acids may be responsible, at least in part, for the interaction of FluPep ligand-conjugated nanoparticles with anionic polysaccharides. To test this idea, gold nanoparticles were functionalised with FluPep ligand and with FluPep ligand lacking this basic tract of amino acids (FluPepΔRRKK). A considerable amount of the FluPep ligand functionalised nanoparticles bound the cells (absorption at 520 nm of 0.55) and 80% of this binding was sensitive to neuraminidase (Fig. 4.5D). However, less gold nanoparticles functionalised with FluPepΔRRKK bound to the cells and neuraminidase treatment only reduced this by 43% (Fig. 4.5D). Thus, the TKIP

sequence itself does engage with these anionic polysaccharides, but the enhanced binding of FluPep ligand observed when it contains the RRKK C-terminal sequence is likely due to this enhancing the interaction of the original Tkip-derived peptide with sialylated glycans and in all likelihood heparan sulfate. The basic tract is less likely to impart any degree of selectivity. Consequently, the lack of effect of chondroitinase ABC digestion may reflect the selectivity of the TKIP sequence for sialic acid and heparan sulfate, with the C-terminal basic tract enhancing binding to these, but unable to override the selectivity.

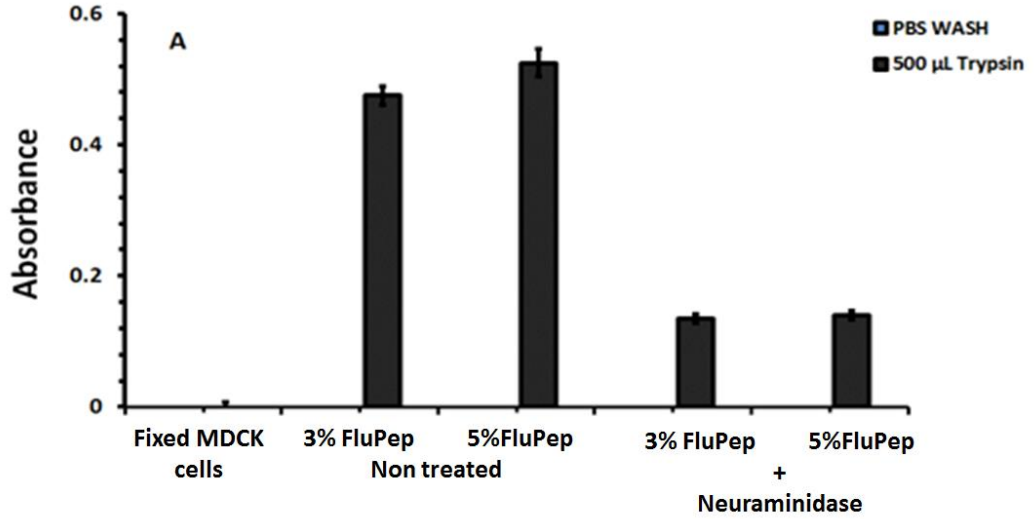

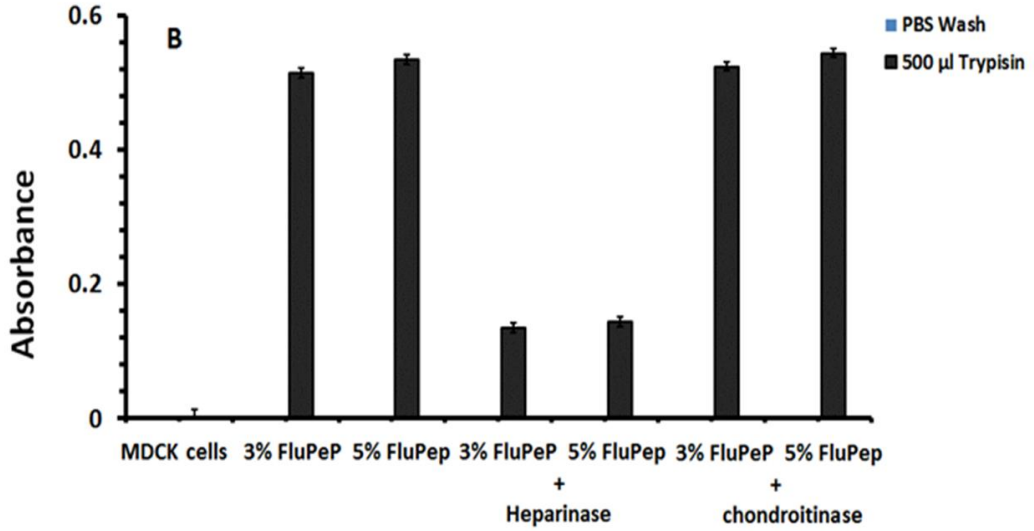

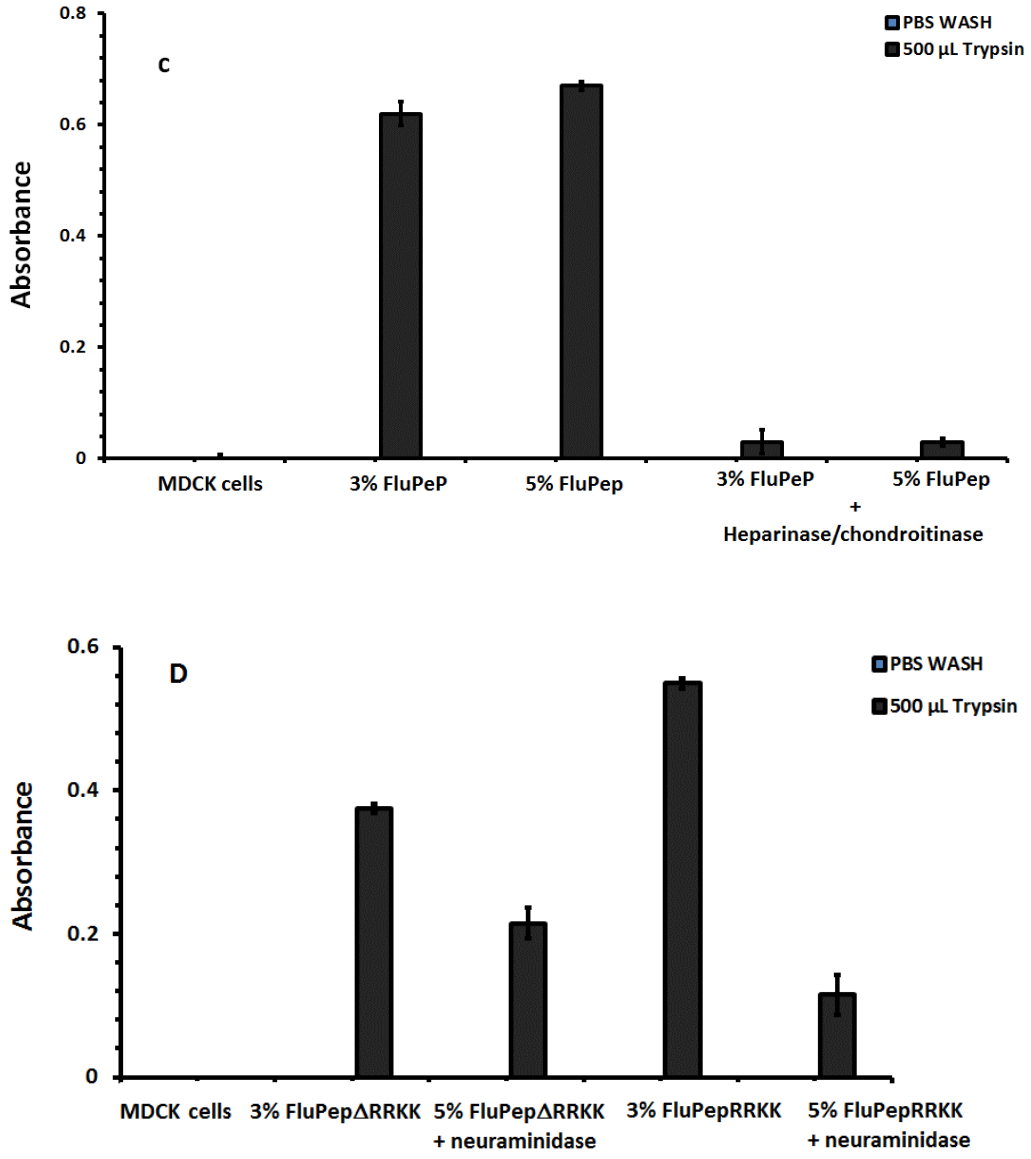

Fig. 4.5. Sensitivity of binding of FluPep functionalised nanoparticles to degradation of cellular polysaccharides. Fixed MDCK cells were subjected to digestion with neuraminidase or heparinases andthen incubated with FluPep functionalised nanoparticles. Cells were then washed with PBS and then trypsinised to enable quantification of the nanoparticles by their absorption at 520 nm. A. Neuraminidase. B heparinase and chondroitinase ABC digestions. C sequential digestion with heparinase and neuraminidase. Treated with enzyme(s) (+) and non-treated (+) D Investigating the effect of RRKK on TKIP ability to engage to anaionic extracellular compounds cells were pre-treated with FluPep ligand and with FluPep lacking RRKK then treated with neuraminidase.

`

4.2.5.4 Anti-viral activity of cell bound gold nanoparticle-FluPep ligand conjugates

Over half of the gold nanoparticle-FluPep ligand conjugate added to cells were bound. Moreover, the C-terminal sequence, RRKK not only enhanced cell binding (Fig. 4.5D), but was also shown to increase the anti-viral activity of the Tkip peptide (Nicol et al., 2012b). Consequently, it seems likely that cells can be loaded with gold nanoparticle-FluPep ligand conjugate, and washed and be protected from viral infection by the pool of cell-associated gold nanoparticle-FluPep ligand conjugates. In a control experiment, cells were washed with 2 M NaCl and then infected with virus. This showed that the 2 M NaCl wash has no effect on viral infectivity, and so on cell viability (Fig. 4.6A). Moreover, the dose response to free FluPep peptide was identical whether the cells had been washed beforehand with 2 M NaCl or not (Fig. 4.6A). Cells were then incubated with gold nanoparticle-FluPep ligand conjugates functionalised with different mole % FluPep ligand, washed with PBS and then subjected to a plaque assay. The results demonstrate that the gold nanoparticle-FluPep ligand conjugate that remains bound to the cells after the PBS wash (Fig. 4.6B) is capable of inhibiting the infectivity of influenza virus (Fig. 4.6B). The IC_{50} is around 734-220 pM, higher than determined previously for the gold nanoparticle-FluPep ligand conjugate without washing (Table 2 chapter 3), presumably due to removal of virus loosely associated with the cells o in the medium residue left after aspiration. When the cells are washed with 2 M NaCl after the incubation with nanoparticle-FluPep ligand conjugate, there was very little inhibition of viral infectivity apparent (Fig. 4.6C). Thus, the fraction of nanoparticle-FluPep ligand conjugate that can be removed from the cells with 2 M

NaCl and so which is interacting with anionic components of the cell surface seems responsible for much of the anti-viral activity. Analogous experiments with heparinases and sialidase were not possible, since these would also affect the ability of the virus to bind and infect cells, so confounding the analysis.

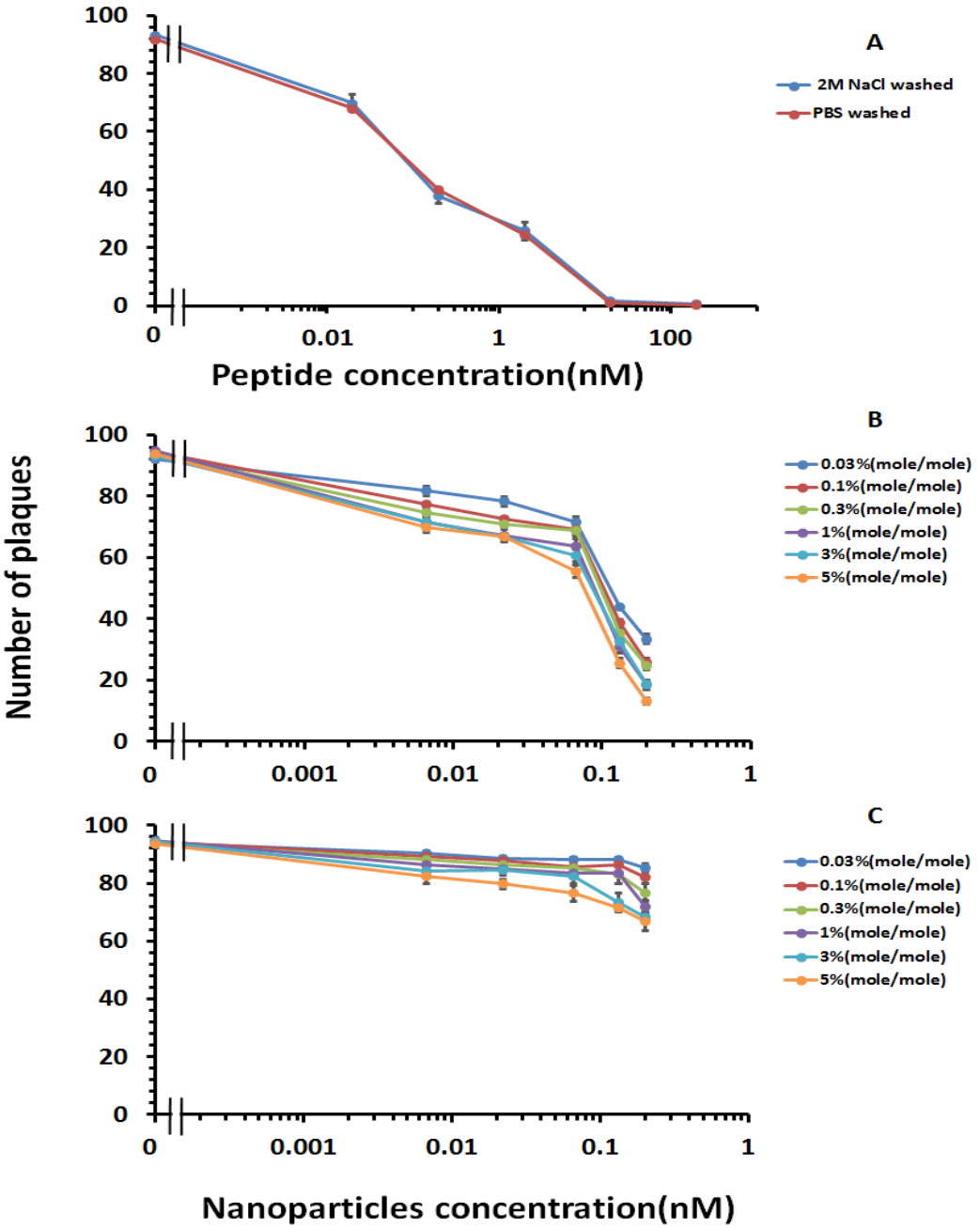

Fig. 4.6. Anti-viral activity of cell bound gold nanoparticle-FluPep ligand conjugates. MDCK cells were pre-treated with nanoparticles functionalised with different mole % of FluPep ligand one hour before virus treatment. Cells were, where applicable, washed with the indicated solutions and then infected with 'flu virus and a plaque assay performed. A. Comparison of the anti-viral effect of FluPep ligand on cells washed with PBS or 2 M NaCl to determine if the short exposure to a hyper osmolar solution affected cell viability and so viral infectivity. Cells were washed with the respective solution and then incubated with FluPep ligand and virus and plaques measured. B, C cells were incubated with nanoparticles functoinalised with different mole % FluPep and then washed with PBS (B) or 2 M NaCl (C), after which cells were infected with 'flu virus and the number of playes determined. Results are the mean ± SD (n=3).

`

4.2.5.5 Antiviral activity of FluPep, FluPep ligand and gold nanoparticles - FluPep ligand conjugates with respect to RRKK

We next determined the contribution of the RRKK sequence to antiviral activity of the peptides alone, of the peptide ligands (so incorporating the N-terminal sequence required for nanoparticle functionalisation) and of FluPep ligand-nanoparticle conjugates (Table 4.1). With the peptides alone, FluPep had the greatest antiviral activity, while RRKKFluPep (so with the basic tract at the N-terminus, rather than the usual C-terminal position) possessed a slightly lower antiviral activity and finally FluPepΔRRKK had the lowest antiviral activity (Fig. 4.7A Table 4.3). The antiviral activity of the corresponding the ligands was lower, in agreement with previous data that show that the N-terminal sequence CVVVTAA reduces antiviral activity (Chapter 3), and the rank order of potency of the peptides was slightly different: the postion of the RRKK sequence (N- or C-terminal to the TKIP sequence) has little effect, though the absence of this basic tract again reduced the anti-viral activity of the peptides (Fig. 4.7B, Table 4.3). The four basic residues on their own were without effect (Fig. 4.7B).

When gold nanoparticles were functionalised with these peptides, the position of the basic tetrapeptide, RRKK, made little difference to the antiviral activity of the nanoparticles (Figs 4.7C). However, as found for the free peptides, the absence of this basic sequence reduced the potency of the functionalised nanoparticles considerably (Fig. 4.7C and Table 4.6). Thus, gold nanoparticles functionalised with FluPep ΔRRKK, possessed IC_{50} values, of 59 pM (5% mole/mole) and 278 pM (0.3% mole/mole) (Fig. 4.7C), which are considerably higher than found for FluPep ligand (Table 4.6).

Table 4.3: **(IC_{50}) of different free FluPep in a plaque assay**. Results are the mean ±SD (n=3).

Peptide	**IC_{50} (nM)**
FluPep	0.14
RRKK FluPep	1.52
FluPep Δ RRKK	2.57
FluPep ligand	2.13
RRKK FluPep ligand	3
FluPep ligand Δ RRKK	3.2
Super FluPep 1	0.9
Super FluPep 2	0.09

Table 4.6: IC_{50} of different mole% of gold nanoparticles-FluPep, RRKK FluPep and FluPep Δ RRKK with respect to gold nanoparticles. Results are the mean ±SD (n=3).

Peptide	**FluPep ligand**	**RRKK FluPep**	**FluPep ΔRRKK**
mole%	**IC_{50} nM**	**IC_{50} nM**	**IC_{50} nM**
0.03%	0.072	0.126	0.27
0.1%	0.068	0.075	0.21
0.3%	0.058	0.060	0.16
1%	0.023	0.032	0.088
3%	0.016	0.018	0.068
5%	0.015	0.018	0.059

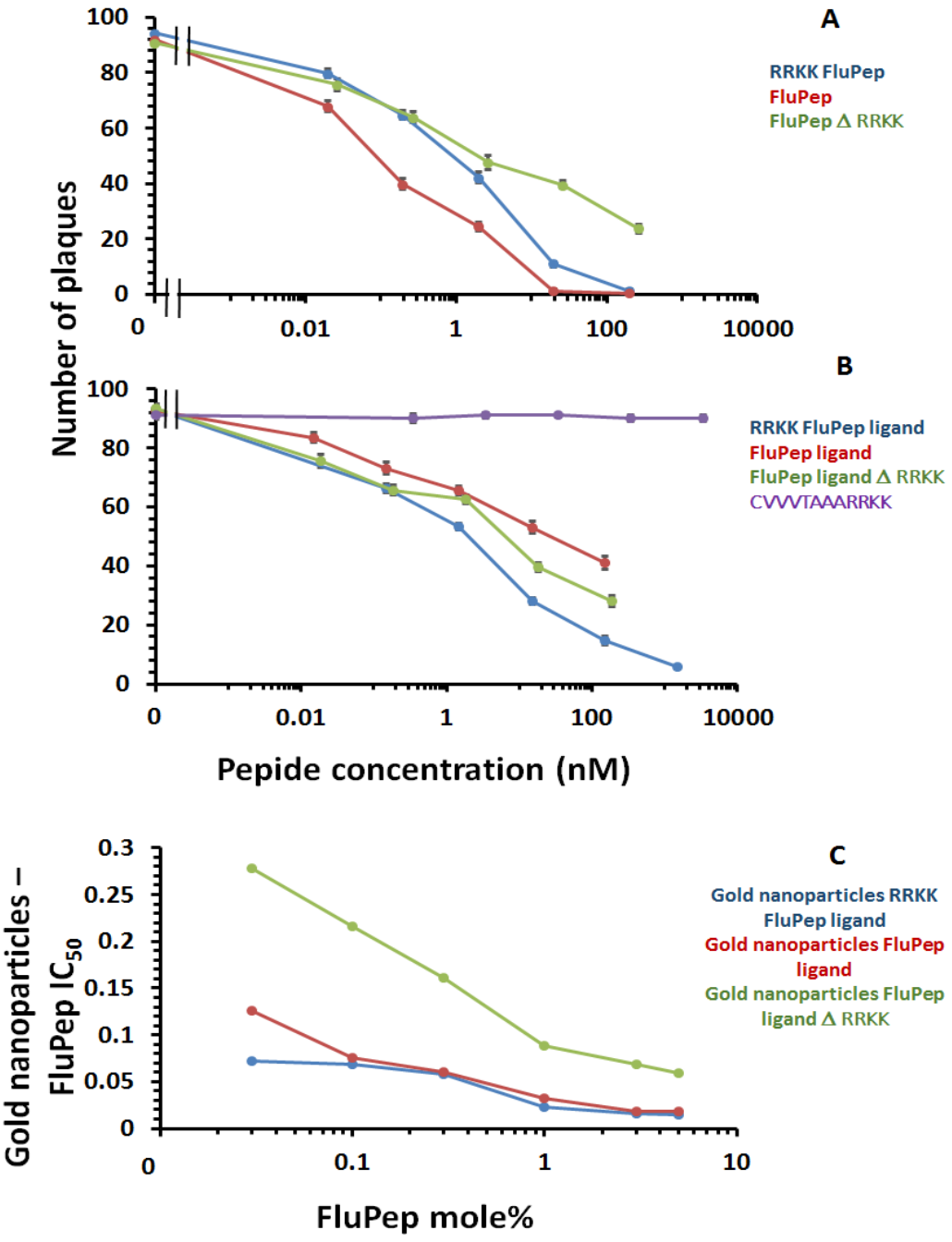

Fig. 4.7. Influence of the RRKK sequence on the antiviral activity of FluPep ligand. (A) A comparison of the antiviral activity of TKIP peptides lacking the RRKK sequence (ΔFluPep) or with this sequence at the C-terminus (FluPep) or the N-terminus. (B) A comparison of the same peptides in (A), but in the form of nanoparticle ligands, so with CVVVTAAA at the N-terminus. In addition, the antiviral activity of a peptide without the TKIP sequence, so just RRKK, was measured. (C) A comparison of the antiviral activity of gold nanoparticles functionalised with different mole % of the peptide ligands in (B). Results are the mean ± SD (n=3).

`

4.2.5.6 FluPep ligand with protein-derived heparin binding sites

FluPep ligand -functionalised gold nanoparticles bound to both sialic acid and heparan sulfate on cells and to heparin-affinity columns (Figs. 4.5A, B). Moreover, a variety of chemically modified heparin derivatives, some with very weak anticoagulant activity, have been shown to inhibit ‘flu virus H5N1 entry into cells using a pseudo virus type assay (Skidmore et al., 2015). Selectivity of the virus for particular sulfation patterns in heparin that would be more commo0n in cellular heparin sulfate was demonstrated by virtue of 6-O desulfated heparin possessing much less inhibitory activity that heparin itself, whereas 2-O desulfated heparin was considerably more active. There is a considerable amount of published data on protein structures and sequences that bind to heparin and heparan sulfate (Ori et al., 2008, Ghezzi et al., 2017). We reasoned that incorporating such sequences in place of the RRKK sequence might enhance the activity of the FluPep ligand further, by providing a more selective and higher affinity interaction with heparan sulfate. Indeed, such an approach has been used to increase the binding to heparan sulfate and activity of growth factors (Martino et al., 2014). Two sequences were chosen. One was derived from placental growth factor2 (PLGF2), and corresponds to a sequence used to enhance growth factor heparan sulfate binding (Martino et al., 2014) and the other from the cannonical heparan binding site of fibroblast growth factor7 (FGF7) (Xu et al., 2012) and are termed “super FluPep 1” and ‘super FluPep 2”, respectively (Table 4.1). Nanoparticles functionalised with either of these peptides were as stable as ones functionalised with FluPep, in terms of their resistance to ligand exchange (Fig. S 1-2. The relative affinity for heparin of gold nanoparticles functionalised with 0.1 % (mole/mole) FluPep ligand, Super FluPep

1,2 was determined in terms of the concentration of NaCl required for elution from a heparin affinity column. Elution of FluPep ligand functionalised nanoparticles is apparent at 0.6 M NaCl and 1 M NaCl (Fig. 4.8). In contrast, both super FluPep 1 2 functionalised nanoparticle required 1.5 M to 2 M NaCl for elution, demonstrating that these had a stronger electrostatic interaction with the polysaccharide (Fig. 4.8).

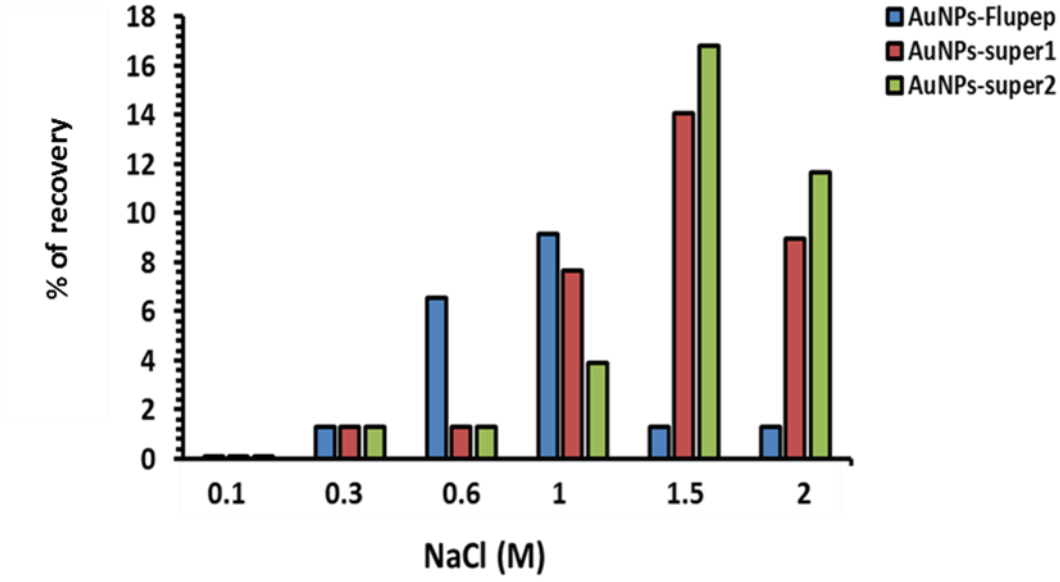

Fig. 4.8. Comparison of concentration of NaCl required to elute gold nanoparticles functionalised with FluPep, super Flupep1 and super Flupep2 from heparin affinity columns. The nanoparticles functionalised with the respective FluPep ligand were applied to a heparin affinity column, which was then eluted with increasing concentrations of NaCl. Nanoparticles were quantified by their absorption at 450 nm. Results are the mean ± SD (n=2).

4.2.5.7 Antiviral activity of super FluPep 1 and 2

The antiviral activity of the super FluPep 1 and 2 peptides (Table 4.1) alone and conjugated to gold nanoparticles was measured. Both peptides inhibited viral infectivity in a concentration-dependent manner and were more effective than FluPep ligand (Fig. 4.9). Thus IC_{50} of the super FluPep 1 and 2 ligands was 900 and

90 pM, respectively. As noted previously (Chapter 3) the FluPep ligand is less potent than FluPep, likely due to the N-terminal CVVVTAA sequence necessary for incorporation into nanoparticle ligand shells. Thus, addition of the heparin binding sequences derived from PLGF and FGF7 rendered the FluPep ligand peptide as potent as the FluPep peptide.

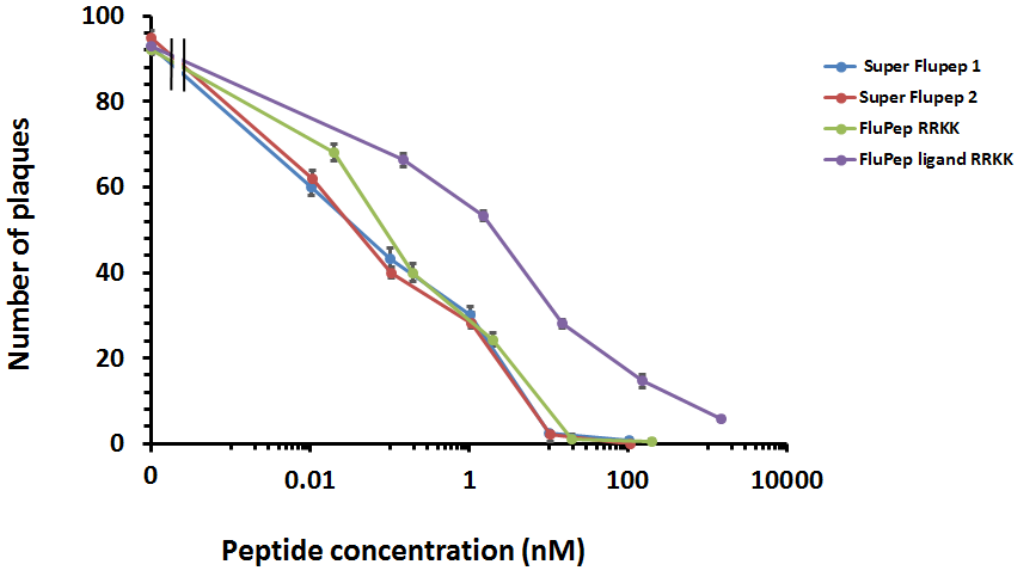

Fig. 4.9. Anti-viral activity of TKIP peptides carrying various basic sequence extensions. Virus infection of a monolayer of MDCK cells was performed in the presence of FluPep, FluPep ligand, with the N-terminal extension necessary for conjugation to gold nanoparticles, and two peptides where the RRKK sequence of FluPep is replaced by a known heparin-binding sequence, Super FluPep 1 and Super FluPep2. Results are the mean ±SD (n=3). Error bars may be smaller than the symbol

The antiviral activity of nanoparticles functionalised with different mole % of super FluPep 1 and 2 was measured. The number of viral plaques was reduced as the concentration of gold nanoparticles functionalised with either super FluPep 1 ligand or Super FluPep 2 ligand increased (Figs 4.10 A, B). Thus, for gold nanoparticles functionalised with 0.03% (mole/mole) Super FluPep 1 and 2, the number of

plaques started to decrease at 20 pM gold nanoparticles and reached a minimum of around 13-17 plaques at 200 pM (Figs 4.10. A, B). As the grafting density of Super FluPep ligands was increased, so did the antiviral activity, to reach a maximum at 5 % (mole/mole) super FluPep1,2 (Figs 4.10. A, B). This is reflected by the decreased IC_{50}, which shows a 5-fold greater potency of nanoparticles functionalised with 5 % (mole/mole) super FluPep1 and super FluPep2 ligand compared to nanoparticles functionalised with just 0.03 % (mole/mole) of these ligands (Tables 4.4 and 4.5). It is noteworthy that the antiviral activity of super FluPep1 and 2 conjugated to gold nanoparticles is greater than that of the free peptides (Tables 4.4 and 4.5).

Table 4.4: (IC_{50}) of different mole % of super FluPep 1 with respect to gold nanoparticles. Results are the mean ±SD (n=3).

Mole % super FluPep1	**IC_{50} nM**
0.03	0.060
0.10	0.058
0.30	0.027
1	0.018
3	0.013
5	0.012

Table 4.5: (**IC_{50}) of different mole% of super FluPep 2 with respect to gold nanoparticles.** Results are the mean ±SD (n=3).

Mole % super FluPep 2	**IC_{50} nM**
0.03	0.063
0.1	0.057
0.3	0.028
1	0.01
3	0.013
5	0.013

However, the data also demonstrate that free FluPep and FluPep ligand are less active than nanoparticles grafted with a single FluPep ligand. This was suggested to be due to FluPep weakly self-associating, perhaps due to its hydrophobicity (with FluPep ligand being more hydrophobic than FluPep), while the monomeric species is the most active with respect to inhibiting influenza virus infectivity (Chapter 3). Such self-association might be greater for a nanoparticle surface with several grafted functional ligands. The association of functional peptides grafted into a peptide ligand shell on nanoparticles has been observed directly previously (Duchesne et al., 2008b). Alternatively, the targets for FluPep may be separated by a distance similar or greater than their average physical separation on nanoparticle surface, resulting in only some of the grafted FluPep ligands on the nanoparticle surface being able to exert an antiviral activity.

The IC_{50} values for Super FluPep 1 and 2 were compared to those of the other peptides and it is clear that the addition of the heparin-biding sequences for PLGF and FGF7 enhanced the antiviral activity of the peptide and peptide-nanoparticle conjugates considerably (Fig. 4.10. C) (Table 4.3). Thus, enhancing the interaction of FluPep with extracellular/pericellular matrix appears to be a valid strategy for enhancing its inhibition of infectivity in at least the MDCK model.

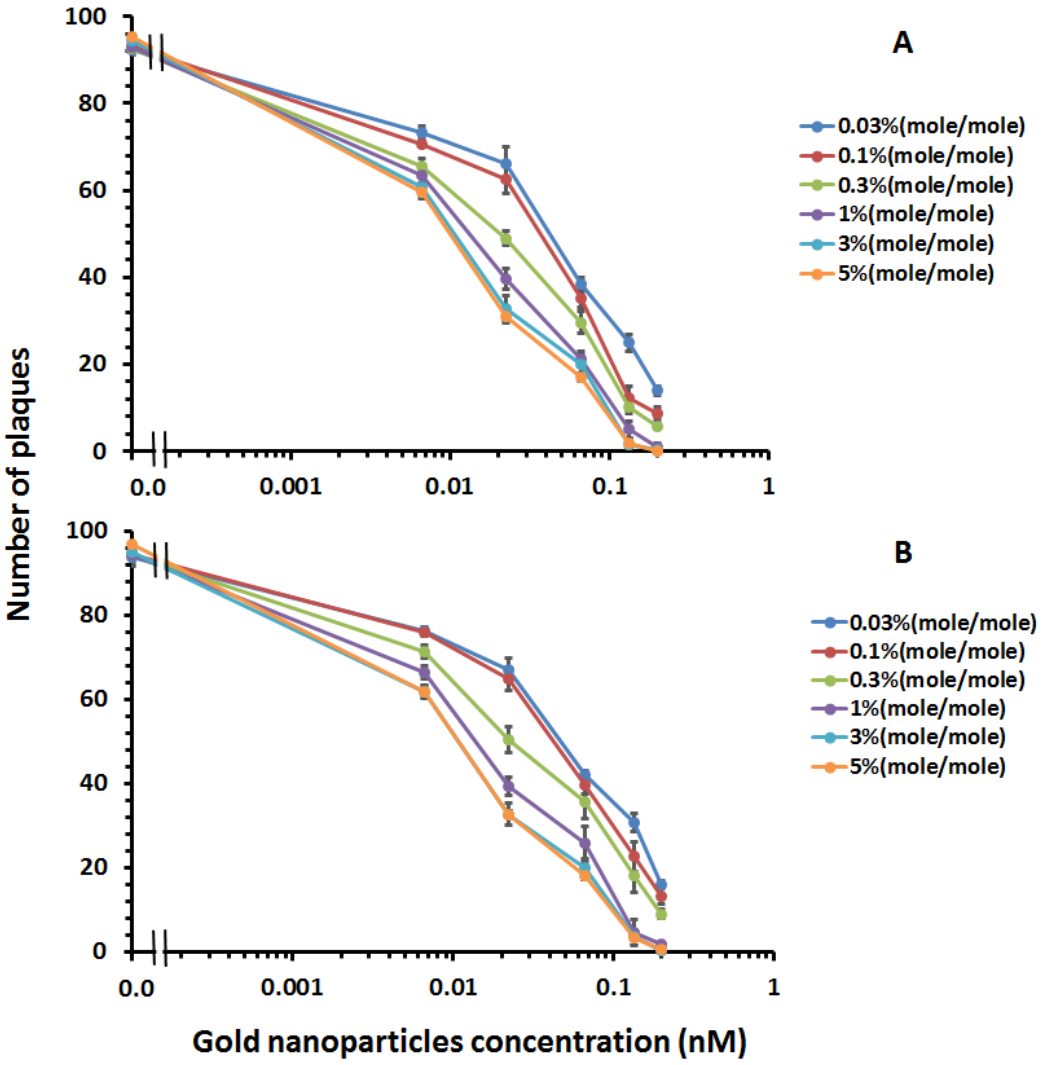

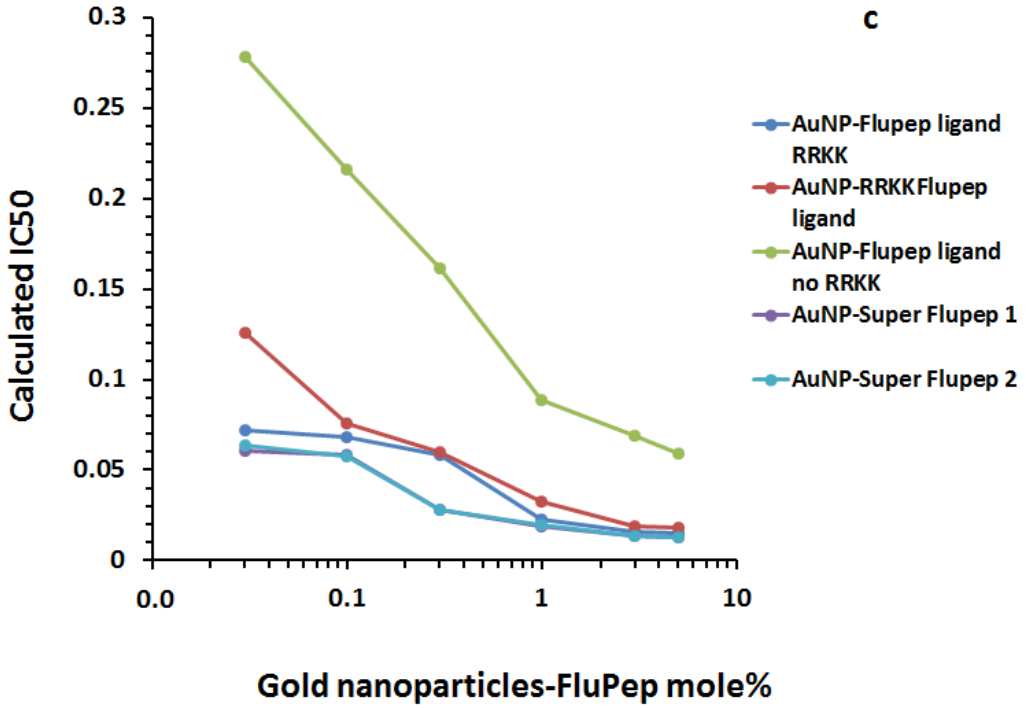

Fig. 4.10. Anti-viral activity of gold nanoparticles functionalised with super FluPep 1 and super FluPep 2. MDCK monolayers were incubated with influenza virus and nanoparticles functionalised with different mole % of super FluPep 1 and super FluPep 2, following which the number of plaques was determined. Dependence of inhibition of plaque formation on the concentration of gold nanoparticles and the % (mole/mole) of super FluPep 1 ligand (A) and super FluPep ligand 2 (B). (C) Comparison of IC_{50} values for nanoparticles functionalised with super FluPep ligand 1 and 2 and FluPep ligand variants. Results are the mean ±SD (n=3).

4.2.6 Conclusion

The FluPep ligand, when conjugated to nanoparticles binds to cells, rather than virus. Cell binding is likely to be key to the mechanism of FluPep's antiviral activity, since enhancing cell binding enhances the antiviral activity of the peptide. Interestingly, cell binding is relatively selective, since FluPep ligand binding was sensitive to neuraminidase and heparinase, but not chondroitinase ABC treatment, despite chondroitin sulfates possessing a high charge density. Thus, while the RRKK basic tract enhanced the activity of FluPep ligand, this is likely to be relative non-elective in terms of its interactions with sulfated polysaccharides; the selectivity is, therefore likely to reside within the TKIP-derived sequence and may involve a combination of ionic bonding and H-bonding, the latter through the amides of the peptide bond. In terms of the mode of action of FluPep ligand, its glycan selectivity is consistent with the documented importance of sialic acid binding in infectivity and the anti-viral activity of heparin compounds (Bateman et al., 2008),(Hosoya et al., 1991). This indicates that engineering an even more effective FluPep, by analogy with the engineering of more potent growth factors (Martino et al., 2014) depends on increasing the interaction of the peptides with some of the charged glycans of the pericellular matrix of cells. Given the very substantial literature on the structures in proteins responsible for binding heparan sulfate (Ori et al., 2008, Ghezzi et al., 2017), it should be possible to design FluPep type sequences with even more potent anti-viral activity.

4.2.7 Supplementary information

An anti-'flu peptide that interacts with sulfated glycosaminoglycans

Table of contents **Page**

`

4.2.7.1 Purification of superFluPep functionalised AuNPs

Since FluPep ligand and the two super FluPep ligands will carry a net positive charge at neutral pH, cation-exchange chromatography was used to purify functionalised gold nanoparticles. As for FluPep (Chapter 3), super FluPep 1 and 2 functionalised gold nanoparticles bound to CM Sepharose and were eluted by increasing electrolyte concentrations (Fig. SI 1). To functionalise the nanoparticles, functional ligands, are included in the ligand mix, and their mole % in relation to the matrix ligand reflects their grafting density on the gold nanoparticles (Levy, 2006, Duchesne et al., 2008a, Duchesne et al., 2012) (Free et al., 2012, Paramelle et al., 2015, Nieves et al., 2014, Levy et al., 2006a). Gold nanoparticles with a range of mole % of ligands were synthesized and applied to a CM-Sepharose column and those that were functionalised eluted with 1.5-2 M NaCl. Quantification of the gold nanoparticles by UV-Vis spectrophotometry then allowed the relation of bound and unbound GNPs to the mole % of FluPep in the original ligand mixture to be analysed. The data indicate that at 0.03% mole % ligand, ~10% of the nanoparticles bound the column and thus most (~95 %) of these gold nanoparticles will possess just a single functional ligand (Levy, 2006). At higher mole % the number of ligands per nanoparticle will increase.

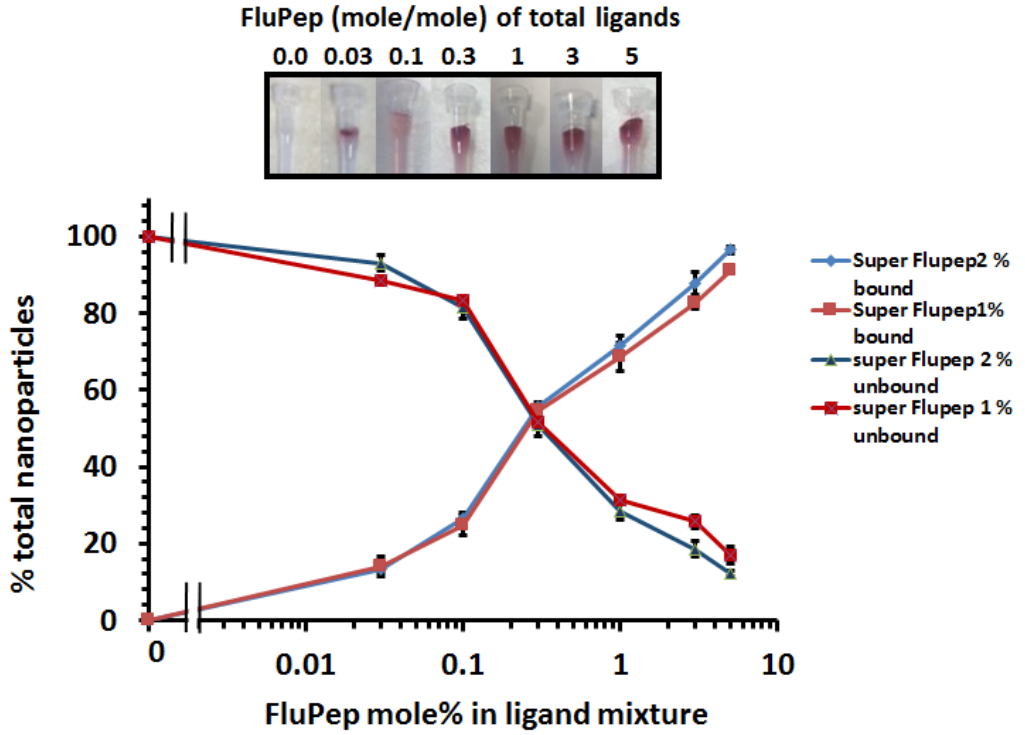

Fig. S 1. Purification of super FluPep ligand functionalised gold nanoparticles by CM-Sepharose cation-exchange chromatography. Gold nanoparticles functionalised with different mole % super FluPep ligand were subjected to chromatography on CM-Sepharose. Top, images of columns after loading and washing with PBS. Bottom, quantification of unbound (through and PBS wash fractions) and bound (eluted with 2 M NaCl) fractions. Results are the mean ± SD (n=3).

`

4.2.7.2 Stability of super FluPep 1 and 2 functionalised gold nanoparticles

Gold nanoparticles with a ligand shell incorporating 5% (mole/mole) super FluPep 1 and 2 ligand had a very similar resistance to ligand exchange with DTT as the control mix matrix protected gold nanoparticles. Thus, their aggregation parameter was unchanged up to 10 mM DTT, even after 48 h incubation (Figs. S2,B, C). At 25 mM DTT after 48 h there was some evidence for ligand exchange, as the aggregation parameter was above 1.0 and the ligand shell was clearly compromised (Figs S3, S4, A-F). Consequently, the incorporation up to 5% (mole/mole) FluPep ligand in the ligand mixture did not reduce the stability of the gold nanoparticles with respect to ligand exchange.

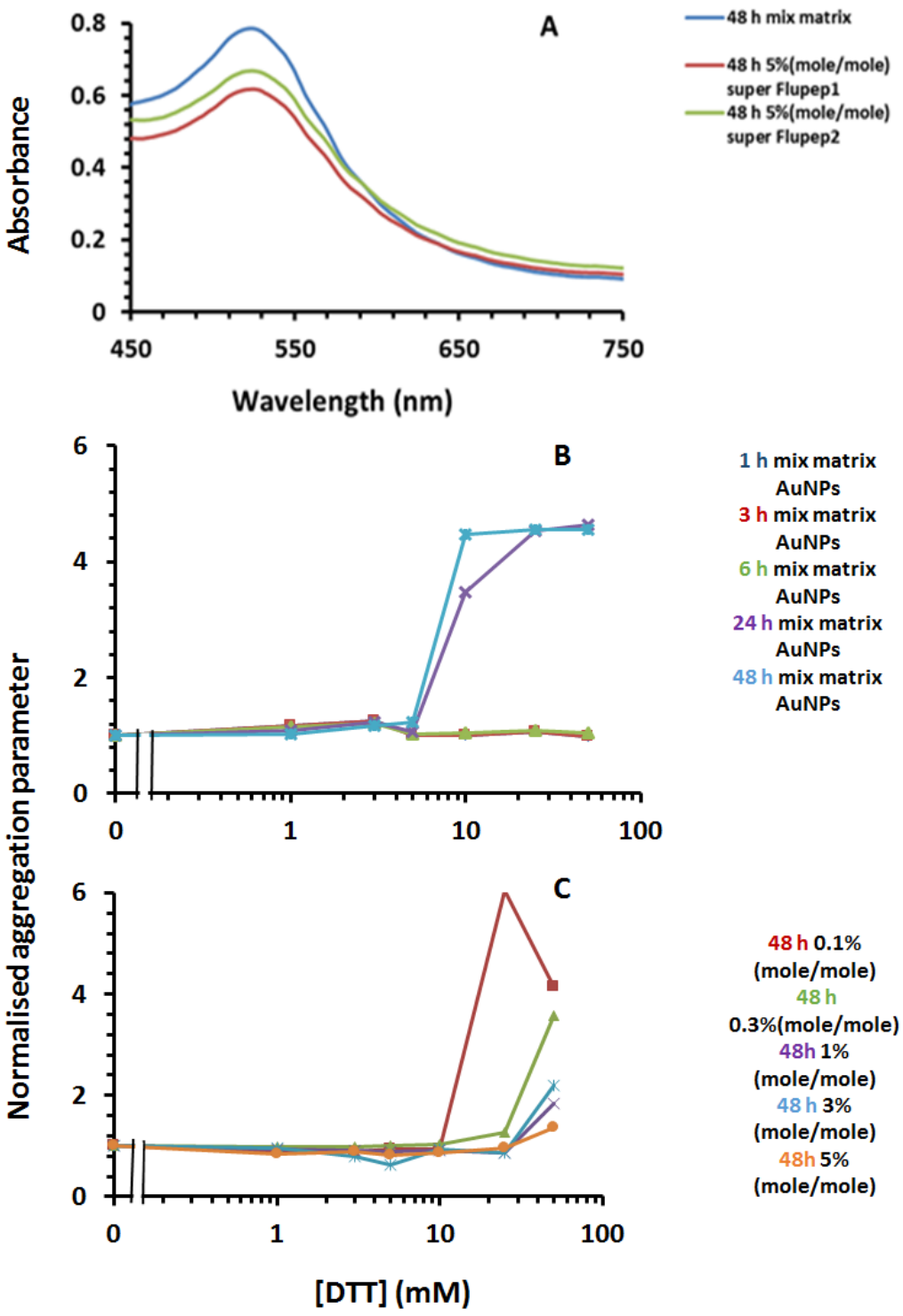

Fig. S 2. Stability of gold nanoparticles to DTT ligand exchange (A) UV-Vis spectra of mix matrix capped gold nanoparticles and mix matrix capped gold nanoparticles incorporating 5% (mole/mole) super FluPep ligand 1 and 2 in PBS. (B)Time and dose-dependence of DTT ligand exchange for (C) mix matrix gold nanoparticles with a ligand shell incorporating 5% (mole/mole) super FluPep ligand1. Results in (b) and (C) are the mean ± SD (n=3)

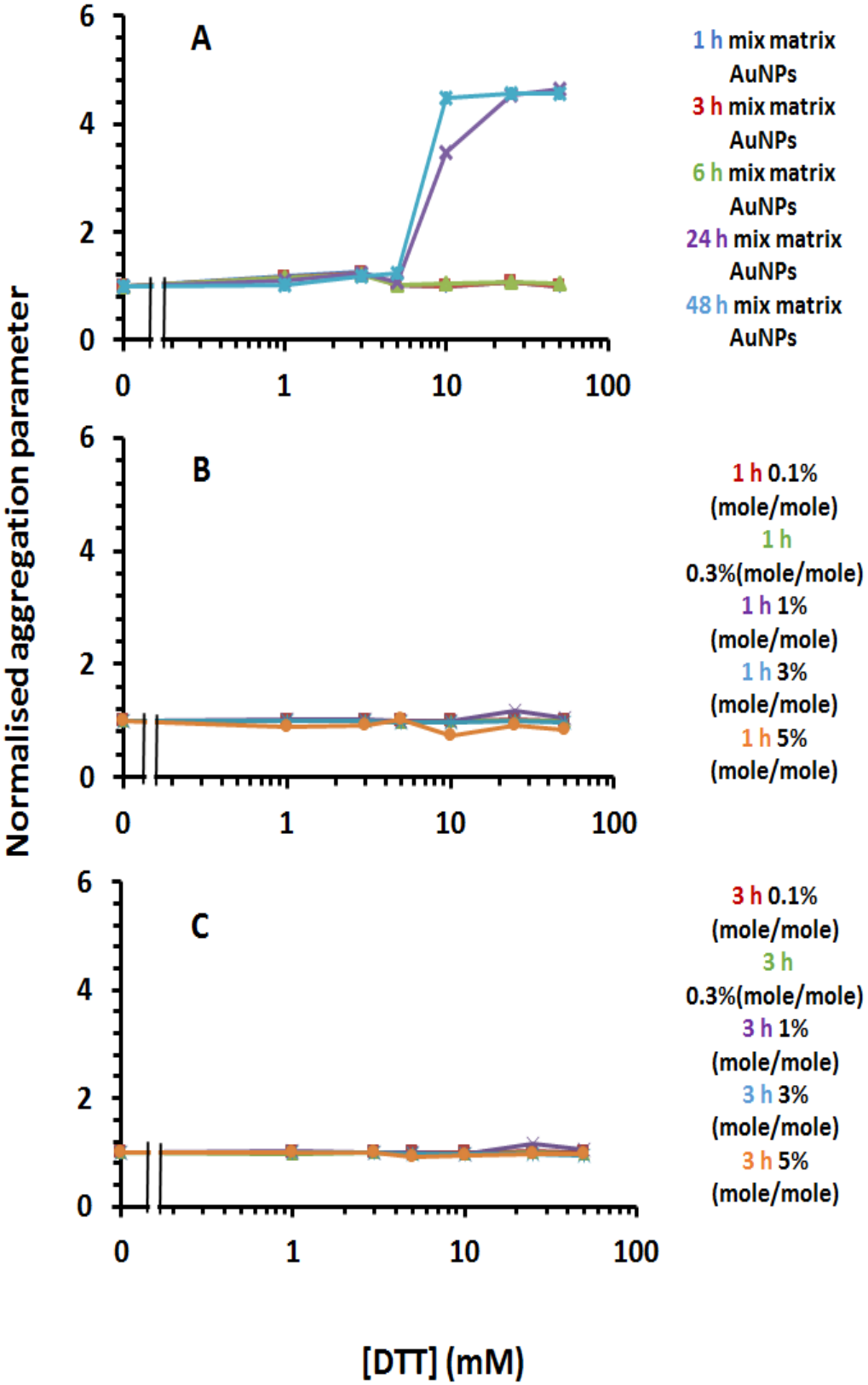
A
B
C
Normalised aggregation parameter
[DTT] (mM)
0
2
4
6
0
1
10
100
1 h mix matrix AuNPs
3 h mix matrix AuNPs
6 h mix matrix AuNPs
24 h mix matrix AuNPs
48 h mix matrix AuNPs
1 h 0.1% (mole/mole)
1 h 0.3%(mole/mole)
1 h 1% (mole/mole)
1 h 3% (mole/mole)
1 h 5% (mole/mole)
3 h 0.1% (mole/mole)
3 h 0.3%(mole/mole)
3 h 1% (mole/mole)
3 h 3% (mole/mole)
3 h 5% (mole/mole)

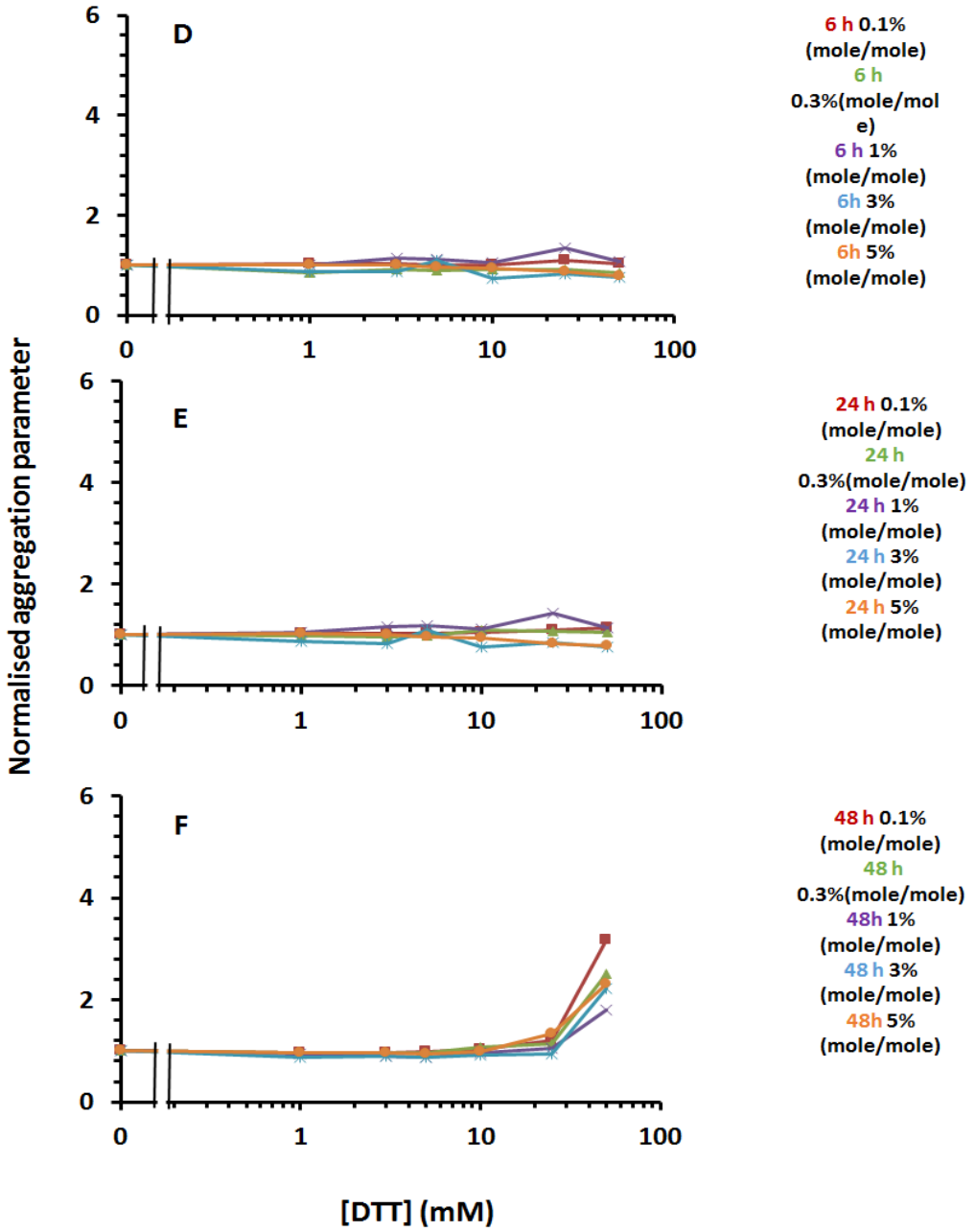

Fig. S 3. DTT Stability test of gold nanoparticles functionalised with super FluPep 1. Gold nanoparticles were incubated with varying concentrations of DTT for different time intervals, UV-Vis spectrum and the normalised aggregation parameter was calculated. A 70:30 CVVVT-ol HS-$(CH_2)_{11}$-EG_4-OH mix matrix Gold nanoparticles. B 0.1%(mole/mole) FluPep functionalised Gold nanoparticles. C 0.3% (mole/mole) FluPep functionalised Gold nanoparticles. D 1 %(mole/mole) FluPep functionalised Gold nanoparticles. E 3% (mole/mole) FluPep functionalised Gold nanoparticles. F 5 % (mole/mole) FluPep functionalised Gold nanoparticles. Results are the mean ± SD (n=3).

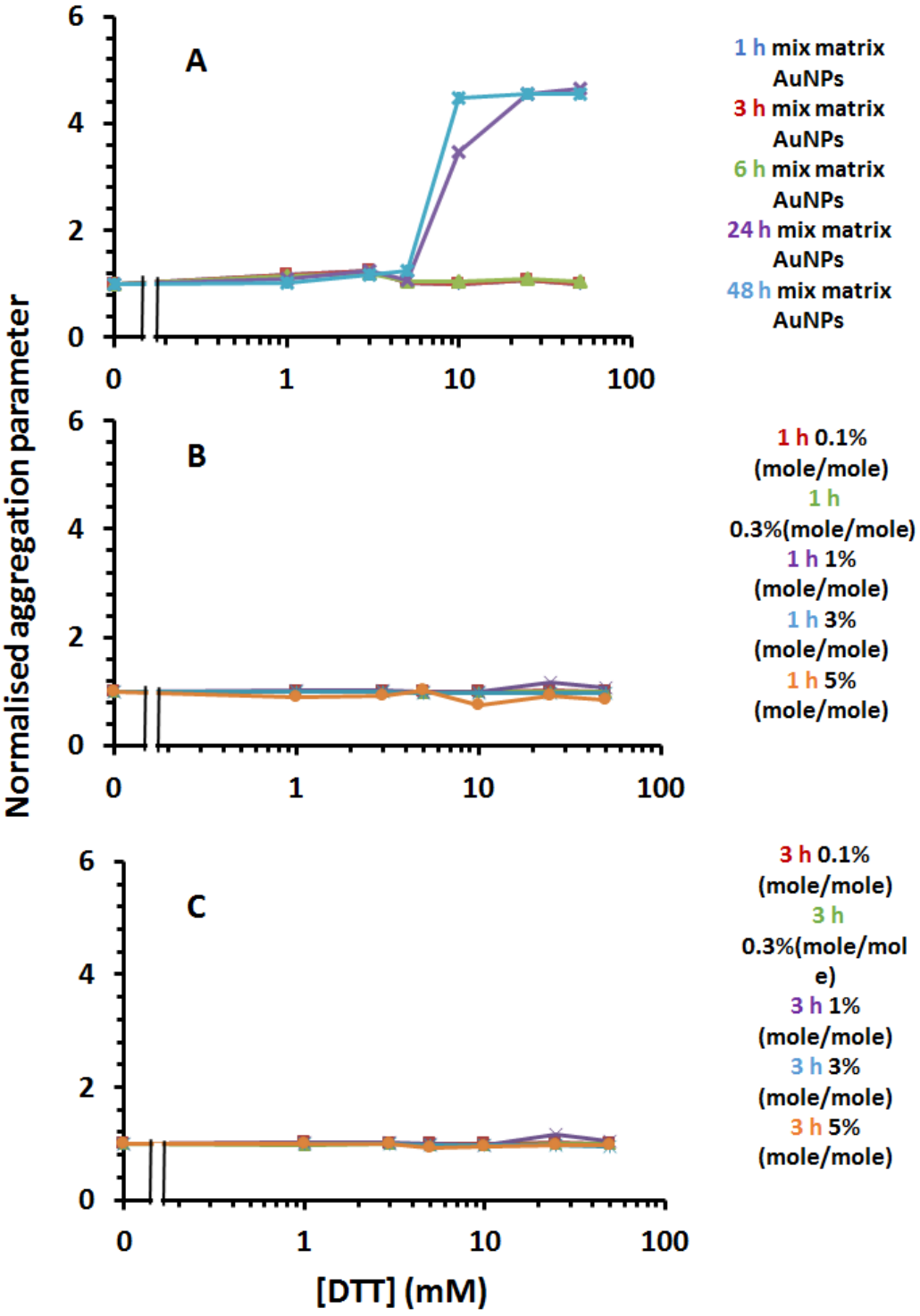
A
B
C
Normalised aggregation parameter
[DTT] (mM)
0
2
4
6
0
1
10
100
1 h mix matrix AuNPs
3 h mix matrix AuNPs
6 h mix matrix AuNPs
24 h mix matrix AuNPs
48 h mix matrix AuNPs
1 h 0.1% (mole/mole)
1 h 0.3%(mole/mole)
1 h 1% (mole/mole)
1 h 3% (mole/mole)
1 h 5% (mole/mole)
3 h 0.1% (mole/mole)
3 h 0.3%(mole/mole)
3 h 1% (mole/mole)
3 h 3% (mole/mole)
3 h 5% (mole/mole)

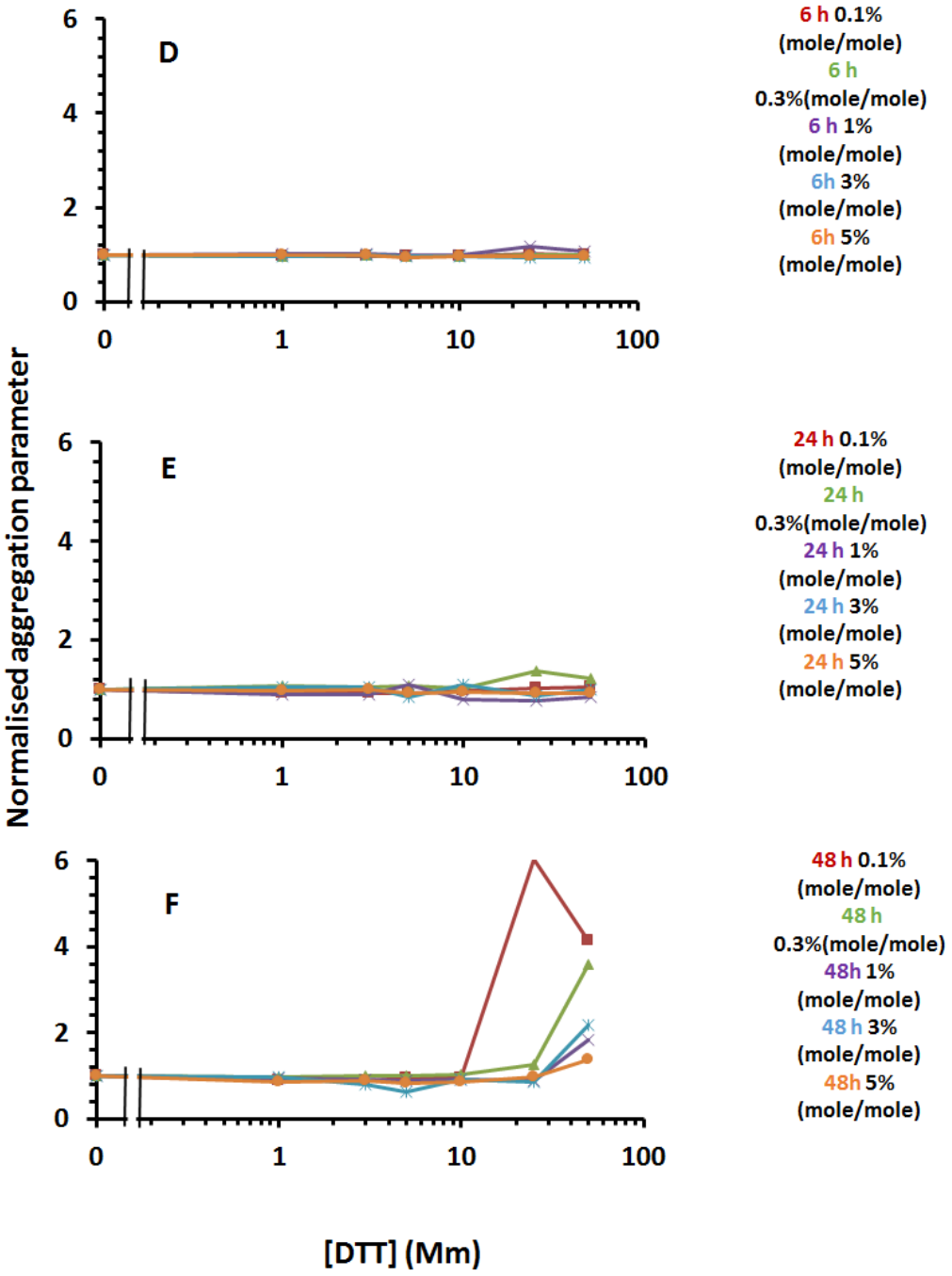

Fig. S 4: Stability of gold nanoparticles functionalised with super FluPep 2. Gold nanoparticles were incubated with varying concentrations of DTT for different times intervals, UV-Vis spectrum and the normalised aggregation parameter was calculated. A 70:30 CVVVT-ol HS-$(CH_2)_{11}$-EG_4-OH mix matrix Gold nanoparticles. B 0.1%(mole/mole) FluPep functionalised Gold nanoparticles. C 0.3% (mole/mole) FluPep functionalised Gold nanoparticles. D 1 %(mole/mole) FluPep functionalised Gold nanoparticles. E 3% (mole/mole) FluPep functionalised Gold nanoparticles. F 5 % (mole/mole) FluPep functionalised Gold nanoparticles. Results are the mean ± SD (n=3)

4.3 Discussion

It was demonstrated in the current work that gold nanoparticles-FluPep ligand conjugates didn't bind to the virus. In contrast, these nanoparticles associated with cells. The majority of the cell-associated FluPep ligand functionalised nanoparticles were bound to heparan sulfate and sialic acids; these interactions were additive, in that digestion of cells with both heparinases and neuraminidase reduced binding of nanoparticles to a greater extent than digestion with either alone. It was interesting to observe that chondroitinase ABC digestion had not effect on the interaction of FluPep conjugated nanoparticles with MDCK cells. Since these cells produce chondroitin sulfate proteoglycans and these are found in their pericellular matrix (Borges et al., 2005), these data indicate that FluPep is somehow selective for sialic acid and heparan sulfate.

The interactions with sialic acid and heparan sulfate are linked to the mechanism of action of FluPep. For example, the FluPep functionalised nanoparticles bound to the cell were able to protect the cell from subsequent viral infection. The affinity of FluPep for heparin, so in all likelihood heparan sulfate, was increased by replacing the RRKK C-terminal sequence with those from protein heparin binding sites. This was shown to increase the anti-viral activity of the peptides and nanoparticle conjugates produced with these peptides. The IC_{50} values for the peptides and the peptide-nanoparticle conjugates are generally in the mid to high pM-nM. The affinity for sialic acid and heparan sulfate is unlikely to be equivalent. For example, heparin-binding proteins generally have affinities in the mid to high nM range for heparin/heparan sulfate (Ori et al., 2008), whereas the various FluPep peptides will present a relatively unstructured set of basic side chains for binding. Moreover, the number of binding sites on these polysaccharides is extremely high, for example in fibroblasts it is of the order of one million heparan sulfate binding sites for FGF2 (Duchesne et al., 2012). These considerations suggest that direct competition for viral binding sites may not be the underlying mechanism for the anti-viral action of FluPep. However, there are two mitigating considerations that suggest direct competition cannot be completely ruled out at this stage. One is that a large amount of the peptide/nanoparticle binds to the cell pericellular matrix, so its effective

concentration in this small volume will be much higher. From this perspective direct competition might still be a valid mechanism. The other is that not all sialic acids and heparan sulfates are equivalent: sialic acid can occur on different structures and the underlying glycans for N-glycans, can have different numbers of branches; heparan sulfate itself is very polydisperse with a vast array of sulfation patterns produced by cells (Ori et al., 2008). In addition, it is not evident that for virus internalisation that binding sites on, e.g.., sialic acid, are the receptor. That is not all glycoproteins with sialic acids are likely to be able to trigger virus internalisation. There is thus the possibility that FluPep selectively binds to the polysaccharide/protein unit that represents the receptor for internalisation. The alternative is that FluPep activates a cell surface receptor that in turn activates a cellular anti-viral response. These ideas are explored in more detail in the following chapter.

4.4 Conclusion

After the successful functionalisation of gold nanoparticles with FluPep ligand and investigating their potential antiviral activity, the next step of work moved to investigate the possible FluPep ligand mechanism of action. It was believed by the group of Edinburgh University (Nicol et al., 2012) that the FluPep mechanism by interacting with viral hemagglutinin. However, FluPep ligand didn't interact with hemagglutinin. Based on initial work, gold nanoparticles-FluPep ligand conjugates were bound to heparin column, this means gold nanoparticles-FluPep ligand conjugates bind to carbohydrates and possibly one of the extracellular anionic sulfated GAGs. Pretreatment of MDCK cells with gold nanoparticles-FluPep ligand conjugates showed that the hypothesis is true since the pretreatment significantly reduced the viral activity. Enzyme degradation assay with heparinises, neuraminidase and chondroitinase ABC demonstrated that FluPep ligand binding sites are heparan sulfate and sialic acids but not chondroitin sulfate, these data indicate that FluPep is somehow selective for sialic acid and heparan sulfate. New designed FluPep with an extensions from protein to replace RRKK with heparin binding sites called super FluPep 1, 2. Their antiviral activity were significantly high as their mechanism of action by increasing the local concentration in the pericellular matrix.

Chapter 5

General Discussion

5.1 Overview

Peptides as therapeutics have gained traction ever since the FDA approved Enfuvirtidie against HIV (Cooper and Lange, 2004). A number of peptides have been discovered to possess antiviral activity in cell and animal models (Section 1.5) The initial work on FluPep (Nicol et al., 2012b) demonstrated that it effectively inhibited viral activity in cell and animal models (Section 1.5). Importantly, the latter work demonstrated that nasal delivery was sufficient. This means that a future drug based on FluPep would be simple to administer via a standard nebuliser. 'Flu remains a major health concern; the occurrence of epidemics and pandemics is certain, what is uncertain is when and what will be the virus strain responsible. Vaccines are unable, within the current economic model to cover all the population and they are not always fully effective and have a long lead time. Therefore, the development of drugs that prevent 'flu infection is a high priority (Section 1.2.3). Thus, FluPep is a potential lead to a drug that prevents 'flu infection.

There are major gaps in our understanding of how FluPep exerts its antiviral activity (Section 1.5). The synthesis of a FluPep with a probe that can be detected with high sensitivity is one key step if the mode of action of FluPep is to be established. In this thesis noble metal nanoparticles were chosen as the probes. This is because they can be detected optically with high sensitivity, and at the limit at the single nanoparticle level (Section 1.4.3). Radioactive peptides would also be very sensitive, but would limit analysis to cultured cells, would present longer time delays between experiment and acquisition of measurement data, and restrictions

on their use could limit the range of possible experiments. Fluorescent labels may have a greater impact on the physicochemical properties of the peptide, because unlike noble metal nanoparticles their interaction with molecules in the environment is not physically separated from their optical detection (Section 1.4.6). Moreover, the complete optical stability of noble metal nanoparticles, e.g., no photobleaching, and their high density relative to biological molecules means they can be used to purify an associated functional peptide from a biological system.

This first aim of the thesis was to establish whether FluPep ligand functionalised nanoparticles retained any antiviral activity. Considerable effort was put into redesigning nanoparticle ligand shells, which were found to be sufficiently hydrophobic to bind strongly to hydrophobic interaction chromatography matrices. Beyond demonstrating that the mix matrix ligand shell was rather hydrophobic, this work did not yield a new, non-hydrophobic ligand shell that imparted good stability to the nanoparticles (Chapter 2). However, the successful functionalisation of nanoparticles with FluPep ligand and the purification route of these nanoparticles from non-functionalised ones on CM-Sepharose was demonstrated (Section 2.9.2), essential steps for the analysis of the antiviral activity of the functionalised nanoparticles.

FluPep ligand functionalised gold and silver nanoparticles were found to possess antiviral activity (Chapter 3). The observation that silver nanoparticles functionalised with FluPep ligand possessed anti-viral activity illustrates the potential to design a future entity with two active substances: the anti-viral peptide and silver, as the latter is demonstrated to have anti-bacterial and antiviral activity in its own right.

A first question regarding the mechanism of action of FluPep ligand was whether it bound to virus or cells, or both. The experimental data (Chapter 4) demonstrate that FluPep ligand functionalised nanoparticles interacted solely with cells. A series of experiments were designed to establish the classes of molecules FluPep ligand interact with. These were found to comprise sialic acid and heparan sulfate, but not chondroitin sulfate, demonstrating an unexpected degree of selectivity on the part of the peptide. These discoveries led to a hypothesis: that binding to pericellular matrix would enhance the activity of FluPep ligand. This was tested using sequences of amino acids known to bind heparan sulfate and designing two new version of FluPep ligand, super FluPep 1 and super FluPep2. Both showed enhanced antiviral activity, demonstrating that this strategy, at least in the context of a cell based assay, will increase the antiviral activity of the peptide.

5.2 Future work

The experimental results presented in this thesis lay the foundation for future work that aims to establish fully the mechanism of action of FluPep ligand in cultured cells and in animal models, and the engineering of FluPep derived peptides that provide long-lasting protection against ‘flu infection. Should this future work be successful, this would pave the way for clinical trials.

The current evidence suggests that FluPep ligand may exert its antiviral activity by preventing the virus from either binding or delivering its genome to the cell’s cytosol. An alternative mechanism would be the delivery of the peptide to the cytosol. This seems unlikely due to the likelihood of proteolysis in endosomes and the cytosol, the absence of any negative effect of the nanoparticle on the antiviral activity of FluPep and of the addition of substantial sequences of amino acids in super FluPep 1 and super FluPep2. To provide direct evidence for an extracellular mode of action the presence of virus in the cells needs to be measured, along with the longevity of the protection of cells from infection by FluPep. Virus in cells can be determined using RT-PCR to measure viral RNA. By performing the measurements over days-weeks, the presence of any virus in the cells long after intracellular FluPep would be degraded will provide the necessary evidence. In addition, the by adding FluPep at different times after virus infection has been initiated may show whether it prevents spread of the infection (so acts outside the cells) or prevents replication of existing virus in already infected cells (so acts in cells).

FluPep's likely inhibition of virus infectivity by preventing its interaction with its receptors seems unlikely to be based on direct competition within the framework of current model for virus binding (Section 1.1.4). Only very modest concentrations of FluPep are required activity and given the consequent low IC_{50} of FluPep direct competition cannot account for the anti-viral activity of the peptide. The number of sialic acid and heparan sulfate binding sites on a cell is high (for example, over 10^6 heparan sulfate binding sites per cell for FGF2, which binds a fairly common sequence of saccharides (Duchesne et al., 2012) that it is difficult to see how FluPep at pM concentrations could block these. However, it should be noted that the actual receptors responsible for 'flu virus endocytosis are not well defined beyond the level of the glycan (Air, 2014). Viral HA binds to sialic acid and this is deemed by the field to be how the virus triggers its internalisation into endosomes (Section 1.1.4). Sialic acid is a common terminal sugar on N- and O-glycans, so is present on most glycoprotein; most cell surface proteins are glycoproteins (Varki, 2008). It is not clear why binding to any of these will trigger a signalling response inside the cell that will cause internalisation. It seems more likely that only binding to a subset of these cell-surface glycoproteins will cause internalisation and thus all sialic acid containing glycoproteins may not be equivalent from the virus' perspective. Moreover, it is not obvious whether the observed inhibition of virus infectivity by heparins (Skidmore et al., 2015) is due to inhibition of virus binding to heparan sulfate or to sialic acid. Thus, it may be that our understanding of the molecular targets of 'flu virus on the cell surface is insufficient. In this respect, a paper demonstrating that inhibition of the fibroblast growth factor receptor kinase prevented viral infectivity (Liu et al., 2015) is suggestive. Like all receptor tyrosine

kinases, fibroblast growth factor receptors are N-glycosylated and the latter are documented to be sialylated (Duchesne et al., 2006). Thus, internalisation of the virus may requires glycans (sialic acid and/or heparan sulfate) associated with particular cell surface receptors. The remaining glycan binding sites would then act as a reservoir, preventing the virus from leaving the vicinity of the cell and *in vivo* being swept away by the mucocilary escalator of the respiratory tract. This would allow a re-interpretation of the concept of 'balance' between HS and NA (Byrd-elotis et al., 2017), whereby NA activity cleaving sialic acids would enable HA to 'explore' the array of glycoproteins on the cell surface and in time enable the virus HA to bind sialic acids associated with a true receptor, that is a glycoprotein capable of triggering endocytosis. In this case, FluPep may exert its activity by binding both the protein and the glycan partner, so it possesses a dual receptor system. By analogy with the many natural dual receptor systems, including that of the fibroblast growth factors, affinity for each individual receptors is likely relatively low, but combined is high. The interaction with a high capacity binding site such as heparan sulfate ensures a pool of pericellularly located peptide at high local concentration.

Thus, to define the mechanism of action of FluPep, it is also necessary to define the receptors of 'flu virus at the cell surface. One obvious route to achieve this is mass spectrometry. Protection and labelling approaches, as used to define heparin binding sites in proteins, (Ori et al., 2009) would at the least uncover the basic residues in the viral proteins responsible for interaction with anionic species on the cell surface; they might also identify basic residues in cellular proteins involved directly or indirectly in virus binding. Label transfer reactions such at APEX fusion proteins (Martell et al., 2012) would be more challenging, as they would involve

insertion of APEX into viral envelope proteins. Should such viruses remain infective, they could then be used to biotinylated molecules within `20 nm of the virus. Analogous experiments would be performed with FluPep. This work would establish the binding sites and receptors for both virus and FluPep. Genetic disruption with e.g., SiRNA, would enable validation of receptor candidates and from there mechanism of action of FluPep.

In vivo work would have three aims.

First would be to determine the extent to which the observation *in vitro* that heparin-binding peptide sequences enhance antiviral activity. Should this be the case, then this work would pave the way to the design of more effective peptides.

Second is the pharmacokinetics (so the fate of FluPep) in the respiratory tract. This would include the extent of its access to different parts of the respiratory tract, its lifetime and its route of clearance. Nanoparticle-FluPep conjugates might be useful for at least the first phase of work, since they can readily be detected. N-terminal biotinylation of FluPep is unlikely to affect its activity, since FluPep ligand and FluPep nanoparticle conjugates possess antiviral activity. The biotinylated FluPep could then be recovered by affinity chromatography and analysed by mass spectrometry from different parts of the respiratory tract over time. An isotope labelled FluPep (using heavy arginine) would allow administration of light then heavy FluPep and their ratios measured over time by mass spectrometry to provide quantitative data on the clearance of FluPep. Since the FluPep would be delivered nasally, it is likely the the amounts that eventually reach the body might be very

low, and to establish whether this is the case would be an important objective, since it would reduce the potential for harmful side-effects.

Third would be the extension of the lifetime of FluPep, since increasing FluPep lifetime would reduce the frequency of its administration. With peptides, this is generally achieved by the incorporation of some D amino acids into the sequence or the incorporation of an unnatural peptide bon, e.g., isopeptide bond.

References

ABE, K., NOZAKI, A., TAMURA, K., IKEDA, M., NAKA, K., DANSAKO, H., HOSHINO, H., TANAKA, K. & KATO, N. 2007a. Tandem repeats of lactoferrin-derived anti-hepatitis C virus peptide enhance antiviral activity in cultured human hepatocytes. *Microbiology and Immunology,* 51**,** 117-125.

ABE, K., NOZAKI, A., TAMURA, K., IKEDA, M., NAKA, K., DANSAKO, H., HOSHINO, H. O., TANAKA, K. & KATO, N. 2007b. Tandem repeats of lactoferrin-derived anti-hepatitis C virus peptide enhance antiviral activity in cultured human hepatocytes. *Microbiol Immunol,* 51**,** 117-25.

AHMED, C. M., DABELIC, R., WAIBOCI, L. W., JAGER, L. D., HERON, L. L. & JOHNSON, H. M. 2009. SOCS-1 Mimetics Protect Mice against Lethal Poxvirus Infection: Identification of a Novel Endogenous Antiviral System. *Journal of Virology,* 83**,** 1402-1415.

AIR, G. M. 2014. Influenza virus-glycan interactions. *Current Opinion in Virology,* 7**,** 128-133.

ANSARI, S. A., SPRINGTHORPE, V. S., SATTAR, S. A., RIVARD, S. & RAHMAN, M. 1991. Potential Role of Hands in the Spread of Respiratory Viral-Infections - Studies with Human Parainfluenza Virus-3 and Rhinovirus-14. *Journal of Clinical Microbiology,* 29**,** 2115-2119.

ASHARANI, P. V., LOW KAH MUN, G., HANDE, M. P. & VALIYAVEETTIL, S. 2009. Cytotoxicity and genotoxicity of silver nanoparticles in human cells. *ACS Nano,* 3**,** 279-90.

AUDSLEY, J. M. & TANNOCK, G. A. 2004. The role of cell culture vaccines in the control of the next influenza pandemic. *Expert Opin Biol Ther,* 4**,** 709-17.

BAEK, J. H., SEO, Y. B., CHOI, W. S., KEE, S. Y., JEONG, H. W., LEE, H. Y., EUN, B. W., CHOO, E. J., LEE, J., KIM, S. R., KIM, Y. K., SONG, J. Y., WIE, S. H., LEE, J. S., CHEONG, H. J., KIM, W. J. & PANDE, T. E. 2014. Guideline on the prevention and control of seasonal influenza in healthcare setting. *Korean Journal of Internal Medicine,* 29**,** 265-280.

BARKER, J., STEVENS, D. & BLOOMFIELD, S. F. 2001. Spread and prevention of some common viral infections in community facilities and domestic homes. *Journal of Applied Microbiology,* 91**,** 7-21.

BARKER, W. H. 1986. Excess Pneumonia and Influenza Associated Hospitalization during Influenza Epidemics in the United-States, 1970-78. *American Journal of Public Health,* 76**,** 761-765.

BARKER, W. H. & MULLOOLY, J. P. 1980. Impact of Epidemic Type a Influenza in a Defined Adult-Population. *American Journal of Epidemiology,* 112**,** 798-813.

BATEMAN, A. C., BUSCH, M. G., KARASIN, A. I., BOVIN, N. & OLSEN, C. W. 2008. Amino acid 226 in the hemagglutinin of H4N6 influenza virus determines binding affinity for alpha-2,6-linked sialic acid and infectivity levels in primary swine and human respiratory epithelial cells. *Journal of Virology,* 82**,** 8204-8209.

BAWENDI, M. G., STEIGERWALD, M. L. & BRUS, L. E. 1990. The Quantum-Mechanics of Larger Semiconductor Clusters (Quantum Dots). *Annual Review of Physical Chemistry,* 41**,** 477-496.

BLUMEL, J., BURGER, R., DROSTEN, C., GRONER, A., GURTLER, L., HEIDEN, M., HILDEBRANDT, M., JANSEN, B., KLAMM, H., MONTAG-LESSING, T., OFFERGELD, R., PAULI, G., SEITZ, R., SCHLENKRICH, U., SCHOTTSTEDT, V., WILLKOMMEN, H.,

VON KONIG, C. H., BLUT, A. & BLUTASSOZIIERTE, U. B. 2009. Influenza Virus. *Transfusion Medicine and Hemotherapy,* 36**,** 32-39.
BORGDORFF, A. J. & CHOQUET, D. 2002. Regulation of AMPA receptor lateral movements. *Nature,* 417**,** 649-653.
BORGES, F. T., MICHELACCI, Y. M., AGUIAR, J. A. K., DALBONI, M. A., GAROFALO, A. S. & SCHOR, N. 2005. Characterization of glycosaminoglycans in tubular epithelial cells: Calcium oxalate and oxalate ions effects. *Kidney International,* 68**,** 1630-1642.
BOUVIER, N. M. & PALESE, P. 2008. The biology of influenza viruses. *Vaccine,* 26**,** D49-D53.
BRIGHT, R. A., MEDINA, M. J., XU, X. Y., PEREZ-ORONOZ, G., WALLIS, T. R., DAVIS, X. H. M., POVINELLI, L., COX, N. J. & KLIMOV, A. I. 2005. Incidence of adamantane resistance among influenza A (H3N2) viruses isolated worldwide from 1994 to 2005: a cause for concern. *Lancet,* 366**,** 1175-1181.
BRUNOTTE, L., FLIES, J., BOLTE, H., REUTHER, P., VREEDE, F. & SCHWEMMLE, M. 2014. The Nuclear Export Protein of H5N1 Influenza A Viruses Recruits Matrix 1 (M1) Protein to the Viral Ribonucleoprotein to Mediate Nuclear Export. *Journal of Biological Chemistry,* 289**,** 20067-20077.
CADY, S. D., SCHMIDT-ROHR, K., WANG, J., SOTO, C. S., DEGRADO, W. F. & HONG, M. 2010. Structure of the amantadine binding site of influenza M2 proton channels in lipid bilayers. *Nature,* 463**,** 689-U127.
CAVALETTI, G., OGGIONI, N., SALA, F., PEZZONI, G., CAVALLETTI, E., MARMIROLI, P., PETRUCCIOLI, M. G., FRATTOLA, L. & TREDICI, G. 2000. Effect on the peripheral nervous system of systemically administered dimethylsulfoxide in the rat: a neurophysiological and pathological study. *Toxicology Letters,* 118**,** 103-107.
CEDERLUND, A., GUDMUNDSSON, G. H. & AGERBERTH, B. 2011. Antimicrobial peptides important in innate immunity. *Febs Journal,* 278**,** 3942-3951.
CHAVAS, L. M., KATO, R., SUZUKI, N., VON ITZSTEIN, M., MANN, M. C., THOMSON, R. J., DYASON, J. C., MCKIMM-BRESCHKIN, J., FUSI, P., TRINGALI, C., VENERANDO, B., TETTAMANTI, G., MONTI, E. & WAKATSUKI, S. 2010. Complexity in influenza virus targeted drug design: interaction with human sialidases. *J Med Chem,* 53**,** 2998-3002.
CHEN, X. Y., QOUTAH, W. W., FREE, P., HOBLEY, J., FERNIG, D. G. & PARAMELLE, D. 2012. Features of Thiolated Ligands Promoting Resistance to Ligand Exchange in Self-Assembled Monolayers on Gold Nanoparticles. *Australian Journal of Chemistry,* 65**,** 266-274.
CHOI, K. Y. & MOOKHERJEE, N. 2012. Multiple immune-modulatory functions of catheticidin host defense peptides. *Frontiers in Immunology,* 3.
COHEN, D. 2014. ANTIVIRAL DRUGS Oseltamivir: another case of regulatory failure? *Bmj-British Medical Journal,* 348.
COLMAN, P. M., HOYNE, P. A. & LAWRENCE, M. C. 1993. Sequence and Structure Alignment of Paramyxovirus Hemagglutinin-Neuraminidase with Influenza-Virus Neuraminidase. *Journal of Virology,* 67**,** 2972-2980.
COOPER, D. A. & LANGE, J. M. A. 2004. Peptide inhibitors of virus-cell fusion: enfuvirtide as a case study in clinical discovery and development. *Lancet Infectious Diseases,* 4**,** 426-436.
COSTANZO, P. J. & BEYER, F. L. 2007. Thermally driven assembly of nanoparticles in polymer matrices. *Macromolecules,* 40**,** 3996-4001.
COWLING, B. J., IP, D. K. M., FANG, V. J., SUNTARATTIWONG, P., OLSEN, S. J., LEVY, J., UYEKI, T. M., LEUNG, G. M., PEIRIS, J. S. M., CHOTPITAYASUNONDH, T.,

NISHIURA, H. & SIMMERMAN, J. M. 2013. Aerosol transmission is an important mode of influenza A virus spread. *Nature Communications,* 4.

CRESPILHO, F. N., LIMA, F. C. A., DA SILVA, A. B. F., OLIVEIRA, O. N. & ZUCOLOTTO, V. 2009. The origin of the molecular interaction between amino acids and gold nanoparticles: A theoretical and experimental investigation. *Chemical Physics Letters,* 469**,** 186-190.

CURRIE, S. M., FINDLAY, E. G., MCFARLANE, A. J., FITCH, P. M., BOTTCHER, B., COLEGRAVE, N., PARAS, A., JOZWIK, A., CHIU, C., SCHWARZE, J. & DAVIDSON, D. J. 2016. Cathelicidins Have Direct Antiviral Activity against Respiratory Syncytial Virus In Vitro and Protective Function In Vivo in Mice and Humans. *Journal of Immunology,* 196**,** 2699-2710.

DAS, K., ARAMINI, J. M., MA, L. C., KRUG, R. M. & ARNOLD, E. 2010. Structures of influenza A proteins and insights into antiviral drug targets. *Nature Structural & Molecular Biology,* 17**,** 530-538.

DELATORRE, J. C., SURGEON, J. W., ERNEST, T. & WOLLMANN, R. 1981. Sub-Acute Toxicity of Intravenous Dimethylsulfoxide in Rhesus-Monkeys. *Journal of Toxicology and Environmental Health,* 7**,** 49-57.

DEYDE, V. M., XU, X. Y., BRIGHT, R. A., SHAW, M., SMITH, C. B., ZHANG, Y., SHU, Y. L., GUBAREVA, L. V., COX, N. J. & KLIMOV, A. I. 2007. Surveillance of resistance to adamantanes among influenza A(H3N2) and A(H1N1) viruses isolated worldwide. *Journal of Infectious Diseases,* 196**,** 249-257.

DIAZGRANADOS, C. A., DUNNING, A. J., ROBERTSON, C. A., TALBOT, H. K., LANDOLFI, V. & GREENBERG, D. P. 2016. Effect of Previous-Year Vaccination on the Efficacy, Immunogenicity, and Safety of High-Dose Inactivated Influenza Vaccine in Older Adults. *Clinical Infectious Diseases,* 62**,** 1092-1099.

DONG, G. Y., PENG, C., LUO, J., WANG, C. M., HAN, L., WU, B., JI, G. J. & HE, H. X. 2015. Adamantane-Resistant Influenza A Viruses in the World (1902-2013): Frequency and Distribution of M2 Gene Mutations. *Plos One,* 10.

DOTY, R. C., TSHIKHUDO, T. R., BRUST, M. & FERNIG, D. G. 2005. Extremely stable water-soluble Ag nanoparticles. *Chemistry of Materials,* 17**,** 4630-4635.

DUCHESNE, L., GENTILI, D., COMES-FRANCHINI, M. & FERNIG, D. G. 2008a. Robust Ligand Shells for Biological Applications of Gold Nanoparticles. *Langmuir,* 24**,** 13572-13580.

DUCHESNE, L., OCTEAU, V., BEARON, R. N., BECKETT, A., PRIOR, I. A., LOUNIS, B. & FERNIG, D. G. 2012. Transport of Fibroblast Growth Factor 2 in the Pericellular Matrix Is Controlled by the Spatial Distribution of Its Binding Sites in Heparan Sulfate. *Plos Biology,* 10.

DUCHESNE, L., TISSOT, B., RUDD, T. R., DELL, A. & FERNIG, D. G. 2006. N-glycosylation of fibroblast growth factor receptor 1 regulates ligand and heparan sulfate co-receptor binding. *Journal of Biological Chemistry,* 281**,** 27178-27189.

DUCHESNE, L., WELLS, G., FERNIG, D. G., HARRIS, S. A. & LEVY, R. 2008b. Supramolecular domains in mixed peptide self-assembled monolayers on gold nanoparticles. *Chembiochem,* 9**,** 2127-34.

DYKMAN, L. A. & KHLEBTSOV, N. G. 2011. Gold Nanoparticles in Biology and Medicine: Recent Advances and Prospects. *Acta Naturae,* 3**,** 34-55.

ENDO, T., KERMAN, K., NAGATANI, N. & TAMIYA, E. 2007. Excitation of localized surface plasmon resonance using a core-shell structured nanoparticle layer substrate and its application for label-free detection of biomolecular interactions. *Journal of Physics-Condensed Matter,* 19.

FAULK, W. P. & TAYLOR, G. M. 1971. Immunocolloid Method for Electron Microscope. *Immunochemistry,* 8**,** 1081-&.

FRANCI, G., FALANGA, A., GALDIERO, S., PALOMBA, L., RAI, M., MORELLI, G. & GALDIERO, M. 2015. Silver Nanoparticles as Potential Antibacterial Agents. *Molecules,* 20**,** 8856-8874.

FREE, P., PARAMELLE, D., BOSMAN, M., HOBLEY, J. & FERNIG, D. G. 2012. Synthesis of Silver Nanoparticles with Monovalently Functionalized Self-Assembled Monolayers. *Australian Journal of Chemistry,* 65**,** 275-282.

GAIKWAD, S., INGLE, A., GADE, A., RAI, M., FALANGA, A., INCORONATO, N., RUSSO, L., GALDIERO, S. & GALDIERO, M. 2013. Antiviral activity of mycosynthesized silver nanoparticles against herpes simplex virus and human parainfluenza virus type 3. *Int J Nanomedicine,* 8**,** 4303-14.

GAJAN, D., GUILLOIS, K., DELICHERE, P., BASSET, J. M., CANDY, J. P., CAPS, V., COPERET, C., LESAGE, A. & EMSLEY, L. 2009. Gold Nanoparticles Supported on Passivated Silica: Access to an Efficient Aerobic Epoxidation Catalyst and the Intrinsic Oxidation Activity of Gold. *Journal of the American Chemical Society,* 131**,** 14667-+.

GAMBLIN, S. J. & SKEHEL, J. J. 2010. Influenza Hemagglutinin and Neuraminidase Membrane Glycoproteins. *Journal of Biological Chemistry,* 285**,** 28403-28409.

GAUSH, C. R., HARD, W. L. & SMITH, T. F. 1966. Characterization of an Established Line of Canine Kidney Cells (Mdck). *Proceedings of the Society for Experimental Biology and Medicine,* 122**,** 931-&.

GHEZZI, S., COOPER, L., RUBIO, A., PAGANI, I., CAPOBIANCHI, M. R., IPPOLITO, G., PELLETIER, J., MENEGHETTI, M. C. Z., LIMA, M. A., SKIDMORE, M. A., BROCCOLI, V., YATES, E. A. & VICENZI, E. 2017. Heparin prevents Zika virus induced-cytopathic effects in human neural progenitor cells. *Antiviral Research,* 140**,** 13-17.

GREEN, I. J. 1962. Serial Propagation of Influenza B (Lee) Virus in a Transmissible Line of Canine Kidney Cells. *Science,* 138**,** 42-&.

GUINEA, R. & CARRASCO, L. 1995. Requirement for Vacuolar Proton-Atpase Activity during Entry of Influenza-Virus into Cells. *Journal of Virology,* 69**,** 2306-2312.

GUO, C. T., SUN, X. L., KANIE, O., SHORTRIDGE, K. F., SUZUKI, T., MIYAMOTO, D., HIDARI, K. I. P. J., WONG, C. H. & SUZUKI, Y. 2002. An O-glycoside of sialic acid derivative that inhibits both hemagglutinin and sialidase activities of influenza viruses. *Glycobiology,* 12**,** 183-190.

GUPTA, Y. K., MEENU, M. & MOHAN, P. 2015. The Tamiflu fiasco and lessons learnt. *Indian Journal of Pharmacology,* 47**,** 11-16.

HAISS, W., THANH, N. T. K., AVEYARD, J. & FERNIG, D. G. 2007. Determination of size and concentration of gold nanoparticles from UV-Vis spectra. *Analytical Chemistry,* 79**,** 4215-4221.

HAMILTON, B. S., WHITTAKER, G. R. & DANIEL, S. 2012. Influenza Virus-Mediated Membrane Fusion: Determinants of Hemagglutinin Fusogenic Activity and Experimental Approaches for Assessing Virus Fusion. *Viruses-Basel,* 4**,** 1144-1168.

HAN, M. Y., GAO, X. H., SU, J. Z. & NIE, S. 2001. Quantum-dot-tagged microbeads for multiplexed optical coding of biomolecules. *Nature Biotechnology,* 19**,** 631-635.

HE, Y. Q., LIU, S. P., KONG, L. & LIU, Z. F. 2005. A study on the sizes and concentrations of gold nanoparticles by spectra of absorption, resonance Rayleigh scattering and resonance non-linear scattering. *Spectrochimica Acta Part a-Molecular and Biomolecular Spectroscopy,* 61**,** 2861-2866.

HEILIGTAG, F. J. & NIEDERBERGER, M. 2013. The fascinating world of nanoparticle research. *Materials Today,* 16**,** 262-271.

HILL, E. M., TILDESLEY, M. J. & HOUSE, T. 2017. Evidence for history-dependence of influenza pandemic emergence (vol 7, pg 43623, 2017). *Scientific Reports,* 7.

HOSOYA, M., BALZARINI, J., SHIGETA, S. & DECLERCQ, E. 1991. Differential Inhibitory Effects of Sulfated Polysaccharides and Polymers on the Replication of Various Myxoviruses and Retroviruses, Depending on the Composition of the Target Amino-Acid-Sequences of the Viral Envelope Glycoproteins. *Antimicrobial Agents and Chemotherapy,* 35**,** 2515-2520.

HSUEH, Y. H., LIN, K. S., KE, W. J., HSIEH, C. T., CHIANG, C. L., TZOU, D. Y. & LIU, S. T. 2015. The Antimicrobial Properties of Silver Nanoparticles in Bacillus subtilis Are Mediated by Released Ag+ Ions. *PLoS One,* 10**,** e0144306.

JAIN, P. K., LEE, K. S., EL-SAYED, I. H. & EL-SAYED, M. A. 2006. Calculated absorption and scattering properties of gold nanoparticles of different size, shape, and composition: Applications in biological imaging and biomedicine. *Journal of Physical Chemistry B,* 110**,** 7238-7248.

JAISHANKAR, D., YAKOUB, A. M., BOGDANOV, A., VALYI-NAGY, T. & SHUKLA, D. 2015. Characterization of a proteolytically stable D-peptide that suppresses herpes simplex virus 1 infection: implications for the development of entry-based antiviral therapy. *J Virol,* 89**,** 1932-8.

JAYABAL, S., PANDIKUMAR, A., LIM, H. N., RAMARAJ, R., SUN, T. & HUANG, N. M. 2015. A gold nanorod-based localized surface plasmon resonance platform for the detection of environmentally toxic metal ions. *Analyst,* 140**,** 2540-2555.

JEFFERSON, T., JONES, M. A., DOSHI, P., DEL MAR, C. B., HENEGHAN, C. J., HAMA, R. & THOMPSON, M. J. 2012. Neuraminidase inhibitors for preventing and treating influenza in healthy adults and children. *Cochrane Database of Systematic Reviews*.

JEFFERSON, T., JONES, M. A., DOSHI, P., DELMAR, C. B., HAMA, R., THOMPSON, M. J., SPENCER, E. A., ONAKPOYA, I., MAHTANI, K. R., NUNAN, D., HOWICK, J. & HENEGHAN, C. J. 2014. Neuraminidase inhibitors for preventing and treating influenza in healthy adults and children. *Cochrane Database of Systematic Reviews*.

JENSSEN, H. 2005. Anti herpes simplex virus activity of lactoferrin/lactoferricin - an example of antiviral activity of antimicrobial protein/peptide. *Cellular and Molecular Life Sciences,* 62**,** 3002-3013.

JONES, J. C., TURPIN, E. A., BULTMANN, H., BRANDT, C. R. & SCHULTZ-CHERRY, S. 2006a. Inhibition of influenza virus infection by a novel antiviral peptide that targets viral attachment to cells. *Journal of Virology,* 80**,** 11960-11967.

JONES, J. C., TURPIN, E. A., BULTMANN, H., BRANDT, C. R. & SCHULTZ-CHERRY, S. 2006b. Inhibition of influenza virus infection by a novel antiviral peptide that targets viral attachment to cells. *J Virol,* 80**,** 11960-7.

JUVE, V., CARDINAL, M. F., LOMBARDI, A., CRUT, A., MAIOLI, P., PEREZ-JUSTE, J., LIZ-MARZAN, L. M., DEL FATTI, N. & VALLEE, F. 2013. Size-Dependent Surface Plasmon Resonance Broadening in Nonspherical Nanoparticles: Single Gold Nanorods. *Nano Letters,* 13**,** 2234-2240.

KATZ, J. M., WANG, M. L. & WEBSTER, R. G. 1990. Direct Sequencing of the Ha Gene of Influenza (H3n2) Virus in Original Clinical-Samples Reveals Sequence Identity with Mammalian Cell-Grown Virus. *Journal of Virology,* 64**,** 1808-1811.

KEVLES, D. J. 1993. Dulbecco,Renato and the New Animal Virology - Medicine, Methods, and Molecules. *Journal of the History of Biology,* 26**,** 409-442.

KIM, K. J., SUNG, W. S., MOON, S. K., CHOI, J. S., KIM, J. G. & LEE, D. G. 2008. Antifungal effect of silver nanoparticles on dermatophytes. *Journal of Microbiology and Biotechnology,* 18**,** 1482-1484.

KIM, M., SCHMITT, S. K., CHOI, J. W., KRUTTY, J. D. & GOPALAN, P. 2015. From Self-Assembled Monolayers to Coatings: Advances in the Synthesis and Nanobio Applications of Polymer Brushes. *Polymers,* 7**,** 1346-1378.

KLAUS, T., JOERGER, R., OLSSON, E. & GRANQVIST, C. G. 1999. Silver-based crystalline nanoparticles, microbially fabricated. *Proceedings of the National Academy of Sciences of the United States of America,* 96**,** 13611-13614.

KREUTER, J. 2007. Nanoparticles - a historical perspective. *International Journal of Pharmaceutics,* 331**,** 1-10.

KRIZANOVA, O. & RATHOVA, V. 1969. Serum inhibitors of myxoviruses. *Curr Top Microbiol Immunol,* 47**,** 125-51.

KUSUMI, A., SAKO, Y. & YAMAMOTO, M. 1993. Confined Lateral Diffusion of Membrane-Receptors as Studied by Single-Particle Tracking (Nanovid Microscopy) - Effects of Calcium-Induced Differentiation in Cultured Epithelial-Cells. *Biophysical Journal,* 65**,** 2021-2040.

LADNER, S. K., OTTO, M. J., BARKER, C. S., ZAIFERT, K., WANG, G. H., GUO, J. T., SEEGER, C. & KING, R. W. 1997. Inducible expression of human hepatitis B virus (HBV) in stably transfected hepatoblastoma cells: A novel system for screening potential inhibitors of HBV replication. *Antimicrobial Agents and Chemotherapy,* 41**,** 1715-1720.

LAMB, R. A. & CHOPPIN, P. W. 1983. The Gene Structure and Replication of Influenza-Virus. *Annual Review of Biochemistry,* 52**,** 467-506.

LEE, N., WALKER, E., EGERER, L., BUNNELL, B. A., MONDAL, D., VON LAER, D. & BRAUN, S. E. 2014. The Therapeutic Potential of Secreted Antiviral Entry Inhibitor (SAVE) Peptides Expressed By Transduced MSCs To Block HIV Infection. *Molecular Therapy,* 22**,** S183-S183.

LENZER, S. B. A. J. 2009. *The Truth About Tamiflu* [Online]. Available: https://www.theatlantic.com/magazine/archive/2009/12/the-truth-about-tamiflu/307801/ [Accessed].

LESER, G. P. & LAMB, R. A. 2005. Influenza virus assembly and budding in raft-derived microdomains: A quantitative analysis of the surface distribution of HA, NA and M2 proteins. *Virology,* 342**,** 215-227.

LEVY, R. 2006. Peptide-capped gold nanoparticles: Towards artificial proteins. *Chembiochem,* 7**,** 1141-1145.

LEVY, R., THANH, N. T., DOTY, R. C., HUSSAIN, I., NICHOLS, R. J., SCHIFFRIN, D. J., BRUST, M. & FERNIG, D. G. 2004a. Rational and combinatorial design of peptide capping ligands for gold nanoparticles. *J Am Chem Soc,* 126**,** 10076-84.

LEVY, R., THANH, N. T. K., DOTY, R. C., HUSSAIN, I., NICHOLS, R. J., SCHIFFRIN, D. J., BRUST, M. & FERNIG, D. G. 2004b. Rational and combinatorial design of peptide capping Ligands for gold nanoparticles. *Journal of the American Chemical Society,* 126**,** 10076-10084.

LEVY, R., WANG, Z., DUCHESNE, L., DOTY, R. C., COOPER, A. I., BRUST, M. & FERNIG, D. G. 2006a. A generic approach to monofunctionalized protein-like gold nanoparticles based on immobilized metal ion affinity chromatography. *Chembiochem,* 7**,** 592-4.

LEVY, R., WANG, Z. X., DUCHESNE, L., DOTY, R. C., COOPER, A. I., BRUST, M. & FERNIG, D. G. 2006b. A generic approach to monofunctionalized protein-like gold

nanoparticles based on immobilized metal ion affinity chromatography. *Chembiochem,* 7**,** 592-594.
LI, X. M., SHEN, D. K., YANG, J. P., YAO, C., CHE, R. C., ZHANG, F. & ZHAO, D. Y. 2013. Successive Layer-by-Layer Strategy for Multi-Shell Epitaxial Growth: Shell Thickness and Doping Position Dependence in Upconverting Optical Properties. *Chemistry of Materials,* 25**,** 106-112.
LI, Y. H., LIN, Z. F., ZHAO, M. Q., GUO, M., XU, T. T., WANG, C. B., XIA, H. M. & ZHU, B. 2016. Reversal of H1N1 influenza virus-induced apoptosis by silver nanoparticles functionalized with amantadine. *Rsc Advances,* 6**,** 89679-89686.
LIU, X., LAI, C. C., WANG, K. Y., XING, L., YANG, P. H., DUAN, Q. & WANG, X. L. 2015. A Functional Role of Fibroblast Growth Factor Receptor 1 (FGFR1) in the Suppression of Influenza A Virus Replication. *Plos One,* 10.
LIZ-MARZAN, L. M., GIERSIG, M. & MULVANEY, P. 1996. Synthesis of nanosized gold-silica core-shell particles. *Langmuir,* 12**,** 4329-4335.
LOWEN, A. & PALESE, P. 2009. Transmission of influenza virus in temperate zones is predominantly by aerosol, in the tropics by contact: a hypothesis. *PLoS Curr,* 1**,** RRN1002.
LU, L., SUN, R. W. Y., CHEN, R., HUI, C. K., HO, C. M., LUK, J. M., LAU, G. K. K. & CHE, C. M. 2008. Silver nanoparticles inhibit hepatitis B virus replication. *Antiviral Therapy,* 13**,** 253-262.
LU, Y., YIN, Y. D., LI, Z. Y. & XIA, Y. N. 2002. Synthesis and self-assembly of Au@SiO2 core-shell colloids. *Nano Letters,* 2**,** 785-788.
LUGOVTSEV, V. Y., MELNYK, D. & WEIR, J. P. 2013. Heterogeneity of the MDCK Cell Line and Its Applicability for Influenza Virus Research. *Plos One,* 8.
MA, C. L., POLISHCHUK, A. L., OHIGASHI, Y., STOUFFER, A. L., SCHON, A., MAGAVERN, E., JING, X. H., LEAR, J. D., FREIRE, E., LAMB, R. A., DEGRADO, W. F. & PINTO, L. H. 2009. Identification of the functional core of the influenza A virus A/M2 proton-selective ion channel. *Proceedings of the National Academy of Sciences of the United States of America,* 106**,** 12283-12288.
MADJET, M., GUET, C. & JOHNSON, W. R. 1995. Comparative study of exchange-correlation effects on the electronic and optical properties of alkali-metal clusters. *Phys Rev A,* 51**,** 1327-1339.
MAIR, C. M., LUDWIG, K., HERRMANN, A. & SIEBEN, C. 2014. Receptor binding and pH stability - How influenza A virus hemagglutinin affects host-specific virus infection. *Biochimica Et Biophysica Acta-Biomembranes,* 1838**,** 1153-1168.
MARTELL, J. D., DEERINCK, T. J., SANCAK, Y., POULOS, T. L., MOOTHA, V. K., SOSINSKY, G. E., ELLISMAN, M. H. & TING, A. Y. 2012. Engineered ascorbate peroxidase as a genetically encoded reporter for electron microscopy. *Nature Biotechnology,* 30**,** 1143-+.
MARTINO, M. M., BRIQUEZ, P. S., GUC, E., TORTELLI, F., KILARSKI, W. W., METZGER, S., RICE, J. J., KUHN, G. A., MULLER, R., SWARTZ, M. A. & HUBBELL, J. A. 2014. Growth Factors Engineered for Super-Affinity to the Extracellular Matrix Enhance Tissue Healing. *Science,* 343**,** 885-888.
MATERIALS, A. 2012. *The Discovery of Metals* [Online]. Available: https://www.azom.com/article.aspx?ArticleID=6101 [Accessed].
MATROSOVICH, M. & KLENK, H. D. 2003. Natural and synthetic sialic acid-containing inhibitors of influenza virus receptor binding. *Reviews in Medical Virology,* 13**,** 85-97.
MATSUBARA, T., ONISHI, A., SAITO, T., SHIMADA, A., INOUE, H., TAKI, T., NAGATA, K., OKAHATA, Y. & SATO, T. 2010. Sialic Acid-Mimic Peptides As Hemagglutinin

Inhibitors for Anti-Influenza Therapy. *Journal of Medicinal Chemistry,* 53**,** 4441-4449.

MOHAN, T., SHARMA, C., BHAT, A. A. & RAO, D. N. 2013. Modulation of HIV peptide antigen specific cellular immune response by synthetic alpha- and beta-defensin peptides. *Vaccine,* 31**,** 1707-16.

MOON, H. J., NIKAPITIYA, C., LEE, H. C., PARK, M. E., KIM, J. H., KIM, T. H., YOON, J. E., CHO, W. K., MA, J. Y., KIM, C. J., JUNG, J. U. & LEE, J. S. 2017. Inhibition of highly pathogenic avian influenza (HPAI) virus by a peptide derived from vFLIP through its direct destabilization of viruses. *Scientific Reports,* 7.

MOORE, T. L., RODRIGUEZ-LORENZO, L., HIRSCH, V., BALOG, S., URBAN, D., JUD, C., ROTHEN-RUTISHAUSER, B., LATTUADA, M. & PETRI-FINK, A. 2015. Nanoparticle colloidal stability in cell culture media and impact on cellular interactions. *Chemical Society Reviews,* 44**,** 6287-6305.

MORENS, D. M., FOLKERS, G. K. & FAUCI, A. S. 2009. What Is a Pandemic? *Journal of Infectious Diseases,* 200**,** 1018-1021.

MUBAREKA, S., LOWEN, A. C., STEEL, J., COATES, A. L., GARCIA-SASTRE, A. & PALESE, P. 2009. Transmission of influenza virus via aerosols and fomites in the guinea pig model. *J Infect Dis,* 199**,** 858-65.

MUTHURI, S. G., VENKATESAN, S., MYLES, P. R., LEONARDI-BEE, J., AL KHUWAITIR, T. S. A., AL MAMUN, A., ANOVADIYA, A. P., AZZIZ-BAUMGARTNER, E., BAEZ, C., BASSETTI, M., BEOVIC, B., BERTISCH, B., BONMARIN, I., BOOY, R., BORJA-ABURTO, V. H., BURGMANN, H., CAO, B., CARRATALA, J., DENHOLM, J. T., DOMINGUEZ, S. R., DUARTE, P. A. D., DUBNOV-RAZ, G., ECHAVARRIA, M., FANELLA, S., GAO, Z. C., GERARDIN, P., GIANNELLA, M., GUBBELS, S., HERBERG, J., IGLESIAS, A. L. H., HOGER, P. H., HU, X. Y., ISLAM, Q. T., JIMENEZ, M. F., KANDEEL, A., KEIJZERS, G., KHALILI, H., KNIGHT, M., KUDO, K., KUSZNIERZ, G., KUZMAN, I., KWAN, A. M. C., AMINE, I. L., LANGENEGGER, E., LANKARANI, K. B., LEO, Y. S., LINKO, R., LIU, P., MADANAT, F., MAYO-MONTERO, E., MCGEER, A., MEMISH, Z., METAN, G., MICKIENE, A., MIKIC, D., MOHN, K. G. I., MORADI, A., NYMADAWA, P., OLIVA, M. E., OZKAN, M., PAREKH, D., PAUL, M., POLACK, F. P., RATH, B. A., RODRIGUEZ, A. H., SARROUF, E. B., SEALE, A. C., SERTOGULLARINDAN, B., SIQUEIRA, M. M., SKRET-MAGIERLO, J., STEPHAN, F., TALAREK, E., TANG, J. W., TO, K. K. W., TORRES, A., TORUN, S. H., TRAN, D., UYEKI, T. M., VAN ZWOL, A., VAUDRY, W., VIDMAR, T., YOKOTA, R. T. C., ZAROGOULIDIS, P., NGUYEN-VAN-TAM, J. S. & INVESTIGATORS, P. C. 2014. Effectiveness of neuraminidase inhibitors in reducing mortality in patients admitted to hospital with influenza A H1N1pdm09 virus infection: a meta-analysis of individual participant data. *Lancet Respiratory Medicine,* 2**,** 395-404.

NEHL, C. L. & HAFNER, J. H. 2008. Shape-dependent plasmon resonances of gold nanoparticles. *Journal of Materials Chemistry,* 18**,** 2415-2419.

NICOL, M. Q., LIGERTWOOD, Y., BACON, M. N., DUTIA, B. M. & NASH, A. A. 2012a. A novel family of peptides with potent activity against influenza A viruses. *J Gen Virol,* 93**,** 980-6.

NICOL, M. Q., LIGERTWOOD, Y., BACON, M. N., DUTIA, B. M. & NASH, A. A. 2012b. A novel family of peptides with potent activity against influenza A viruses. *Journal of General Virology,* 93**,** 980-986.

NIEVES, D. J., AZMI, N. S., XU, R., LEVY, R., YATES, E. A. & FERNIG, D. G. 2014. Monovalent maleimide functionalization of gold nanoparticles via copper-free click chemistry. *Chemical Communications,* 50**,** 13157-13160.

NIEVES, D. J., LI, Y., FERNIG, D. G. & LEVY, R. 2015. Photothermal raster image correlation spectroscopy of gold nanoparticles in solution and on live cells. *R Soc Open Sci,* 2**,** 140454.

NUNE, S. K., CHANDA, N., SHUKLA, R., KATTI, K., KULKARNI, R. R., THILAKAVATHY, S., MEKAPOTHULA, S., KANNAN, R. & KATTI, K. V. 2009. Green nanotechnology from tea: phytochemicals in tea as building blocks for production of biocompatible gold nanoparticles. *Journal of Materials Chemistry,* 19**,** 2912-2920.

O'KEEFE, B. R., SMEE, D. F., TURPIN, J. A., SAUCEDO, C. J., GUSTAFSON, K. R., MORI, T., BLAKESLEE, D., BUCKHEIT, R. & BOYD, M. R. 2003. Potent anti-influenza activity of cyanovirin-N and interactions with viral hemagglutinin. *Antimicrobial Agents and Chemotherapy,* 47**,** 2518-2525.

OCTEAU, V., COGNET, L., DUCHESNE, L., LASNE, D., SCHAEFFER, N., FERNIG, D. G. & LOUNIS, B. 2009. Photothermal Absorption Correlation Spectroscopy. *Acs Nano,* 3**,** 345-350.

ORI, A., FREE, P., COURTY, J., WILKINSON, M. C. & FERNIG, D. G. 2009. Identification of Heparin-binding Sites in Proteins by Selective Labeling. *Molecular & Cellular Proteomics,* 8**,** 2256-2265.

ORI, A., WILKINSON, M. C. & FERNIG, D. G. 2008. The heparanome and regulation of cell function: structures, functions and challenges. *Frontiers in Bioscience-Landmark,* 13**,** 4309-4338.

PARAMELLE, D., NIEVES, D., BRUN, B., KRAUT, R. S. & FERNIG, D. G. 2015. Targeting Cell Membrane Lipid Rafts by Stoichiometric Functionalization of Gold Nanoparticles with a Sphingolipid-Binding Domain Peptide. *Advanced Healthcare Materials,* 4**,** 911-917.

PARAMELLE, D., PENG, T., FREE, P., FERNIG, D. G., LIM, S. & TOMCZAK, N. 2016. Specific Internalisation of Gold Nanoparticles into Engineered Porous Protein Cages via Affinity Binding. *Plos One,* 11.

PARAMELLE, D., SADOVOY, A., GORELIK, S., FREE, P., HOBLEY, J. & FERNIG, D. G. 2014. A rapid method to estimate the concentration of citrate capped silver nanoparticles from UV-visible light spectra. *Analyst,* 139**,** 4855-61.

PASRICHA, G., MISHRA, A. C. & CHAKRABARTI, A. K. 2013. Comprehensive global amino acid sequence analysis of PB1F2 protein of influenza A H5N1 viruses and the influenza A virus subtypes responsible for the 20th-century pandemics. *Influenza and Other Respiratory Viruses,* 7**,** 497-505.

PESSI, A., INGALLINELLA, P., BIANCHI, E., WANG, Y. J., HRIN, R., VENEZIANO, M., BONELLI, F., KETAS, T., MOORE, J. & MILLER, M. 2009. Dramatic Increase of Antiviral Potency of an Hiv Peptide Fusion Inhibitor by Targeting to Lipid Rafts Via Addition of a Cholesterol Group. *Biopolymers,* 92**,** 302-302.

PIELAK, R. M., SCHNELL, J. R. & CHOU, J. J. 2009. Mechanism of drug inhibition and drug resistance of influenza A M2 channel. *Proceedings of the National Academy of Sciences of the United States of America,* 106**,** 7379-7384.

PIETRANTONI, A., DI BIASE, A. M., TINARI, A., MARCHETTI, M., VALENTI, P., SEGANTI, L. & SUPERTI, F. 2003. Bovine lactoferrin inhibits adenovirus infection by interacting with viral structural polypeptides. *Antimicrobial Agents and Chemotherapy,* 47**,** 2688-2691.

POOLEY, F. D. 1982. Bacteria Accumulate Silver during Leaching of Sulfide Ore Minerals. *Nature,* 296**,** 642-643.

PUIG-BASAGOITI, F., FUKUHARA, T., TAMURA, T., ONO, C., UEMURA, K., KAWACHI, Y., YAMAMOTO, S., MORI, H., KURIHARA, T., OKAMOTO, T., AIZAKI, H. &

MATSUURA, Y. 2016. Human Cathelicidin Compensates for the Role of Apolipoproteins in Hepatitis C Virus Infectious Particle Formation. *J Virol,* 90**,** 8464-77.

QU, L. & PENG, X. 2002. Control of photoluminescence properties of CdSe nanocrystals in growth. *J Am Chem Soc,* 124**,** 2049-55.

REIMANN, S. M. & MANNINEN, M. 2002. Electronic structure of quantum dots. *Reviews of Modern Physics,* 74**,** 1283-1342.

REUTER, J. D., MYC, A., HAYES, M. M., GAN, Z. H., ROY, R., QIN, D. J., YIN, R., PIEHLER, L. T., ESFAND, R., TOMALIA, D. A. & BAKER, J. R. 1999. Inhibition of viral adhesion and infection by sialic-acid-conjugated dendritic polymers. *Bioconjugate Chemistry,* 10**,** 271-278.

ROBERTSON, J. D., RIZZELLO, L., AVILA-OLIAS, M., GAITZSCH, J., CONTINI, C., MAGON, M. S., RENSHAW, S. A. & BATTAGLIA, G. 2016. Purification of Nanoparticles by Size and Shape. *Scientific Reports,* 6.

RODEWALD, L. E., ORENSTEIN, W. A., MASON, D. D. & COCHI, S. L. 2006. Vaccine supply problems: A perspective of the Centers for Disease Control and Prevention. *Clinical Infectious Diseases,* 42**,** S104-S110.

ROSI, N. L., GILJOHANN, D. A., THAXTON, C. S., LYTTON-JEAN, A. K. R., HAN, M. S. & MIRKIN, C. A. 2006. Oligonucleotide-modified gold nanoparticles for intracellular gene regulation. *Science,* 312**,** 1027-1030.

ROSSMAN, J. S., JING, X. H., LESER, G. P. & LAMB, R. A. 2010. Influenza Virus M2 Protein Mediates ESCRT-Independent Membrane Scission. *Cell,* 142**,** 902-913.

RUDAVSKY, S. 2018. *Tamiflu may have odd side effects, particularly in children, experts say* [Online]. Available: https://eu.indystar.com/story/news/2018/02/13/tamiflu-may-have-odd-side-effects-particularly-children-experts-say/324846002/ [Accessed].

RUGGIERO, G. & UTILI, R. 1992. [Usefulness and limitations of vaccination against influenza]. *Recenti Prog Med,* 83**,** 337-40.

SAINSBURY, T., IKUNO, T., OKAWA, D., PACILE, D., FRECHET, J. M. J. & ZETTL, A. 2007. Self-assembly of gold nanoparticles at the surface of amine- and thiol-functionalized boron nitride nanotubes. *Journal of Physical Chemistry C,* 111**,** 12992-12999.

SAITO, T., NAKAYA, Y., SUZUKI, T., ITO, R., SAITO, T., SAITO, H., TAKAO, S., SAHARA, K., ODAGIRI, T., MURATA, T., USUI, T., SUZUKI, Y. & TASHIRO, M. 2004. Antigenic alteration of influenza B virus associated with loss of a glycosylation site due to host-cell adaptation. *Journal of Medical Virology,* 74**,** 336-343.

SALVATORE, M., GARCIA-SASTRE, A., RUCHALA, P., LEHRER, R. I., CHANG, T. & KLOTMAN, M. E. 2007. alpha-Defensin inhibits influenza virus replication by cell-mediated mechanism(s). *J Infect Dis,* 196**,** 835-43.

SANTAK, M., LANG-BALIJA, M., IVANCIC-JELECKI, J., KOSUTIC-GULIJA, T., LJUBIN-STERNAK, S. & FORCIC, D. 2013. Antigenic differences between vaccine and circulating wild-type mumps viruses decreases neutralization capacity of vaccine-induced antibodies. *Epidemiology and Infection,* 141**,** 1298-1309.

SAUNDERS-HASTINGS, P. R. & KREWSKI, D. 2016. Reviewing the History of Pandemic Influenza: Understanding Patterns of Emergence and Transmission. *Pathogens,* 5.

SCHULZ, F., DAHL, G. T., BESZTEJAN, S., SCHROER, M. A., LEHMKUHLER, F., GRUBEL, G., VOSSMEYER, T. & LANGE, H. 2016. Ligand Layer Engineering To Control Stability and Interfacial Properties of Nanoparticles. *Langmuir,* 32**,** 7897-7907.

SCHULZ, F., VOSSMEYER, T., BASTUS, N. G. & WELLER, H. 2013. Effect of the Spacer Structure on the Stability of Gold Nanoparticles Functionalized with Monodentate Thiolated Poly(ethylene glycol) Ligands. *Langmuir,* 29**,** 9897-9908.

SHAALAN, N. M., HAMAD, D., ABDEL-LATIEF, A. Y. & ABDEL-RAHIM, M. A. 2016. Preparation of quantum size of tin oxide: Structural and physical characterization. *Progress in Natural Science-Materials International,* 26**,** 145-151.

SHAH, R. & CHANG, T. L. 2012. Defensins in Viral Infection. *Small Wonders: Peptides for Disease Control,* 1095**,** 137-171.

SHAO, W. H., LI, X. X., GORAYA, M. U., WANG, S. & CHEN, J. L. 2017. Evolution of Influenza A Virus by Mutation and Re-Assortment. *International Journal of Molecular Sciences,* 18.

SKALICKOVA, S., HEGER, Z., KREJCOVA, L., PEKARIK, V., BASTL, K., JANDA, J., KOSTOLANSKY, F., VARECKOVA, E., ZITKA, O., ADAM, V. & KIZEK, R. 2015a. Perspective of Use of Antiviral Peptides against Influenza Virus. *Viruses-Basel,* 7**,** 5428-5442.

SKALICKOVA, S., HEGER, Z., KREJCOVA, L., PEKARIK, V., BASTL, K., JANDA, J., KOSTOLANSKY, F., VARECKOVA, E., ZITKA, O., ADAM, V. & KIZEK, R. 2015b. Perspective of Use of Antiviral Peptides against Influenza Virus. *Viruses,* 7**,** 5428-42.

SKEHEL, J. J. & WILEY, D. C. 2000. Receptor binding and membrane fusion in virus entry: The influenza hemagglutinin. *Annual Review of Biochemistry,* 69**,** 531-569.

SKIDMORE, M. A., KAJASTE-RUDNITSKI, A., WELLS, N. M., GUIMOND, S. E., RUDD, T. R., YATES, E. A. & VICENZI, E. 2015. Inhibition of influenza H5N1 invasion by modified heparin derivatives. *Medchemcomm,* 6**,** 640-646.

SLAWSON, R. M., VANDYKE, M. I., LEE, H. & TREVORS, J. T. 1992. Germanium and Silver Resistance, Accumulation, and Toxicity in Microorganisms. *Plasmid,* 27**,** 72-79.

SMITHA, S. L., GOPCHANDRAN, K. G., SMIJESH, N. & PHILIP, R. 2013. Size-dependent optical properties of Au nanorods. *Progress in Natural Science-Materials International,* 23**,** 36-43.

SOKOLOV, K., AARON, J., HSU, B., NIDA, D., GILLENWATER, A., FOLLEN, M., MACAULAY, C., ADLER-STORTHZ, K., KORGEL, B., DESCOUR, M., PASQUALINI, R., ARAP, W., LAM, W. & RICHARDS-KORTUM, R. 2003. Optical systems for In vivo molecular imaging of cancer. *Technology in Cancer Research & Treatment,* 2**,** 491-504.

SONDI, I. & SALOPEK-SONDI, B. 2004. Silver nanoparticles as antimicrobial agent: a case study on E-coli as a model for Gram-negative bacteria. *Journal of Colloid and Interface Science,* 275**,** 177-182.

SPADARO, J. A., BERGER, T. J., BARRANCO, S. D., CHAPIN, S. E. & BECKER, R. O. 1974. Antibacterial Effects of Silver Electrodes with Weak Direct-Current. *Antimicrobial Agents and Chemotherapy,* 6**,** 637-642.

STORM-VERSLOOT, M. N., VOS, C. G., UBBINK, D. T. & VERMEULEN, H. 2010. Topical silver for preventing wound infection. *Cochrane Database of Systematic Reviews*.

STUBBS, T. M. & TE VELTHUIS, A. J. W. 2014. The RNA-dependent RNA polymerase of the influenza A virus. *Future Virology,* 9**,** 863-876.

SUN, C., MARCELLO, M., LI, Y., MASON, D., LEVY, R. & FERNIG, D. G. 2016. Selectivity in glycosaminoglycan binding dictates the distribution and diffusion of fibroblast growth factors in the pericellular matrix. *Open Biol,* 6.

SUN, R. W. Y., CHEN, R., CHUNG, N. P. Y., HO, C. M., LIN, C. L. S. & CHE, C. M. 2005. Silver nanoparticles fabricated in Hepes buffer exhibit cytoprotective activities toward HIV-1 infected cells. *Chemical Communications*, 5059-5061.

TAKIMOTO, T., TAYLOR, G. L., CONNARIS, H. C., CRENNELL, S. J. & PORTNER, A. 2002. Role of the hemagglutinin-neuraminidase protein in the mechanism of paramyxovirus-cell membrane fusion. *Journal of Virology,* 76**,** 13028-13033.

TAUBENBERGER, J. K. & MORENS, D. M. 2006. 1918 influenza: the mother of all pandemics. *Emerging Infectious Diseases,* 12**,** 15-22.

TOOVEY, S., RAYNER, C., PRINSSEN, E., CHU, T., DONNER, B., THAKRAR, B., DUTKOWSKI, R., HOFFMANN, G., BREIDENBACH, A., LINDEMANN, L., CAREY, E., BOAK, L., GIESCHKE, R., SACKS, S., SOLSKY, J., SMALL, I. & REDDY, D. 2008. Assessment of Neuropsychiatric Adverse Events in Influenza Patients Treated with Oseltamivir A Comprehensive Review. *Drug Safety,* 31**,** 1097-1114.

TOTANI, K., KUBOTA, T., KURODA, T., MURATA, T., HIDARI, K. I. P. J., SUZUKI, T., SUZUKI, Y., KOBAYASHI, K., ASHIDA, H., YAMAMOTO, K. & USUI, T. 2003. Chemoenzymatic synthesis and application of glycopolymers containing multivalent sialyloligosaccharides with a poly(L-glutamic acid) backbone for inhibition of infection by influenza viruses. *Glycobiology,* 13**,** 315-326.

TREANOR, J. 2004. Influenza vaccine--outmaneuvering antigenic shift and drift. *N Engl J Med,* 350**,** 218-20.

TSUCHIDA, A., KOBAYASHI, K., MATSUBARA, N., MURAMATSU, T., SUZUKI, T. & SUZUKI, Y. 1998. Simple synthesis of sialyllactose-carrying polystyrene and its binding with influenza virus. *Glycoconjugate Journal,* 15**,** 1047-1054.

TURZHITSKY, V., QIU, L., ITZKAN, I., NOVIKOV, A. A., KOTELEV, M. S., GETMANSKIY, M., VINOKUROV, V. A., MURADOV, A. V. & PERELMAN, L. T. 2014. Spectroscopy of Scattered Light for the Characterization of Micro and Nanoscale Objects in Biology and Medicine. *Applied Spectroscopy,* 68**,** 133-154.

UNG, T., LIZ-MARZAN, L. M. & MULVANEY, P. 1998. Controlled method for silica coating of silver colloids. Influence of coating on the rate of chemical reactions. *Langmuir,* 14**,** 3740-3748.

VARKI, A. 2008. Sialic acids in human health and disease. *Trends in Molecular Medicine,* 14**,** 351-360.

VENKATESH, P. & PRASAD, C. R. 1983. The Scattering of Light and Other Electromagnetic-Radiation. *Applied Optics,* 22**,** 645-645.

WANG, F., TAN, W. B., ZHANG, Y., FAN, X. P. & WANG, M. Q. 2006. Luminescent nanomaterials for biological labelling. *Nanotechnology,* 17**,** R1-R13.

WANG, J. X., LI, J. H., GUO, G. Y., WANG, Q. J., TANG, J., ZHAO, Y. C., QIN, H., WAHAFU, T., SHEN, H., LIU, X. Y. & ZHANG, X. L. 2016. Silver-nanoparticles-modified biomaterial surface resistant to staphylococcus: new insight into the antimicrobial action of silver. *Scientific Reports,* 6.

WILSON, S. S., WIENS, M. E. & SMITH, J. G. 2013. Antiviral Mechanisms of Human Defensins. *Journal of Molecular Biology,* 425**,** 4965-4980.

WORTHLEY, E. G. & SCHOTT, C. D. 1969. Toxicity of 4 Concentrations of Dmso. *Toxicology and Applied Pharmacology,* 15**,** 275-&.

XIANG, D. X., CHEN, Q., PANG, L. & ZHENG, C. L. 2011. Inhibitory effects of silver nanoparticles on H1N1 influenza A virus in vitro. *J Virol Methods,* 178**,** 137-42.

XU, R. Y., ORI, A., RUDD, T. R., UNIEWICZ, K. A., AHMED, Y. A., GUIMOND, S. E., SKIDMORE, M. A., SILIGARDI, G., YATES, E. A. & FERNIG, D. G. 2012. Diversification of the Structural Determinants of Fibroblast Growth Factor-

Heparin Interactions IMPLICATIONS FOR BINDING SPECIFICITY. *Journal of Biological Chemistry,* 287.

YOFFE, A. D. 2001. Semiconductor quantum dots and related systems: electronic, optical, luminescence and related properties of low dimensional systems. *Advances in Physics,* 50**,** 1-208.

ZHAO, L., JIANG, D., CAI, Y., JI, X., XIE, R. & YANG, W. 2012. Tuning the size of gold nanoparticles in the citrate reduction by chloride ions. *Nanoscale,* 4**,** 5071-6.

ZHU, J., HUANG, L. Q., ZHAO, J. W., WANG, Y. C., ZHAO, Y. R., HAO, L. M. & LU, Y. M. 2005. Shape dependent resonance light scattering properties of gold nanorods. *Materials Science and Engineering B-Solid State Materials for Advanced Technology,* 121**,** 199-203.

ZOST, S. J., PARKHOUSE, K., GUMINA, M. E., KIM, K., PEREZ, S. D., WILSON, P. C., TREANOR, J. J., SANT, A. J., COBEY, S. & HENSLEY, S. E. 2017. Contemporary H3N2 influenza viruses have a glycosylation site that alters binding of antibodies elicited by egg-adapted vaccine strains. *Proceedings of the National Academy of Sciences of the United States of America,* 114**,** 12578-12583.

ZOU, Y., LIU, P., LIU, C. H. & ZHI, X. T. 2015. Doxorubicin-loaded mesoporous magnetic nanoparticles to induce apoptosis in breast cancer cells. *Biomedicine & Pharmacotherapy,* 69**,** 355-360.